

NASA/CR-2012-217562
NIA Report No. 2012-01



Development and Application of Benchmark Examples for Mixed-Mode I/II Quasi-Static Delamination Propagation Predictions

Ronald Krueger
National Institute of Aerospace, Hampton, Virginia

NASA STI Program . . . in Profile

Since its founding, NASA has been dedicated to the advancement of aeronautics and space science. The NASA scientific and technical information (STI) program plays a key part in helping NASA maintain this important role.

The NASA STI program operates under the auspices of the Agency Chief Information Officer. It collects, organizes, provides for archiving, and disseminates NASA's STI. The NASA STI program provides access to the NASA Aeronautics and Space Database and its public interface, the NASA Technical Report Server, thus providing one of the largest collections of aeronautical and space science STI in the world. Results are published in both non-NASA channels and by NASA in the NASA STI Report Series, which includes the following report types:

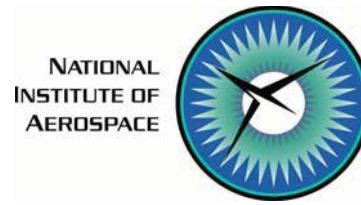
- **TECHNICAL PUBLICATION.** Reports of completed research or a major significant phase of research that present the results of NASA programs and include extensive data or theoretical analysis. Includes compilations of significant scientific and technical data and information deemed to be of continuing reference value. NASA counterpart of peer-reviewed formal professional papers, but having less stringent limitations on manuscript length and extent of graphic presentations.
- **TECHNICAL MEMORANDUM.** Scientific and technical findings that are preliminary or of specialized interest, e.g., quick release reports, working papers, and bibliographies that contain minimal annotation. Does not contain extensive analysis.
- **CONTRACTOR REPORT.** Scientific and technical findings by NASA-sponsored contractors and grantees.
- **CONFERENCE PUBLICATION.** Collected papers from scientific and technical conferences, symposia, seminars, or other meetings sponsored or co-sponsored by NASA.
- **SPECIAL PUBLICATION.** Scientific, technical, or historical information from NASA programs, projects, and missions, often concerned with subjects having substantial public interest.
- **TECHNICAL TRANSLATION.** English-language translations of foreign scientific and technical material pertinent to NASA's mission.

Specialized services also include creating custom thesauri, building customized databases, and organizing and publishing research results.

For more information about the NASA STI program, see the following:

- Access the NASA STI program home page at <http://www.sti.nasa.gov>
- E-mail your question via the Internet to help@sti.nasa.gov
- Fax your question to the NASA STI Help Desk at 443-757-5803
- Phone the NASA STI Help Desk at 443-757-5802
- Write to:
NASA STI Help Desk
NASA Center for AeroSpace Information
7115 Standard Drive
Hanover, MD 21076-1320

NASA/CR-2012-217562
NIA Report No. 2012-01



Development and Application of Benchmark Examples for Mixed-Mode I/II Quasi-Static Delamination Propagation Predictions

Ronald Krueger
National Institute of Aerospace, Hampton, Virginia

National Aeronautics and
Space Administration

Langley Research Center
Hampton, Virginia 23681-2199

Prepared for Langley Research Center
Under Cooperative Agreement NNL09AA00A

April 2012

The use of trademarks or names of manufacturers in this report is for accurate reporting and does not constitute an official endorsement, either expressed or implied, of such products or manufacturers by the National Aeronautics and Space Administration.

Available from:

NASA Center for AeroSpace Information
7115 Standard Drive
Hanover, MD 21076-1320
443-757-5802

DEVELOPMENT AND APPLICATION OF BENCHMARK EXAMPLES FOR MIXED-MODE I/II QUASI-STATIC DELAMINATION PROPAGATION PREDICTIONS

Ronald Krueger*

ABSTRACT

The development of benchmark examples for quasi-static delamination propagation prediction is presented and demonstrated for a commercial code. The examples are based on finite element models of the Mixed-Mode Bending (MMB) specimen. The examples are independent of the analysis software used and allow the assessment of the automated delamination propagation prediction capability in commercial finite element codes based on the virtual crack closure technique (VCCT). First, quasi-static benchmark examples were created for the specimen. Second, starting from an initially straight front, the delamination was allowed to propagate under quasi-static loading. Third, the load-displacement relationship from a propagation analysis and the benchmark results were compared, and good agreement could be achieved by selecting the appropriate input parameters. Good agreement between the results obtained from the automated propagation analysis and the benchmark results could be achieved by selecting input parameters that had previously been determined during analyses of mode I Double Cantilever Beam and mode II End Notched Flexure specimens. The benchmarking procedure proved valuable by highlighting the issues associated with choosing the input parameters of the particular implementation. Overall, the results are encouraging, but further assessment for mixed-mode delamination fatigue onset and growth is required.

1. INTRODUCTION

Over the past two decades, the use of fracture mechanics has become common practice to characterize the onset and growth of delaminations. In order to predict delamination onset or growth, the calculated strain energy release rate components are compared to interlaminar fracture toughness properties measured over a range from pure mode I loading to pure mode II loading.

The virtual crack closure technique (VCCT) is widely used for computing energy release rates based on results from continuum (2D) and solid (3D) finite element (FE) analyses and to supply the mode separation required when using the mixed-mode fracture criterion [1, 2]. The virtual crack closure technique was recently implemented into several commercial finite element codes. As new methods for analyzing composite delamination are incorporated into finite element codes, the need for comparison and benchmarking becomes important since each code requires specific input parameters unique to its implementation. These parameters are unique to the numerical approach chosen and do not reflect real *physical* differences in delamination behavior.

An approach for assessing the mode I, mode II and mixed-mode I and II, delamination propagation capabilities in commercial finite element codes under static loading was recently presented and demonstrated for VCCT for ABAQUS^{®1} [3,4] as well as MD Nastran[™] and Marc^{™2} [5]. First, benchmark results were created manually for finite element models of the mode I Double

*R. Krueger, National Institute of Aerospace, 100 Exploration Way, Hampton, VA, 23666, resident at Durability, Damage Tolerance and Reliability Branch, MS 188E, NASA Langley Research Center, Hampton, VA, 23681, USA.

¹ ABAQUS[®] is a product of Dassault Systèmes Simulia Corp. (DSS), Providence, RI, USA

² MD Nastran[™] and Marc[™] are manufactured by MSC.Software Corp., Santa Ana, CA, USA. NASTRAN[®] is a registered trademark of NASA.

Cantilever Beam (DCB), the mode II End Notched Flexure (ENF) and the mixed-mode I/II Single Leg Bending (SLB) specimen. Second, starting from an initially straight front, the delamination was allowed to propagate using the automated procedure implemented in the finite element software. The approach was then extended to allow the assessment of the delamination fatigue growth prediction capabilities in commercial finite element codes [4,6]. As for the static case, benchmark results were created manually first for the mode I Double Cantilever Beam (DCB) and the mode II End Notched Flexure (ENF) specimen. Second, the delamination was allowed to grow under cyclic loading in a finite element model of a commercial code. In general, good agreement between the results obtained from the propagation and growth analysis and the benchmark results could be achieved by selecting the appropriate input parameters. Overall, the results were encouraging but showed that additional assessment for mixed-mode delamination cases is required.

The objective of the present study was to create additional benchmark examples, independent of the analysis software used, which allows the assessment of the quasi-static delamination propagation prediction capabilities in commercial finite element codes. For the simulation of mixed-mode I/II fracture, the Mixed-Mode Bending (MMB) specimen was selected as shown in Figure 1. Dimensions, layup and material properties were taken directly from a related experimental study [7].

Static benchmark results were created for three mixed-mode ratios ($G_{II}/G_T = 0.2, 0.5$ and 0.8) based on the approach developed earlier [3]. To create the benchmark results, two-dimensional finite element models were used for simulating the MMB specimens with different delamination lengths a_0 . For each delamination length modeled, the load, P , and the displacement, w , were monitored. The total strain energy release rate, G_T , and mixed-mode ratio, G_{II}/G_T , were calculated for a fixed applied displacement. It is assumed that the delamination propagates when the computed energy release rate, G_T , reaches the mixed-mode fracture toughness G_c . Thus, critical loads and critical displacements for delamination propagation were calculated for each delamination length modeled. From these critical load/displacement results, benchmark solutions were created. It is assumed that the load/displacement relationship computed during automatic propagation should closely match the benchmark cases.

After creating the benchmark cases, the approach was demonstrated for the commercial finite element code ABAQUS[®]. Starting from an initially straight front, the delamination was allowed to propagate under quasi-static loading based on the algorithms implemented into the software. Input control parameters were varied to study the effect on the computed delamination propagation. The benchmark enabled the selection of the appropriate input parameters that yielded good agreement between the results obtained from the propagation analysis and the benchmark results. Once the parameters have been identified, they may then be used with confidence to model delamination growth for more complex configurations.

In this paper, the development of the benchmark cases for the assessment of the quasi-static delamination propagation is presented. Examples of automated propagation analyses are shown, and the selection of the required code specific input parameters are discussed.

2. METHODOLOGY BASED ON FRACTURE MECHANICS

For the current numerical investigation, the Mixed-Mode Bending (MMB) specimen, as shown in Figure 1, was chosen since it is simple, and exhibits the mixed-mode I/II opening fracture mode over a wide range of mixed-mode ratios G_{II}/G_T . For the current investigation, finite element models were created for three distinct mixed-mode ratios ($G_{II}/G_T = 0.2, 0.5$ and 0.8). The methodology for

delamination propagation, was applied to the MMB specimen to create the benchmark example [8, 9]. For the current study, MMB specimens made of IM7/8552 graphite/epoxy with a unidirectional layup, $[0]_{24}$, were modeled. The material, layup, overall specimen dimensions including initial crack length, a_0 , were identical to specimens used in related experimental studies [7,10,11]. The material properties are given in Tables I and II.

A quasi-static mixed-mode fracture criterion is determined by plotting the interlaminar fracture toughness, G_c , versus the mixed-mode ratio, G_{II}/G_T as shown in Figure 2. The fracture criterion is generated experimentally using pure Mode I ($G_{II}/G_T=0$) Double Cantilever Beam (DCB) tests [11], pure Mode II ($G_{II}/G_T=1$) End-Notched Flexure (ENF) tests [10], and Mixed Mode Bending (MMB) tests of varying ratios of G_I and G_{II} [7]. For the material used in this study, the experimental data (open symbols) and mean values (filled symbols) are shown in Figure 2. A 2D fracture criterion was suggested by Benzeggah and Kenane [12] using a simple mathematical relationship between G_c and G_{II}/G_T

$$G_c = G_{Ic} + (G_{IIc} - G_{Ic}) \cdot \left(\frac{G_{II}}{G_T} \right)^\eta \quad (1)$$

In this expression, G_{Ic} and G_{IIc} are the experimentally determined fracture toughness data for mode I and II as shown in Figure 2. The factor η was determined by a curve fit using the Levenberg-Marquardt algorithm in the KaleidaGraphTM graphing and data analysis software [13]. The parameters G_{Ic} , G_{IIc} and η are required input to perform a VCCT analysis in ABAQUS[®] as discussed in the appendix.

3. FINITE ELEMENT MODELING

3.1 Model description

An example of a two-dimensional finite element model of a Mixed-Mode Bending (MMB) specimen with boundary conditions is shown in Figure 3 for a mixed-mode ratio $G_{II}/G_T=0.2$. Based on previous experience [3,4,6], the specimen was modeled with solid plane strain elements (CPE4I) in ABAQUS[®] Standard 6.10. Along the length, all models were divided into different sections with different mesh refinement as shown in Figure 3a. The MMB specimen was modeled with six elements through the specimen thickness ($2h$) as shown in the detail of Figure 3b. The resulting element length at the delamination tip was $\Delta a=0.5$ mm. The load apparatus was modeled explicitly using rigid beam elements (R2D2) as shown in Figure 3a. Multi-point constraints were used to connect the rigid elements with the planar model of the specimen and enforce the appropriate boundary conditions as shown in Figures 3b and c.

The plane of delamination was modeled as a discrete discontinuity in the center of the specimen. For the analysis with ABAQUS[®] 6.10, the models were created as separate meshes for the upper and lower part of the specimens with identical nodal point coordinates in the plane of delamination [14]. Two surfaces (top and bottom surface) were defined to identify the contact area in the plane of delamination as shown in Figures 3b and c. Additionally, a node set was created to define the intact (bonded nodes) region. Two models, used to simulate mixed-mode ratios $G_{II}/G_T=0.5$ and 0.8, are shown in Figure 4. The mesh of the specimen was kept the same for all three mode ratios. Only the lengths of the rigid elements used to simulate the load apparatus were changed as shown in Figure 4.

Examples of three-dimensional finite element models of the MMB specimen are shown in Figures 5 and 6. Along the length, all models were divided into different sections with different mesh refinement. A refined mesh was used in the center of the MMB specimen as shown in the detail of Figure 5b. Across the width, a uniform mesh (25 elements) was used to avoid potential problems at the transition between a coarse and finer mesh [3-6]. Through the specimen thickness ($2h$), six elements were used as shown in the detail of Figure 5b. The resulting element length at the delamination tip was $\Delta a=0.5$ mm. The specimen was modeled with solid brick elements (C3D8I), which had yielded excellent results in previous studies [3,4,6]. The load apparatus was modeled explicitly using rigid plate elements (R3D4) as shown in Figure 5a. As before for the two-dimensional model, multi-point constraints were used to connect the rigid elements with the solid model of the specimen and enforce the appropriate boundary conditions. Two models used to simulate mixed-mode ratios $G_{II}/G_T=0.5$ and 0.8 are shown in Figure 6. The mesh of the specimen was kept the same for all three mode ratios. Only the lengths of the rigid plate elements used to simulate the load apparatus were changed as shown in Figure 6.

3.2 Static delamination propagation analysis

For the automated delamination propagation analysis, the VCCT implementation in ABAQUS[®] Standard 6.10 was used. The plane of delamination in three-dimensional analyses is modeled using the existing ABAQUS[®]/Standard crack propagation capability based on the contact pair capability [14]. Additional element definitions are not required, and the underlying finite element mesh and model does not have to be modified [14]. The implementation offers a crack and delamination propagation capability in ABAQUS[®]. It is implied that the energy release rate at the crack tip is calculated at the end of a converged increment. Once the energy release rate exceeds the critical strain energy release rate (including the user-specified mixed-mode criteria as shown in Figure 2), the node at the crack tip is released in the following increment, which allows the crack to propagate. To avoid sudden loss of stability when the crack tip is propagated, the force at the crack tip before advancement is released gradually during succeeding increments in such a way that the force is brought to zero no later than the time at which the next node along the crack path begins to open [14,15].

In addition to the mixed-mode fracture criterion, VCCT for ABAQUS[®] requires additional input for the propagation analysis. If a user specified release tolerance is exceeded in an increment $(G-G_c)/G_c > \text{release tolerance}$, a cutback operation is performed which reduces the time increment. In the new smaller increment, the strain energy release rates are recalculated and compared to the user specified release tolerance. The cutback reduces the degree of overshoot and improves the accuracy of the local solution [14]. A release tolerance of 0.2 is suggested in the handbook [14]. To help overcome convergence issues during the propagation analysis, ABAQUS[®] provides:

- *contact stabilization* which is applied across only selected contact pairs and used to control the motion of two contact pairs while they approach each other in multi-body contact. The damping is applied when bonded contact pairs debond and move away from each other [14,15]
- *automatic or static stabilization* which is applied to the motion of the entire model and is commonly used in models that exhibit statically unstable behavior such as buckling [14,15]
- *viscous regularization*, which is applied only to nodes on contact pairs that have just debonded. The viscous regularization damping causes the tangent stiffness matrix of the

softening material to be positive for sufficiently small time increments. Viscous regularization damping in VCCT for ABAQUS[®] is similar to the viscous regularization damping provided for cohesive elements and the concrete material model in ABAQUS[®]/Standard [14,15]. Further details about the required input parameters are discussed in the appendix.

For automated propagation analysis, it was assumed that the computed behavior should closely match the benchmark results created below. For all analyses, the elastic constants (given in Table I) and the input to define the fracture criterion (given in Table II) were kept constant. Based on previous results [3], automatic or static stabilization was not used in this study. To limit the scope of the study, viscous regularization was also not considered. Instead, the study focused on using the default values and parameter combinations that had recently yielded good results [4]. This approach was used to gain confidence in the parameters that had been identified previously and thus determine if the selection of the parameters could be considered problem independent. Therefore, only the following items were varied to study the effect on the automated delamination propagation behavior during the analysis.

- The release tolerance (*reltol*) was varied.
- Analyses were performed with and without contact stabilization. For analyses that included contact stabilization only, a single stabilization factor ($cs=1 \times 10^{-6}$) was used.
- Two- and three-dimensional models with different types of elements were used.

4. DEVELOPMENT OF THE STATIC BENCHMARK CASES

4.1 Benchmark case for 20% mode II

The static benchmark case was created based on the approach developed earlier [3]. Two-dimensional finite element models simulating MMB specimens with 17 different delamination lengths a_0 were created ($25.4 \text{ mm} \leq a_0 \leq 70.6 \text{ mm}$). For each delamination length modeled, the load, P , and displacement, w , were monitored as shown in Figure 7 (colored lines) for the case of 20% mode II ($G_{II}/G_T = 0.2$). Using VCCT, the total strain energy release rate, G_T , and the mixed-mode ratio G_{II}/G_T were computed at the end of the analysis as shown in Figure 7. The failure index G_T/G_c was calculated by correlating the computed total energy release rate, G_T , with the mixed-mode fracture toughness, G_c , of the graphite/epoxy material. As discussed before (see Figure 2), the mixed-mode fracture toughness, G_c , is a function of the mixed-mode ratio G_{II}/G_T . Hence, the mixed-mode fracture toughness, G_c for each computed mixed-mode ratio ($G_{II}/G_T \approx 0.2$) was obtained from the curve fit of the material data (solid red curve) as illustrated in Figure 8 (blue arrows). It is assumed that the delamination propagates when the failure index G_T/G_c reaches unity. Therefore, the critical load, P_{crit} , can be calculated based on the relationship between load, P , and the energy release rate, G [16],

$$G = \frac{P^2}{2} \cdot \frac{\partial C_P}{\partial A} \quad (2)$$

In equation (2), C_P is the compliance of the specimen, and ∂A is the increase in surface area corresponding to an incremental increase in load or displacement at fracture. The critical load, P_{crit} , and critical displacement, w_{crit} , were calculated for each delamination length modeled

$$\frac{G_T}{G_c} = \frac{P^2}{P_{crit}^2} \Rightarrow P_{crit} = P \sqrt{\frac{G_c}{G_T}}, \quad w_{crit} = w \sqrt{\frac{G_c}{G_T}} \quad (3)$$

and the results were included in the load/displacement plots as shown in Figure 9 (solid red circles). These critical load/displacement results indicated that, with increasing delamination length, less load is required to extend the delamination up to $a_0 \approx 48$ mm. To further extend the delamination an increase in load is required past $w=3.5$ mm.

As shown in Figure 10, these critical load/displacement results (solid black dots) can be used to create a benchmark solution (solid red line) for applied displacements, w . The benchmark result may also be visualized by plotting the prescribed displacements, w , at delamination growth onset versus the increase in delamination length, a^* , as illustrated in Figure 11. It is assumed that the load/displacement, or applied displacement/delamination-length relationship computed during automatic propagation should closely match the benchmark cases.

4.2 Benchmark case for 50% mode II

The benchmark case for 50% mode II ($G_{II}/G_T=0.5$) was created similarly. Two-dimensional finite element models simulating MMB specimens with 16 different delamination lengths a_0 were created ($25.4 \text{ mm} \leq a_0 \leq 70.6 \text{ mm}$) to study the case of $G_{II}/G_T=0.5$. For each delamination length modeled, the load, P , and displacement, w , were monitored as shown in Figure 12 (colored lines). Using VCCT, the total energy release rate, G_T , and the mixed-mode ratio G_{II}/G_T were computed at the end of the analysis as shown in Figure 12. The mixed-mode fracture toughness, G_c for each computed mixed-mode ratio ($G_{II}/G_T \approx 0.5$) was obtained from the curve fit of the material data (solid red curve) as illustrated previously in Figure 8 (green arrows). The critical load, P_{crit} , and critical displacement, w_{crit} , were calculated for each delamination length modeled using equation (3), and the results were included in the load/displacement plots as shown in Figure 13 (solid red circles). These critical load/displacement results indicated that, with increasing delamination length, less load is required to extend the delamination up to $a_0 \approx 48$ mm. To further extend the delamination an increase in load is required past $w=2.0$ mm. For the first three delamination lengths, a_0 , plotted in Figure 13, the values of the critical displacements also decreased at the same time. This means that the MMB specimen exhibits unstable delamination propagation under load control as well as displacement control in this region for $G_{II}/G_T=0.5$. The remaining critical load/displacement results indicated stable propagation. From these critical load/displacement results (solid grey circles and dashed line), two benchmark solutions can be created as shown in Figure 14. During the analysis, either prescribed displacements, w , or nodal point loads, P , are applied. For the case of prescribed displacements, w , (dashed blue line), the applied displacement must be held constant over several increments once the critical point (P_{crit} , w_{crit}) is reached, and the delamination front is advanced during these increments. Once the critical path (dashed grey line) is reached, the applied displacement is increased again incrementally. For the case of applied nodal point loads (dashed red line), the applied load must be held constant while the delamination front is advanced during these increments. Once the critical path (dashed grey line) is reached, the applied load is increased again incrementally.

The benchmark result for prescribed displacements may also be visualized by plotting the prescribed displacements, w , at delamination growth onset versus the increase in delamination length, a^* , as illustrated in Figure 15. For the case of applied nodal point loads, the benchmark result may be visualized by plotting the applied loads, P , at delamination growth onset versus the increase in delamination length, a^* , as illustrated in Figure 16. It is assumed that the

load/displacement, load/delamination-length or applied displacement/delamination-length relationship computed during automatic propagation should closely match the benchmark cases.

4.3 Benchmark case for 80% mode II

The benchmark case for 80% mode II ($G_{II}/G_T = 0.8$) was created based on the approach developed earlier [3] and discussed above for 20% and 50% mode II. Two-dimensional finite element models simulating MMB specimens with 15 different delamination lengths a_0 were created ($25.4 \text{ mm} \leq a_0 \leq 70.6 \text{ mm}$) to study the case of $G_{II}/G_T = 0.8$. For each delamination length modeled, the load, P , and displacement, w , were monitored as shown in Figure 17 (colored lines). Using VCCT, the total energy release rate, G_T , and the mixed-mode ratio G_{II}/G_T were computed at the end of the analysis as shown in Figure 17. The mixed-mode fracture toughness, G_c for each computed mixed-mode ratio ($G_{II}/G_T \approx 0.8$) was obtained from the curve fit of the material data (solid red curve) as illustrated previously in Figure 8 (purple arrows). The critical load, P_{crit} , and critical displacement, w_{crit} , were calculated for each delamination length modeled, using equation (3), and the results were included in the load/displacement plots as shown in Figure 18 (solid red circles).

These critical load/displacement results indicated that, with increasing delamination length, less load is required to extend the delamination up to $a_0 \approx 48 \text{ mm}$. To further extend the delamination an increase in load is required past $w=2.0 \text{ mm}$. For the first five delamination lengths, a_0 , plotted in Figure 18, the values of the critical displacements also decreased at the same time. This means that the MMB specimen exhibits unstable delamination propagation under load control as well as displacement control in this region for $G_{II}/G_T = 0.8$. The remaining critical load/displacement results indicated stable propagation. From these critical load/displacement results (solid grey circles and dashed line), two benchmark solutions can be created as shown in Figure 19. During the analysis, either prescribed displacements, w , or nodal point loads, P , are applied. For the case of prescribed displacements, w , (dashed blue line), the applied displacement must be held constant over several increments once the critical point (P_{crit}, w_{crit}) is reached, and the delamination front is advanced during these increments. Once the critical path (dashed grey line) is reached, the applied displacement is increased again incrementally. For the case of applied nodal point loads (dashed red line), the applied load must be held constant while the delamination front is advanced during these increments. Once the critical path (dashed grey line) is reached, the applied load is increased again incrementally.

The benchmark result for prescribed displacements may also be visualized by plotting the prescribed displacements, w , at delamination growth onset versus the increase in delamination length, a^* , as illustrated in Figure 20. For the case of applied nodal point loads, the benchmark result may be visualized by plotting the applied loads, P , at delamination growth onset versus the increase in delamination length, a^* , as illustrated in Figure 21. It is assumed that the load/displacement, load/delamination-length or applied displacement/delamination-length relationship computed during automatic propagation should closely match the benchmark cases.

5. STATIC ANALYSIS BENCHMARKING

5.1 Computed energy release rates and mixed-mode ratios

First, static analyses were performed with propagation disabled to compute the total energy release rate, G_T , the mode II component, G_{II} , and the mixed-mode ratio G_{II}/G_T . For this static analysis, an applied maximum displacement of $w=2.0 \text{ mm}$ was chosen for all models. To ensure that the model geometry and material input data for all models produced consistent results, the

computed results were evaluated. The results were obtained from models shown in Figures 3 through 6.

5.1.1 Comparison of results obtained from two- and three-dimensional models

For all mixed-mode ratios (results for $G_{II}/G_T=0.2$ in blue; 0.5 in green and 0.8 in black) the two-dimensional models (results with open symbols and solid lines) yield total energy release rates, G_T , that are almost identical to the results obtained from three-dimensional models (solid symbols and dashed lines) as shown in Figure 22. Comparing the computed mode II strain energy release rates, G_{II} (plotted in Figure 23), and the mixed-mode ratios, G_{II}/G_T , (plotted in Figure 24), confirms the good agreement between the different models. The computed mixed-mode ratios, G_{II}/G_T , are slightly lower than the targeted values for the test (dashed lines) [7] a trend that appears to increase with increasing applied displacement, w . Based on the current findings, it was assumed that results obtained from two- and three-dimensional models computed later during the assessment phase were easily comparable.

For each of the two-dimensional finite element models representing different delamination lengths ($25.4 \text{ mm} \leq a_0 \leq 76.2 \text{ mm}$), the mixed-mode ratios corresponding to an applied displacement $w=2.0 \text{ mm}$, were computed. The results were plotted versus the increase in delamination length, a^* , as illustrated in Figure 25. For all three mixed-mode ratios studied (results for $G_{II}/G_T=0.2$ in blue; 0.5 in green and 0.8 in black) the computed mixed-mode ratios increase slightly with increasing delamination length until $a^* \approx 20 \text{ mm}$ when the mixed-mode ratios reach the targeted values for the test (dashed lines) [7]. The computed mixed-mode ratios increased further until the delamination tip is located under the loading point. For delaminations extending beyond the load point, the computed mixed-mode ratios increased for models with target values $G_{II}/G_T=0.5$ and 0.8 and decreased for models with target values $G_{II}/G_T=0.2$. It should be noted, that delaminations extending beyond the load point could be included in the current benchmarking process, which is entirely geared toward numerical analysis. For actual physical tests geared towards obtaining mixed-mode fracture toughness values however, delaminations extending beyond the load point become meaningless.

5.1.2 Computed distributions across the specimen width

For all the mixed-mode ratios studied ($G_{II}/G_T=0.2, 0.5$ and 0.8), the total energy release rate, G_T , the mode II component, G_{II} , the mixed-mode ratio, G_{II}/G_T , and the failure index, G_T/G_c , were also computed and plotted versus the normalized width, y/B , as shown in Figures 26 through 29. For a delamination length $a_0=25.4 \text{ mm}$ the computed total energy release rates rates, G_T (results for $G_{II}/G_T=0.2$ blue circles; 0.5 green squares and 0.8 black diamonds), were plotted versus the normalized width, y/B , of the specimen as shown in Figure 26. The results obtained from two-dimensional finite element models (open symbols) are plotted at the center of the specimen $y/B=0$. The values obtained from two-dimensional and three-dimensional analyses are in good agreement as discussed above (see results plotted in Figures 22 through 25). The results obtained from three-dimensional models (solid symbols) indicate that qualitatively, the total strain energy release rate is fairly constant over almost the entire width of the specimen. Only near the edges of the specimen is a decrease in total energy release rate observed for the cases $G_{II}/G_T=0.2$ and 0.5 and an increase in total energy release rate is observed for the mode II dominated case $G_{II}/G_T=0.8$. The mode II components, G_{II} , for each case were plotted in Figure 27. An increase in G_{II} is visible near the edges for the mode II dominated case $G_{II}/G_T=0.8$ and also for the equal mode case $G_{II}/G_T=0.5$. The mixed-mode ratios, G_{II}/G_T , plotted in Figure 28 indicate a relative dominance of G_{II} near the edges of the specimens compared to the distribution in the center of the specimens. For all three-dimensional

models, the failure indices, G_T/G_c , plotted in Figure 29, were somewhat higher across the entire width than the results from two-dimensional planar finite element models. The failure indices dropped near the edges, which suggested that delamination propagation was expected to locally lag behind and turn the initially straight front into a thumbnail front for $G_{II}/G_T = 0.2$ and 0.5 similar to fronts observed in a Double Cantilever Beam (DCB) specimen. For $G_{II}/G_T = 0.8$, the drop of the failure index near the edges was less pronounced and a straight front across the entire width was expected. The computed front shapes will be discussed in detail in a later section.

5.2 Results from automated delamination propagation analysis for 20% mode II

The propagation analysis was performed in two steps using the models shown in Figures 3 and 5 starting from an initial delamination length, $a_0 = 25.4$ mm. In the first step, a displacement of $w = 1.5$ mm was applied which nearly equaled the critical displacement, $w_{crit} = 1.64$ mm, determined earlier. In the second step, the applied displacement was increased to $w = 8.0$ mm. For this second step, automatic incrementation was used in ABAQUS[®] and a small increment size (0.5% of the total step) was chosen at the beginning of the step. To reduce the risk of numerical instability and early termination of the analysis, a minimum allowed increment size (10^{-18} of the total step) was also chosen. The analysis was limited to 5000 increments.

Initially, analyses were performed using two-dimensional planar models (shown in Figure 3) without stabilization or viscous regularization. Based on previous results [3,4], release tolerance values smaller than the default value ($reltol = 0.2$) [14] were used since these values yielded better results. Using $reltol = 0.1$, the load dropped at the critical point, however the computed path stayed above the benchmark as shown in Figure 30 (solid blue line) where the computed resultant force (load P) is plotted versus the applied displacement w . As the displacement continued to increase over 3.0 mm, the computed load/displacement path converged to the benchmark result (solid grey circles and solid grey line). To improve the results, the release tolerance was decreased to $reltol = 0.01$. The results (solid red line) matched the benchmark case. Due to the fine mesh, only a small saw-tooth pattern was observed.

Based on problems identified during previous analyses, automated or static stabilization was not used in this study [3]. The results computed when contact stabilization (cs) was added are plotted in Figure 31. For a small stabilization factor ($cs = 1 \times 10^{-6}$) and a release tolerance suggested in the handbook ($reltol = 0.2$) [14], the load decreased, and delamination propagation started shortly after reaching the critical point of the benchmark solution (solid green line). The load/displacement path then ran parallel to the constant displacement branch of the benchmark result and later converged to the benchmark result. To reduce the observed overshoot, the release tolerance was reduced. For a stabilization factor of $cs = 1 \times 10^{-6}$ and release tolerance $reltol = 0.1$ (solid blue line), the overshoot was reduced, and the computed load/displacement path then ran closer to the constant displacement branch of the benchmark result. This result was practically identical to the results discussed above without stabilization. As above, further reducing the release tolerance ($reltol = 0.01$) yielded results that were in excellent agreement with the benchmark (solid red line) and due to the fine mesh, only a small saw-tooth pattern was observed.

An alternative way to plot the benchmark is shown in Figure 32 where the applied displacement w is plotted versus the increase in delamination length a^* . This way of presenting the results is shown because it may be of advantage for large structures where local delamination propagation may have little effect on the global stiffness of the structure and may therefore not be visible in a global load/displacement plot. However, extracting the delamination length a from the finite element results required more manual, time consuming post-processing of the results compared to

the relatively simple and readily available output of nodal displacements and forces. The results plotted in Figure 30 are the examples that were discussed above and were shown in the global load/displacement plots of Figure 31. The conclusions that can be drawn from this plot are identical to those discussed above.

Results obtained from three-dimensional models are shown in Figures 33 and 34. Based on the results from two-dimensional planar models shown previously, contact stabilization was added to the analyses to help overcome convergence issues. The results (solid blue line) computed for a release tolerance value ($reltol=0.1$) and a small stabilization factor ($cs=1 \times 10^{-6}$) are plotted in Figure 33. The load dropped and delamination propagation started upon reaching the critical point of the benchmark solution (solid circles and solid grey line). The load/displacement path then ran parallel to the benchmark result but was shifted slightly towards lower loads. Deviation from the benchmark may be explained by the fact that the benchmark results were created using two-dimensional planar finite element models of the MMB specimen. As shown in Figure 29, the three-dimensional models yield a failure index which is somewhat higher across the entire width of the specimen compared to the results from two-dimensional planar finite element models. Therefore, delamination propagation is expected to start prior to the benchmark results obtained from two-dimensional planar finite element analysis, which ultimately leads to a shift of the entire results plot towards lower loads.

For three distinct locations across the width of the specimen (two edges and center as shown later in Figure 53) the results from above were plotted in Figure 34, where the applied displacement w is plotted versus the increase in delamination length a^* . The results for all three locations (solid green line for edge 1, solid blue line for center location and solid red line for edge 2) are in excellent agreement with the benchmark case (solid circles and solid grey line). Any deviation from the benchmark results mentioned above is less visible compared to the load/displacement plot of Figure 33.

5.3 Results from automated delamination propagation analysis for 50% mode II

5.3.1 Computed delamination propagation for applied displacement

As discussed above, the propagation analysis was performed in two steps using the models shown in Figures 4a and 6a starting from an initial delamination length, $a_0=25.4$ mm. In the first step, a displacement of $w=1.2$ mm was applied which nearly equaled the critical displacement, $w_{crit}=1.34$ mm, determined earlier. In the second step, the applied displacement was increased to $w=8.0$ mm. For this second step, automatic incrementation was used in ABAQUS[®] and a small increment size (0.5% of the total step) was chosen at the beginning of the step. To reduce the risk of numerical instability and early termination of the analysis, a minimum allowed increment size (10^{-18} of the total step) was also chosen. The analysis was limited to 5000 increments.

Initially, analyses were performed using two-dimensional planar models (shown in Figure 4a) without stabilization or viscous regularization. Release tolerance values equal to the default value ($reltol=0.2$) [14] and smaller were used since these values had yielded better results in the past [3,4]. Using the default value ($reltol=0.2$), the computed load and displacement exceeded the critical point before the initial load drop occurred and delamination propagation started (solid green line) as shown in Figure 35 where the computed resultant force (load P) is plotted versus the applied displacement w . The computed path initially stayed above the benchmark, however, as the displacement continued to increase over 2.5 mm, the computed load/displacement path converged to the benchmark result (solid grey circles and dashed grey line). To reduce the observed overshoot, the release tolerance was decreased. For a release tolerance $reltol=0.1$, the overshoot was reduced

and the results improved (solid blue line) and shifted towards the benchmark case. For a release tolerance $reltol=0.01$, the analysis terminated once the critical point was reached (solid red line) due to convergence problems.

The results computed when contact stabilization (cs) was added are plotted in Figure 36. Using a stabilization factor of $cs=1 \times 10^{-6}$, and a release tolerance ($reltol=0.01$) yielded results that were in excellent agreement with the benchmark (solid red line). Due to the fine mesh, only a small saw-tooth pattern was observed. The result confirms previous observations where small release tolerance values ($reltol=0.01$) in conjunction with a stabilization factor of $cs=1 \times 10^{-6}$ had yielded excellent agreement with the benchmark results [3,4].

An alternative way to plot the benchmark is shown in Figure 37 where the applied displacement w is plotted versus the increase in delamination length a^* . The results plotted in Figure 37 are the examples that were discussed above and were shown in the global load/displacement plots of Figures 35 and 36. The conclusions that can be drawn from this plot are identical to those discussed above.

The result obtained from a three-dimensional analysis is shown in Figure 38. Based on the results from two-dimensional planar models shown above, contact stabilization was added to the analysis to help overcome convergence issues. Since the computer time increases with tighter release tolerances, a tolerance value ($reltol=0.1$) was selected. The result (solid blue line) computed for a release tolerance value $reltol=0.1$ and a small stabilization factor $cs=1 \times 10^{-6}$ are plotted in Figure 38. The load dropped and delamination propagation started upon reaching the critical point of the benchmark solution (solid circles and dashed grey line). The load/displacement path then ran parallel to the benchmark result but was shifted slightly towards lower loads. Deviation from the benchmark may be explained by the fact that the benchmark results were created using two-dimensional planar finite element models of the MMB specimen. As shown in Figure 29, the three-dimensional models yield a failure index which is somewhat higher across the entire width than the results from two-dimensional planar finite element models. Therefore, delamination propagation is expected to start prior to the benchmark results obtained from two-dimensional planar finite element analysis, which ultimately leads to a shift of the entire results plot towards lower loads.

5.3.2 Computed delamination propagation for applied quasi-static load

The propagation analysis was performed in two steps using the models shown in Figures 4a and 6a starting from an initial delamination length, $a_0=25.4$ mm. In the first step, a load $P=360$ N was applied which equaled nearly the critical load, $P_{crit}=385$ N, determined earlier. In the second step, the total load was increased ($P=600$ N). Automatic incrementation was used with a small increment size at the beginning (0.5% of the total step) and a very small minimum allowed increment (10^{-18} of the total step) to reduce the risk of numerical instability and early termination of the analysis. The analysis was limited to 5000 increments.

The same steps discussed in the section on applied displacement were followed. Initially, analyses were performed using two-dimensional planar models without stabilization or viscous regularization. For the default value $reltol=0.2$, the load increase stopped after reaching the critical point, but the analysis terminated immediately (solid green line) due to convergence problems as shown in Figure 39. The release tolerance was not increased as suggested by the ABAQUS® error in the message (.msg) file. Previous analysis had shown that, by increasing the release tolerance ($reltol>0.2$), termination of the analysis could be avoided. However, the results had not been in good agreement with the benchmark [3,4]. Therefore, additional stabilization had to be introduced in order to obtain agreement with the benchmark case.

The results computed when contact stabilization (cs) was added are plotted in Figure 40. A small stabilization factor ($cs=1 \times 10^{-6}$) was used for all cases since it had yielded good results in previous analyses [3, 4]. Initially, the release tolerance value was set at the default value ($reltol=0.2$) (solid green line). For this parameter combination, the load increased up to the critical point, and delamination propagation started while the load remained constant (solid green line). Also for the stable propagation path, the result was in good agreement with the benchmark result (solid grey line). Then, the release tolerance was reduced to $reltol=0.1$ (solid blue line) and further to $reltol=0.01$ (solid red line). For all cases, the results were in good agreement with the benchmark results over the entire load/displacement range.

An alternative way to plot the benchmark is shown in Figure 41 where the applied load P is plotted versus the increase in delamination length a^* . This way of presenting the results may be of advantage for large structures where local delamination propagation may have little effect on the global stiffness of the structure and may therefore not be visible in a global load/displacement plot. However, extracting the delamination length a from the finite element results required more manual, time consuming, post-processing of the results compared to the relatively simple and readily available output of nodal displacements and forces. The results plotted in Figure 41 are the same as those that were discussed above and were shown as global load/displacement plots in Figure 40. The conclusions that can be drawn from the plots in Figure 41 are identical to those discussed in the above for Figure 40.

A result obtained from a three-dimensional model is shown in Figures 42. Based on the results from two-dimensional planar models shown above, contact stabilization was added to help overcome convergence issues. A release tolerance value ($reltol=0.1$) was used which had yielded good results previously. The load/displacement result computed when a small stabilization factor ($cs=1 \times 10^{-6}$) was added is plotted in Figure 42. The load increase stopped and delamination propagation started (solid blue line) shortly before reaching the critical point of the benchmark solution (solid grey line). As mentioned earlier, deviation from the benchmark may be explained by the fact that the benchmark results were created using two-dimensional planar finite element models of the MMB specimen. As shown in Figure 29, the three-dimensional models yield a failure index which is somewhat higher across the entire width than the results from two-dimensional planar finite element models. Therefore, delamination propagation is expected to start prior to the benchmark results obtained from two-dimensional planar finite element analysis, which ultimately leads to a shift of the entire results plot towards lower loads.

5.4 Results from automated delamination propagation analysis for 80% mode II

5.4.1 Computed delamination propagation for applied displacement

As discussed above, the propagation analysis was performed in two steps using the models shown in Figures 4b and 6b starting from an initial delamination length, $a_0=25.4$ mm. In the first step, a displacement of $w=1.5$ mm was applied which nearly equaled the critical displacement, $w_{crit}=1.65$ mm, determined earlier. In the second step, the applied displacement was increased to $w=8.0$ mm. For this second step, automatic incrementation was used in ABAQUS[®] and a small increment size (0.5% of the total step) was chosen at the beginning of the step. To reduce the risk of numerical instability and early termination of the analysis, a minimum allowed increment size (10^{-18} of the total step) was also chosen. The analysis was limited to 5000 increments.

Initially, analyses were performed using two-dimensional planar models (shown in Figure 4a) without stabilization or viscous regularization. Using the default value $reltol=0.2$, the load and displacement exceeded the critical point and the analysis terminated (solid green line) as shown in

Figure 43 where the computed resultant force (load P) is plotted versus the applied displacement w . By increasing the release tolerance to $reltol=0.5$, – as suggested by the ABAQUS® error in the message (.msg) file – it was possible to extend the analysis without an error message until the load drop occurred and delamination propagation started as shown in Figure 43, (solid light blue line). However, the load drop occurred past the critical point and the analysis terminated soon afterwards due to convergence problems. The release tolerance was not increased any further as suggested in the ABAQUS® error in the message (.msg) file. Previous analysis had shown that by increasing the release tolerance ($reltol>0.2$), termination of the analysis could be avoided, however, the results had not been in good agreement with the benchmark [3,4]. Therefore, it was decided to introduce additional stabilization to obtain better agreement with the benchmark case.

The results computed when contact stabilization (cs) was added are plotted in Figure 44. A small stabilization factor ($cs=1 \times 10^{-6}$) was used for all cases since it had yielded good results in previous analyses [3, 4]. Initially, the release tolerance value was set at the default value ($reltol=0.2$) (solid green line). For this parameter combination, the load increased past the critical point and delamination propagation started while the load dropped (solid green line). The load/displacement path then ran parallel to the constant displacement branch of the benchmark result and later followed the stable propagation branch of the benchmark result. To reduce the observed overshoot, the release tolerance was reduced. For a stabilization factor of $cs=1 \times 10^{-6}$ and release tolerance $reltol=0.1$ (solid blue line), the overshoot was reduced, and the computed load/displacement path then ran closer to the constant displacement branch of the benchmark result. However, just before reaching the minimum load, the displacement increased slightly followed by a small load drop. The results then followed the stable propagation branch of the benchmark result. Further reducing the release tolerance ($reltol=0.01$) yielded results that were in excellent agreement with the benchmark (solid red line). Due to the fine mesh, only a small saw-tooth pattern was observed along the stable path.

An alternative way to plot the benchmark is shown in Figure 45 where the applied displacement w is plotted versus the increase in delamination length a^* . The results plotted in Figure 45 are the examples that were discussed above and were shown in the global load/displacement plots of Figure 44. The conclusions that can be drawn from this plot are identical to those discussed above.

The result obtained from a three-dimensional analysis is shown in Figure 46. Based on the results from two-dimensional planar models shown above, contact stabilization was added to the analysis to help overcome convergence issues. Since the computer time increases with tighter release tolerances, i.e. smaller release tolerance values, first a release tolerance value ($reltol=0.1$) was selected. The result (solid blue line) computed for a release tolerance value ($reltol=0.1$) and a small stabilization factor ($cs=1 \times 10^{-6}$) are plotted in Figure 46. The load dropped and delamination propagation started upon reaching the critical point of the benchmark solution (solid grey circles and solid grey line). The load/displacement path then ran parallel to the benchmark result but was shifted slightly towards lower loads. The analysis was stopped after 6.81×10^5 CPU seconds (7.9 days). To improve the results, the release tolerance value was set to $reltol=0.01$. The results (solid red line) are practically identical to the results obtained for $reltol=0.01$, however the computation time increased and the analysis was stopped after 1.97×10^6 CPU seconds (22.8 days). Deviation from the benchmark may be explained by the fact that the benchmark results were created using two-dimensional planar finite element models of the MMB specimen. As shown in Figure 29, the three-dimensional models yield a failure index, which is somewhat higher across the entire width than the results from two-dimensional planar finite element models. Therefore, delamination propagation is expected to start prior to the benchmark results obtained from two-dimensional

planar finite element analysis, which ultimately leads to a shift of the entire results plot towards lower loads. The current results for 80% mode II resemble the results obtained from the analysis of the ENF specimen (pure mode II) [4].

5.4.2 Computed delamination propagation for applied quasi-static load

The propagation analysis was performed in two steps using the models shown in Figures 4b and 6b starting from an initial delamination length, $a_0=25.4$ mm. In the first step, a load $P=730$ N was applied which equaled nearly the critical load, $P_{crit}=751$ N, determined earlier. In the second step, the total load was increased ($P=1000$ N). Automatic incrementation was used with a small increment size at the beginning (0.5% of the total step) and a very small minimum allowed increment (10^{-18} of the total step) to reduce the risk of numerical instability and early termination of the analysis. The analysis was limited to 5000 increments.

The same steps discussed in the section on applied displacement were followed. Initially, analyses were performed using two-dimensional planar models without stabilization or viscous regularization. Using the default value ($reltol=0.2$), the load increase stopped after reaching the critical point, but the analysis terminated immediately (solid green line) due to convergence problems, as shown in Figure 47. The release tolerance was not increased as suggested by the ABAQUS® error in the message (.msg) file. Previous analysis had shown that by increasing the release tolerance ($reltol>0.2$), termination of the analysis could be avoided, however, the results had not been in good agreement with the benchmark [3,4]. Therefore, it was decided to introduce additional stabilization to obtain better agreement with the benchmark case.

The results computed when contact stabilization (cs) was added are plotted in Figure 48. A small stabilization factor ($cs=1 \times 10^{-6}$) was used for all cases since it had yielded good results in previous analyses [3, 4]. Initially, the release tolerance value was set at the default value ($reltol=0.2$) (solid green line). For this parameter combination, the load increased up to the critical point and delamination propagation started while the load remained constant (solid green line). Also for the stable propagation path, the result was in good agreement with the benchmark result (solid grey line). Then, the release tolerance was reduced to $reltol=0.1$ (solid blue line) and further to $reltol=0.01$ (solid red line). For all cases, the results were in good agreement with the benchmark results over the entire load/displacement range.

An alternative way to plot the benchmark is shown in Figure 49 where the applied load P is plotted versus the increase in delamination length a^* . This way of presenting the results may be of advantage for large structures where local delamination propagation may have little effect on the global stiffness of the structure and may therefore not be visible in a global load/displacement plot. The results plotted in Figure 49 are the same as those that were discussed above and were shown as global load/displacement plots in Figure 48. The conclusions that can be drawn from the plots in Figure 49 are identical to those discussed in the above for Figure 48.

A result obtained from a three-dimensional model is shown in Figures 50. Based on the results from two-dimensional planar models shown above, contact stabilization was added to help overcome convergence issues. Since the computer time increases with tighter release tolerances, i.e. smaller release tolerance values, first a release tolerance value $reltol=0.1$ was selected. The result (solid blue line) computed for a release tolerance value ($reltol=0.1$) and a small stabilization factor ($cs=1 \times 10^{-6}$) are plotted in Figure 50. The load increase stopped (solid blue line) and delamination propagation started shortly before reaching the critical point of the benchmark solution (solid grey line). The load/displacement path then ran parallel to the benchmark result but was shifted slightly towards lower loads. To improve the results, the release tolerance value was set to $reltol=0.01$. The

results (solid red line) are practically identical to the results obtained for $reltol=0.1$, however the computational time increased. As discussed earlier, deviation from the benchmark may be explained by the fact that the benchmark results were created using two-dimensional planar finite element models of the MMB specimen. As shown in Figure 29, the three-dimensional models yield a failure index which is somewhat higher across the entire width than the results from two-dimensional planar finite element models. Therefore, delamination propagation is expected to start prior to the benchmark results obtained from two-dimensional planar finite element analysis, which ultimately leads to a shift of the entire results plot towards lower loads. The current results for 80% mode II resemble the results obtained from the analysis of the ENF specimen (pure mode II) [4].

The results from above were plotted for three distinct locations across the width of the specimen (two edges and center as shown later in Figure 56) as shown in Figure 51, where the applied load P is plotted versus the increase in delamination length a^* . This way of presenting the results is shown since it may be of advantage for large structures where local delamination propagation may have little effect on the global stiffness of the structure, and may therefore not be visible in a global load/displacement plot. However, extracting the delamination length a from finite element results required more manual, time consuming post-processing of the results - especially for the three-dimensional models - compared to the relatively simple and readily available output of nodal displacements and forces.

Initially during the unstable growth phase, the results for both simulations ($reltol=0.1$, $cs=1 \times 10^{-6}$ solid lines and $reltol=0.01$, $cs=1 \times 10^{-6}$ dashed lines) and all three locations (green line for edge 1, blue line for center location and red line for edge 2) were practically identical. All the result curves ran parallel to the benchmark result (solid grey line) but were shifted slightly towards lower loads. The unstable phase, however created longer delaminations compared to the benchmark result. For the stable path of delamination propagation, small differences can be observed between the two simulations (solid versus dashed lines). In this respect, more detailed information about the propagation can be obtained from the plot where the applied load is plotted versus the increase in delamination length than from the traditional load/displacement plot. The current results for 80% mode II resemble the results obtained from the analysis of the ENF specimen (pure mode II) [4].

5.5 Computed delamination front shape

Besides matching the load displacement behavior of benchmark results, a delamination propagation analysis should also yield a delamination front shape that is representative of the actual failure. An example of delamination front shapes observed by opening tested MMB specimens are shown in Figure 52 [7]. From the initial straight delamination front, which is formed by the edge of the polytetrafluoroethylene (PTFE) insert, the delamination develops into a curved thumbnail shaped front (blue line) as shown in Figure 52a for 20% mode II. The front is similar to fronts observed in the mode I DCB specimen [3]. A pronounced thumbnail shaped front is observed for the pre-cracks (red line) shown in Figures 52 b and c for 50% and 80% mode II, respectively. The final front (blue line) exhibits less curvature as would be expected from the increased mode II contribution. The fronts are somewhat jagged, suggesting that growth happens in one location then stops and continues at another location across the width. On average, however, the delaminations appear to grow uniformly across the width.

A straight front across almost the entire width of the specimen is to be expected when looking at the failure index distribution plotted in Figure 29. However, due to the drop of the failure index near the edges, delamination propagation is expected to locally lag behind and turn the initially straight front into a thumbnail front for $G_{II}/G_T=0.2$ and 0.5 similar to fronts observed in a Double Cantilever

Beam (DCB) specimen. For $G_{II}/G_T = 0.8$, the drop of the failure index near the edges is less pronounced, and a straight front across the entire width is expected.

Delamination propagation computed using the model with a uniform mesh across the width (Figure 5) is shown in Figure 53 for $G_{II}/G_T = 0.2$. Plotted on the bottom surface (defined in Figure 5) are the contours of the bond state, where the delaminated section appears in blue and the intact (bonded) section in red. The transition between the colors (in green/yellow) indicates the location of the delamination front. The initial straight front is shown in Figure 53a and was added for clarification in Figures 53d and e. The first propagation was observed towards the edges of the specimen (Figure 53b) as expected from the distribution of the failure index (Figure 29) where two local maxima are observed at $y/B \pm 0.33$. Then, as expected, the front advanced more in the center and lagged behind at the edges as shown in Figure 53c. Later in the analysis, the delamination continued to propagate through the entire specimen basically as a straight front as shown in Figures 53d and 53e. Locally however, always one element at each edge lagged behind as shown in Figures 53c and 53d. After the shape stabilized, new propagation usually started in the center first as shown in Figure 53e, the exact location being determined by the maximum of the failure index distribution across the width.

Delamination fronts computed using the model with a uniform mesh across the width (Figure 5) are shown in Figures 54 and 55 for $G_{II}/G_T = 0.5$. For the case of applied displacement, w , the propagation was observed first in the center section of the specimen (Figure 54a) rather than at the location of the two local maxima in the failure index distribution (Figure 29) observed at $y/B \pm 0.33$. Then, the front advanced across the entire width but lagged behind at the edges as shown in Figure 54b. Later, the delamination propagated across the width of the specimen as a straight front shape with only one element at each edge lagging behind as shown in Figure 54c. The final front as shown in Figure 54d, appeared jagged locally but on average moved forward as a straight front across the entire width, which may be explained by the increase in mode II for longer delamination lengths (increased G_{II}/G_T as shown in Figure 25). Delaminations under pure mode II generally exhibit straight fronts [4,10]. For the case of applied load, P , the propagation was observed first in the center section of the specimen (Figure 55a). Then, the front advanced across the entire width but lagged behind at the edges as shown in Figure 55b. Later, the delamination appeared jagged locally but on average moved forward as a straight front across the entire width as shown in Figures 55c and 55d, which may again be explained by the increase in mode II for longer delamination lengths (increased G_{II}/G_T as shown in Figure 25).

Delamination propagation computed using the model with a uniform mesh across the width (Figure 5) is shown in Figure 56 for $G_{II}/G_T = 0.8$. The initial straight front is shown in Figure 56a and 56b and was added for clarification in Figures 56d and 56e. The first propagation was observed towards the edges of the specimen (Figure 56c) as expected from the distribution of the failure index (Figure 29) where two local maxima are observed at $y/B \pm 0.33$. Then, the delamination appeared jagged locally but on average moved forward as a straight front across the entire width as shown in Figures 56d, which may be explained by the already high mode II ratio ($G_{II}/G_T = 0.8$) for this configuration. The front remained jagged until the end of the analysis as shown in Figure 56e. The current results for 80% mode II resemble the results obtained from the analysis of the ENF specimen (pure mode II) [4].

Computed delamination fronts obtained from three-dimensional solid models generally matched the experimentally observed shapes shown in Figure 52. Improved results may be obtained by refining the mesh across the width.

6. SUMMARY AND CONCLUSIONS

The development of benchmark examples, which allow the assessment of the static delamination propagation prediction capabilities was presented and demonstrated for ABAQUS[®] Standard. The examples are based on finite element models of the mixed-mode I/II Mixed-Mode Bending (MMB) specimen. The models are independent of the analysis software used and allow the assessment of the automated delamination growth prediction capabilities in commercial finite element codes based on the virtual crack closure technique (VCCT).

First, quasi-static benchmark results were created based on the approach developed in reference 3. Two-dimensional finite element models were used for simulating the MMB specimens with different mixed-mode ratio (20%, 50% and 80% mode II) and different initial delamination lengths, a_0 . For each delamination length modeled, the load and displacements were monitored. The mixed-mode I/II strain energy release rate was calculated for a fixed applied displacement. It was assumed that the delamination propagated when the total strain energy release rate reached the fracture toughness value. Thus, critical loads and critical displacements for delamination propagation were calculated for each initial delamination length modeled. From these critical load/displacement results, benchmark solutions were created. It was assumed that the load/displacement relationship computed during automatic propagation should closely match the benchmark cases.

After creating the benchmark cases, the approach was demonstrated for the commercial finite element code ABAQUS[®]. Starting from an initially straight front, the delamination was allowed to propagate under quasi-static loading based on the algorithms implemented into the software. Input control parameters were varied to study the effect on the computed delamination propagation and growth.

The results showed the following:

- The benchmarking procedure proved valuable by highlighting the issues associated with choosing the input parameters of the particular implementation.
- In general, good agreement between the results obtained from the automated propagation analysis and the benchmark results could be achieved by selecting input parameters that had previously been determined during analyses of mode I Double Cantilever Beam and mode II End Notched Flexure specimens.
- In particular, the results for automated delamination propagation analysis under quasi-static loading showed the following:
 - Using the default release tolerance ($reltol=0.2$) as suggested in the ABAQUS[®] handbook or increasing the value, as suggested in the user's manual, may help to overcome convergence problems, however, it leads to an undesired overshoot of the computed result compared to the benchmark.
 - A combination of release tolerance and contact stabilization is required to obtain more accurate results.
 - A gradual reduction of the release tolerance and contact stabilization over several analyses is suggested.
 - Good agreement between analysis results and the benchmarks could be achieved for release tolerance values ($reltol<0.1$) in combination with contact stabilization ($cs=1 \times 10^{-6}$).
 - Computed delamination fronts obtained from three-dimensional solid models generally matched the experimentally observed shapes. Improved results may be obtained by refining the mesh across the width.

- The analyses for three-dimensional models of a simple MMB specimen required several days of computation time. Improvements to the implementation are required to make analysis of larger structural components computationally affordable.

Overall, the results are promising and the current findings concur with previously published conclusions [3,4,5]. However, further assessment for mixed-mode delamination fatigue onset and growth is required. Additional studies should also include the assessment of the propagation capabilities in more complex mixed-mode specimens and on a structural level.

Assessing the implementation in one particular finite element code illustrated the value of establishing benchmark solutions since each code requires specific input parameters unique to its implementation. Once the parameters have been identified, they may then be used as a starting point to model delamination growth for more complex configurations.

ACKNOWLEDGEMENTS

This research was supported by the Subsonic Rotary Wing Project as part of NASA's Fundamental Aeronautics Program.

The analyses were performed at the Durability, Damage Tolerance and Reliability Branch at NASA Langley Research Center, Hampton, Virginia, USA.

REFERENCES

1. E. F. Rybicki and M. F. Kanninen, "A Finite Element Calculation of Stress Intensity Factors by a Modified Crack Closure Integral," *Eng. Fracture Mech.*, Vol. 9, pp. 931-938, 1977.
2. R. Krueger, "Virtual Crack Closure Technique: History, Approach and Applications," *Applied Mechanics Reviews*, Vol. 57, pp. 109-143, 2004.
3. R. Krueger, "An Approach to Assess Delamination Propagation Simulation Capabilities in Commercial Finite Element Codes," NASA/TM-2008-215123, 2008.
4. R. Krueger, "Development and Application of Benchmark Examples for Mode II Static Delamination Propagation and Fatigue Growth Predictions," NASA/CR-2011-217305, NIA report no. 2011-02, 2011.
5. A. C. Orifici and R. Krueger, "Assessment of Static Delamination Propagation Capabilities in Commercial Finite Element Codes Using Benchmark Analysis," NASA/CR-2010-216709, NIA report no. 2010-03, 2010.
6. R. Krueger, "Development of a Benchmark Example for Delamination Fatigue Growth Prediction," NASA/CR-2010-216723, NIA report no. 2010-04, 2010.
7. J. G. Ratcliffe, personal communication.
8. I. S. Raju and T. K. O'Brien, "Fracture Mechanics Concepts, Stress Fields, Strain Energy Release Rates, Delamination and Growth Criteria," in *Delamination Behavior of Composites*, S. Sridharan, Ed.: Woodhead Publishing in Materials, 2008.
9. "Composite Fatigue Damage Onset," in *Composite Materials Handbook CMH-17*, Vol. 3, Section 12.6.4, draft of revision G, 2009.
10. T. K. O'Brien, W. M. Johnston, and G. Toland, "Mode II Interlaminar Fracture Toughness and Fatigue Characterization of a Graphite Epoxy Composite Material," NASA/TM-2010-216838, 2010.
11. G. B. Murri, personal communication.
12. M. L. Benzeggagh and M. Kenane, "Measurement of Mixed-Mode Delamination Fracture Toughness of Unidirectional Glass/Epoxy Composites with Mixed-Mode Bending Apparatus," *Composites Science and Technology*, Vol. 56, pp. 439-449, 1996.
13. KaleidaGraph: Version 4.1, 2009.
14. *Abaqus Analysis User's Manual*, ABAQUS® Standard, Version 6.10, DSS Simulia, 2010.
15. *Abaqus Theory Manual*, ABAQUS® Standard, Version 6.10, DSS Simulia, 2010.
16. D. Broek, *The Practical Use of Fracture Mechanics*, Kluwer Academic Publishers, 1991.

TABLE I. MATERIAL PROPERTIES [4].

Unidirectional Graphite/Epoxy Prepreg		
$E_{11} = 161 \text{ GPa}$	$E_{22} = 11.38 \text{ GPa}$	$E_{33} = 11.38 \text{ GPa}$
$\nu_{12} = 0.32$	$\nu_{13} = 0.32$	$\nu_{23} = 0.45$
$G_{12} = 5.2 \text{ GPa}$	$G_{13} = 5.2 \text{ GPa}$	$G_{23} = 3.9 \text{ GPa}$

The material properties are given with reference to the ply coordinate axes where index 11 denotes the ply principal axis that coincides with the direction of maximum in-plane Young's modulus (fiber direction). Index 22 denotes the direction transverse to the fiber in the plane of the lamina and index 33 the direction perpendicular to the plane of the lamina.

TABLE II. FRACTURE PARAMETERS.

Fracture Toughness Data [7,10,11] – Figures 2, A1		
$G_{Ic} = 0.212 \text{ kJ/m}^2$	$G_{IIc} = G_{IIIc} = 0.774 \text{ kJ/m}^2$	$\eta = 2.1$

APPENDIX

Delamination propagation analysis in ABAQUS®

Delamination propagation at the interfaces in laminated composites can be simulated in ABAQUS® [14]. The interface along which the delamination (or crack) propagates must be indicated in the model using a fracture criterion definition. The fracture energy release rates at the crack tips in the interface elements are calculated based on the virtual crack closure technique (VCCT) [14,15].

Required input for ABAQUS®

The input required to perform a delamination propagation analysis under quasi-static load in ABAQUS® Standard is discussed in the following paragraphs. It is assumed that the reader is familiar with ABAQUS® Standard and the syntax used in the input file (.inp). The focus is therefore on the specific input that relates to delamination propagation in ABAQUS®. An example input file is given at the end of this appendix to provide an overview of an entire analysis and assist the readers in creating their own analyses.

Input for delamination propagation

The interface along which the delamination (or crack) propagates must be indicated in the model using a fracture criterion definition:

```
*DEBOND, SLAVE=VCCT_TOP, MASTER=VCCT_BOT, FREQ=1  
*FRACTURE CRITERION, TYPE=VCCT, MIXED MODE BEHAVIOR=BK, TOLERANCE=<reltol>  
  <GIc>, <GIIc>, <GIIIc>, <eta>  
*CONTACT CONTROLS, STABILIZE, MASTER=VCCT_BOT, SLAVE=VCCT_TOP  
  1.E-06, 0, 0.1
```

where **VCCT_TOP** and **VCCT_BOT** are interface surfaces as shown in Figure A1, and **<reltol>** is the release tolerance within which the crack propagation criterion must be satisfied. The critical energy release rates **<GIc>**, **<GIIc>**, **<GIIIc>** and the curve fit parameter **<eta>** are obtained from the mixed-mode failure criterion as shown in Figure A2. A quasi-static mixed-mode fracture criterion is determined for a material by plotting the interlaminar fracture toughness, G_c , versus the mixed-mode ratio, G_{II}/G_T as discussed earlier and shown in Figure A2. The input for contact stabilization is provided in the contact controls definition.

Example input files

An input file is given to provide an overview of an entire analysis and assist the readers in creating their own analyses. The analysis was divided into two steps. In the first step, a displacement just below the critical value, w_{crit} , was applied to avoid delamination propagation in this step. Thus, large increments could be used to get up to the critical point. In the second step, the final desired displacement was defined. Automatic incrementation was used with a small increment size at the beginning (0.5% of the total step) and a very small minimum allowed increment (10^{-18} of the total step) to reduce the risk of numerical instability and early termination of the analysis. The analysis was limited to 5000 increments.

For all analyses, the input to define the fracture criterion (**<GIc>**, **<GIIc>**, **<GIIIc>**, **<eta>**), were kept constant. The ABAQUS® keywords shown in **bold type** were discussed in detail in the previous paragraphs.

Input file for fatigue onset and growth analysis

***HEADING**

```
MMB-UD-IM7/8552, a=30 mm, ratio=0.2
units: mm, N, MPa
*** elements, nodes, material, etc
*ELEMENT, TYPE=CPE4I    , ELSET=EALL
...
...
*NSET, NSET=BONDED, GENERATE
    1069, 1533,    8
**
**** surface and contact definition ****
*SURFACE, TYPE=ELEMENT, NAME=VCCT_BOT
EL_BOT, S3
*SURFACE, TYPE=ELEMENT, NAME=VCCT_TOP
EL_TOP, S1
*INITIAL CONDITION, TYPE=CONTACT
VCCT_TOP, VCCT_BOT, BONDED
*CONTACT PAIR, INTERACTION=VCCT, ADJUST=BONDED
VCCT_TOP, VCCT_BOT
**** VCCT -- STAGE I ****
*SURFACE INTERACTION, NAME=VCCT
    <width>
**** rigid elements to simulate MMB fixture
*** extra nodes for rigid elements
*NSET, NSET=MMBREF, UNSORTED
**** MMB fixture loading
    100006,
**
*NSET, NSET=NPIN, UNSORTED
**** MMB rollers
    100001,
**
*NODE, NSET=NFIXTURE
100001, 2.25, 152.399994, 0.
100002, 34., 152.399994, 0.
100003, 2.25, 102.000168, 0.
100004, 34., 102.000168, 0.
** ratio=0.2
100005, 34., 9.05, 0.,
100006, 3.25, 9.05, 0.,
** ratio=0.5
**100005, 34., 60.72, 0.,
**100006, 3.25, 60.72, 0.,
** ratio=0.8
**100005, 34., 74.75, 0.,
**100006, 3.25, 74.75, 0.,
*** rigid beam elements
*ELEMENT, TYPE=R2D2, ELSET=MMB_RIG
100001, 8, 100002
100002, 100002, 100004
**100003, 272, 100004
100003, 100003, 100004
100004, 100004, 100005
100005, 100005, 100006
```

```

*RIGID BODY, ELSET=MMB_RIG, REF NODE=MMBREF, PIN NSET=NPIN
**
** mode II loading
*EQUATION
2
616,1,1.0,100003,1,-1.0
**** VCCT input
*parameter
** fracture toughness:
  GIc = 0.212
  GIIc = 0.774
  GIIIc = 0.774
** B-K parameter:
  eta=2.1
** Damage and tolerance parameters
damv=0.0
reltol=0.01
** width in the plane stress/strain direction
  width =25.4
***
***** STEP 1 *****
*STEP, NLGEOM, INC=500
*STATIC
  0.1, 1., 0.000000001, 1.
**** MMB loading
*** applied displacement w for MMB, 2D-full model
*BOUNDARY
  100006, 1, 1, -1.5
**
*CONTROLS,PARAMETERS=TIME INCREMENTATION
  ,,,,,,50
*** fracture analysis using VCCT
*DEBOND,SLAVE=VCCT_TOP,MASTER=VCCT_BOT,FREQ=1
*FRACTURE CRITERION,TYPE=VCCT,MIXED MODE BEHAVIOR=BK, TOLERANCE=<reltol>
  <GIc>,<GIIc>,<GIIIc>,<eta>
**
***CONTACT CONTROLS, STABILIZE, MASTER=VCCT_BOT, SLAVE=VCCT_TOP
** 1.E-06, 0, 0.1
**
*OUTPUT, FIELD, VARIABLE=PRESELECT, FREQ=1
*CONTACT OUTPUT, MASTER=VCCT_BOT, SLAVE=VCCT_TOP
  dbt,dbsf,dbs,openbc,crsts,enrrt,efenrrtr,bdstat
**
*Output, history,VARIABLE=PRESELECT,freq=1
*NODE output,NSET=MMBREF
  RF1
*NODE output,NSET=MMBREF
  U1
***NODE output,NSET=NSUP
** RF1, RF2
***NODE output,NSET=NSUP
** U1, U2
*CONTACT OUTPUT, MASTER=VCCT_BOT, SLAVE=VCCT_TOP, NSET=BONDED
  enrrt
*END STEP
***** STEP 2 *****
*STEP, NLGEOM, INC= 5000

```

```

*STATIC
  0.00500000    ,    1.0000    ,    1.0000000E-18,    1.0
**** MMB loading
*** applied displacement w for MMB, 2D-full model
*BOUNDARY
  100006, 1, 1, -8.0
**
*CONTROLS,PARAMETERS=TIME INCREMENTATION
  ,,,,,,50
*CONTACT PRINT
*** fracture analysis using VCCT
**DEBOND,SLAVE=VCCT_TOP,MASTER=VCCT_BOT,FREQ=1
*DEBOND,SLAVE=VCCT_TOP,MASTER=VCCT_BOT,FREQ=1
*FRACTURE CRITERION,TYPE=VCCT,MIXED MODE BEHAVIOR=BK, TOLERANCE=<reltol>
  <GIc>,<GIIc>,<GIIIc>,<eta>
*CONTACT CONTROLS, STABILIZE, MASTER=VCCT_BOT, SLAVE=VCCT_TOP
  1.E-06, 0, 0.1
**
*OUTPUT, FIELD, VARIABLE=PRESELECT, FREQ=1
*CONTACT OUTPUT, MASTER=VCCT_BOT, SLAVE=VCCT_TOP
  dbt,dbsf,dbs,openbc,crsts,enrrt,efenrrtr,bdstat
*Output, history,VARIABLE=PRESELECT,freq=1
*NODE output,NSET=MMBREF
  RF1
*NODE output,NSET=MMBREF
  U1
*CONTACT OUTPUT, MASTER=VCCT_BOT, SLAVE=VCCT_TOP, NSET=BONDED
  enrrt
*END STEP

```

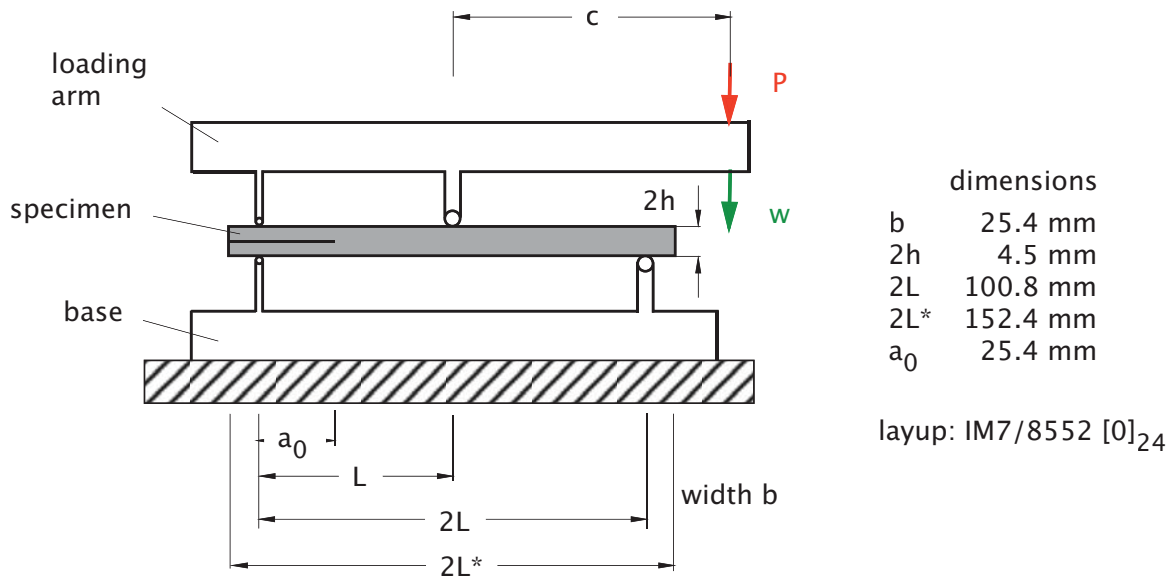


Figure 1. Mixed Mode Bending specimen (MMB) (dimensions from [7]).

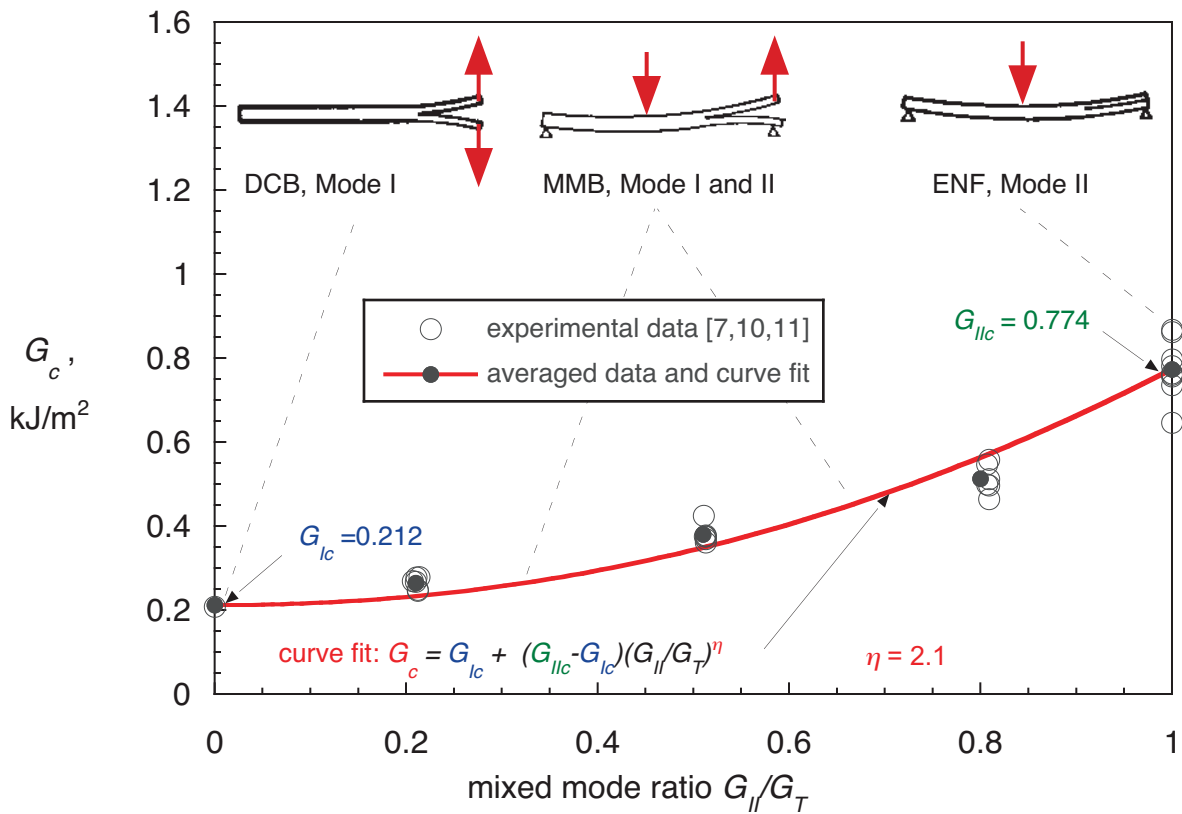
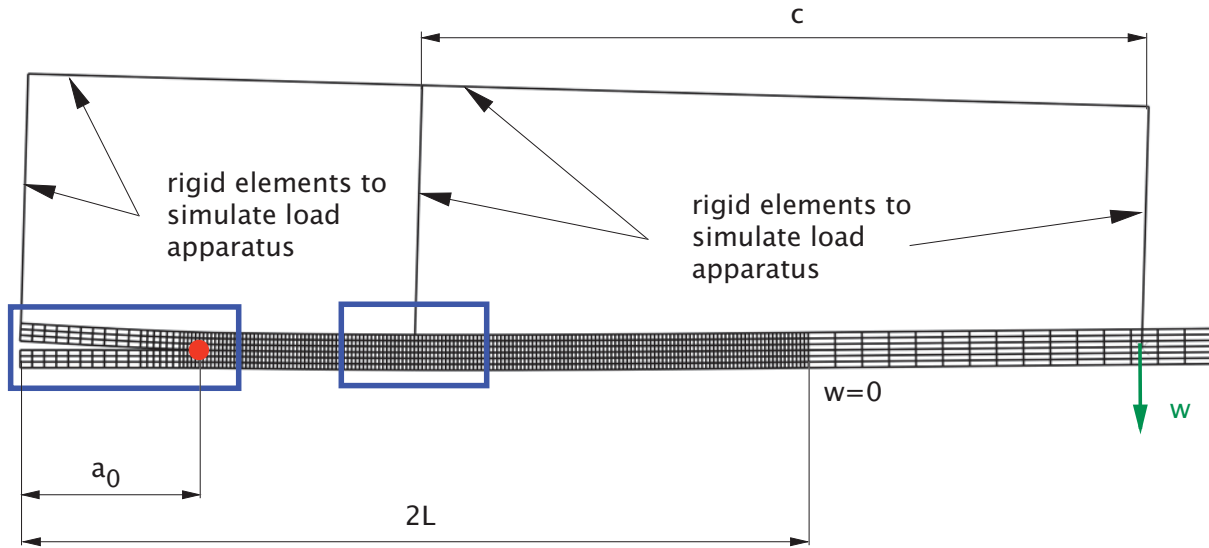
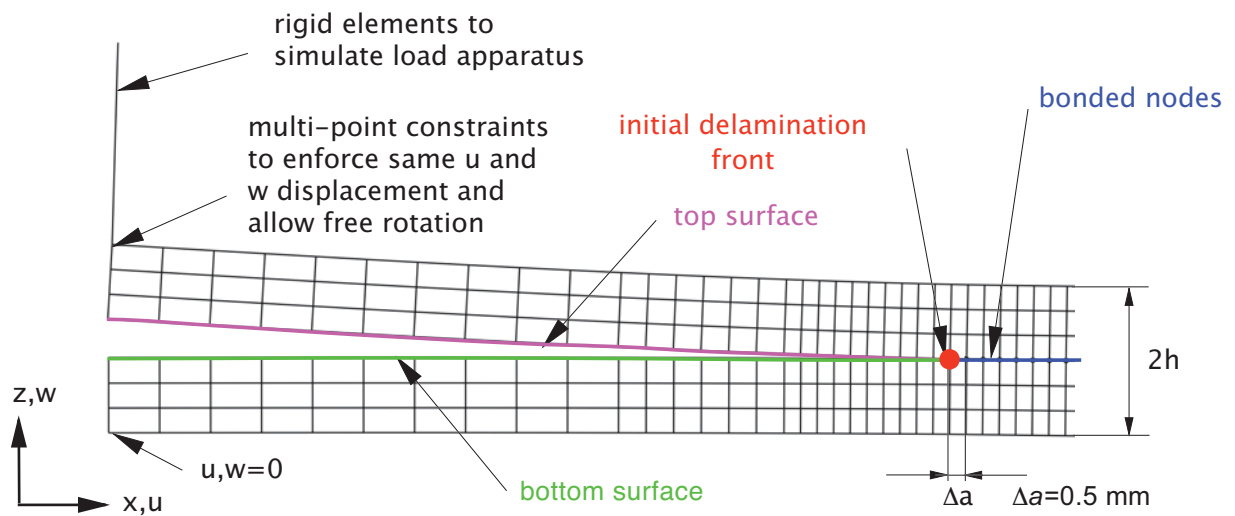


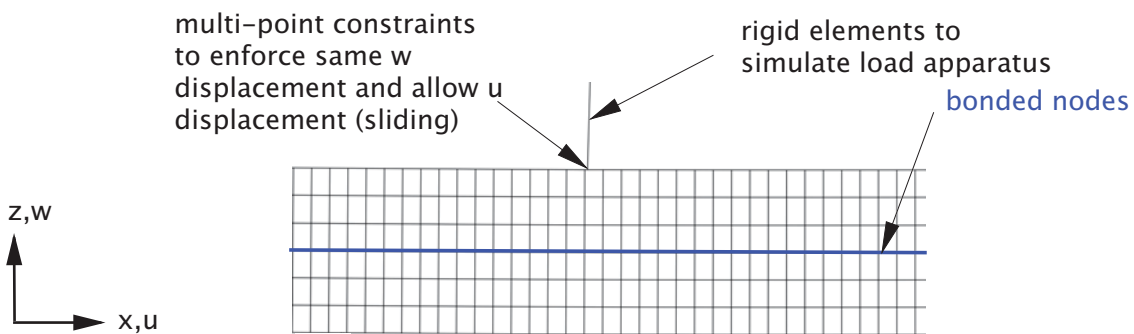
Figure 2. Mixed mode fracture criterion for IM7/8552.



(a). View of full model - $G_{II}/G_T=0.2$, $c=92.9$ mm.

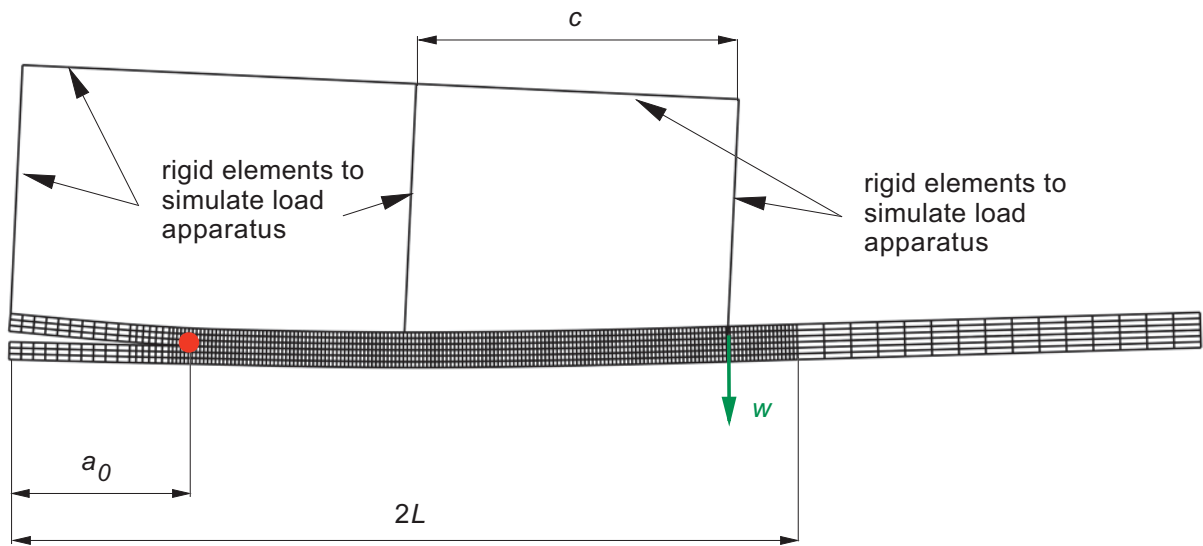


(b). Detail of specimen tip and crack tip zone.

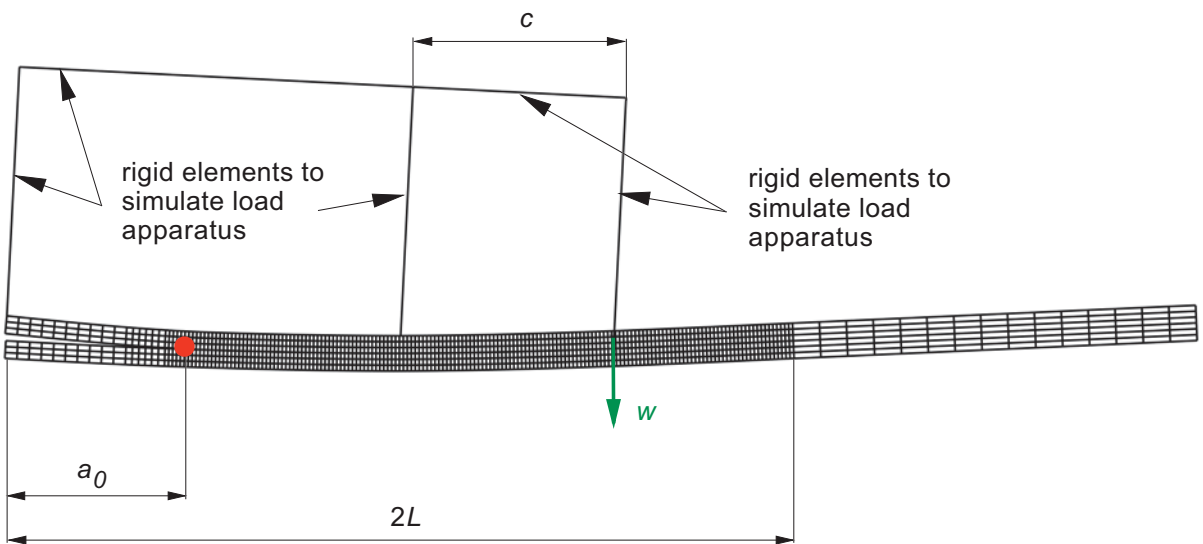


(c). Detail of load introduction zone.

Figure 3. Deformed 2D FE-model of a MMB specimen with mixed mode ratio $G_{II}/G_T=0.2$.

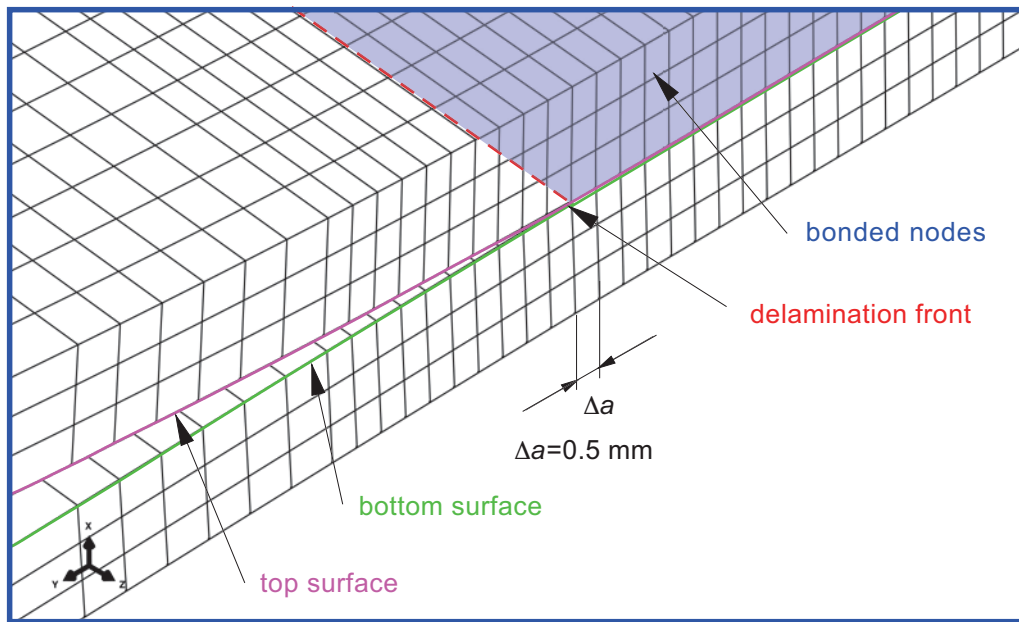
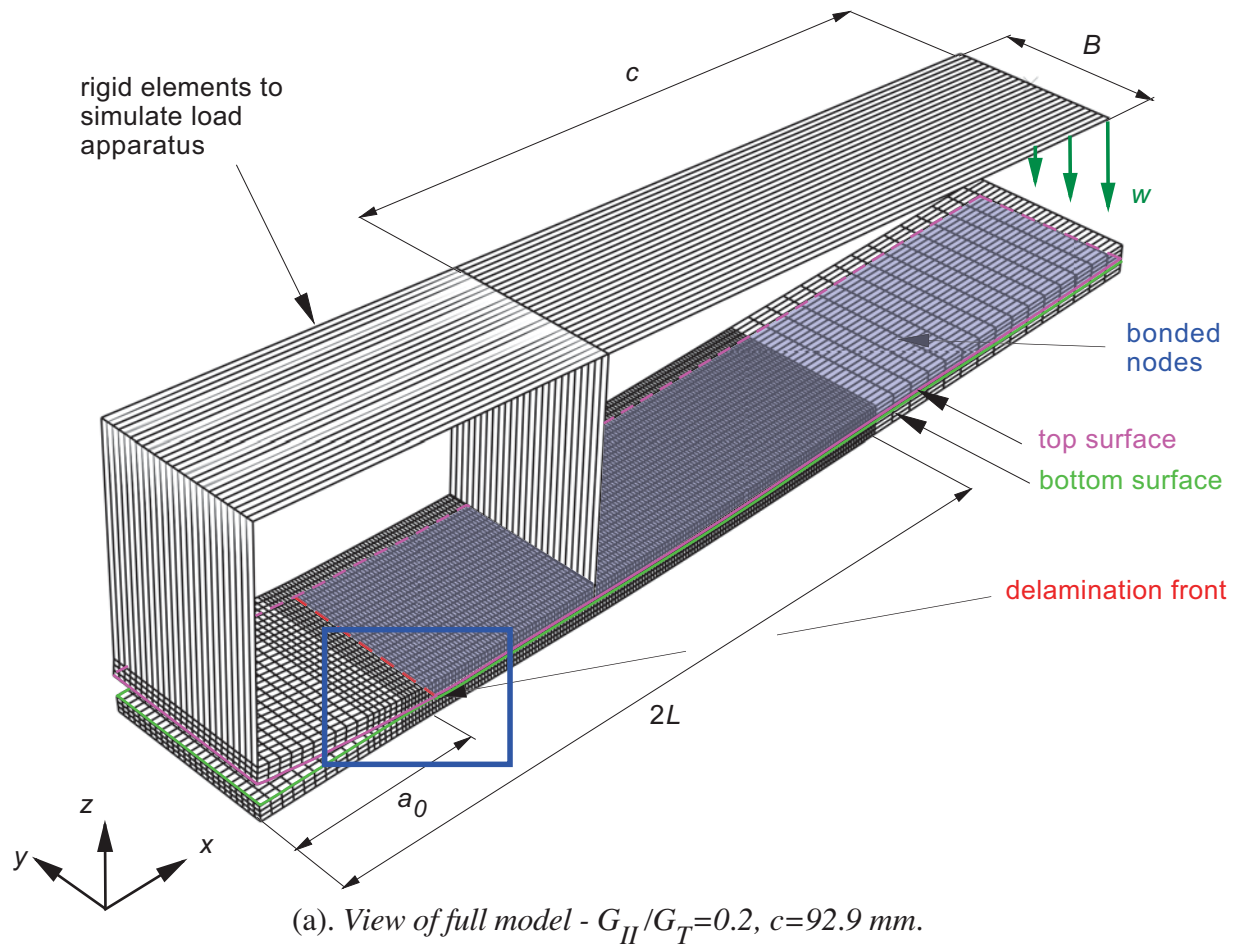


(a). Mixed mode ratio $G_{II}/G_T=0.5$, $c=41.3$ mm.



(b). Mixed mode ratio $G_{II}/G_T=0.8$, $c=27.3$ mm.

Figure 4. Deformed 2D FE models of MMB specimens with different mixed-mode ratios.



(b). Detail of specimen tip and crack tip zone.

Figure 5. Deformed 3D FE-model of a MMB specimen with mixed mode ratio $G_{II}/G_T=0.2$.

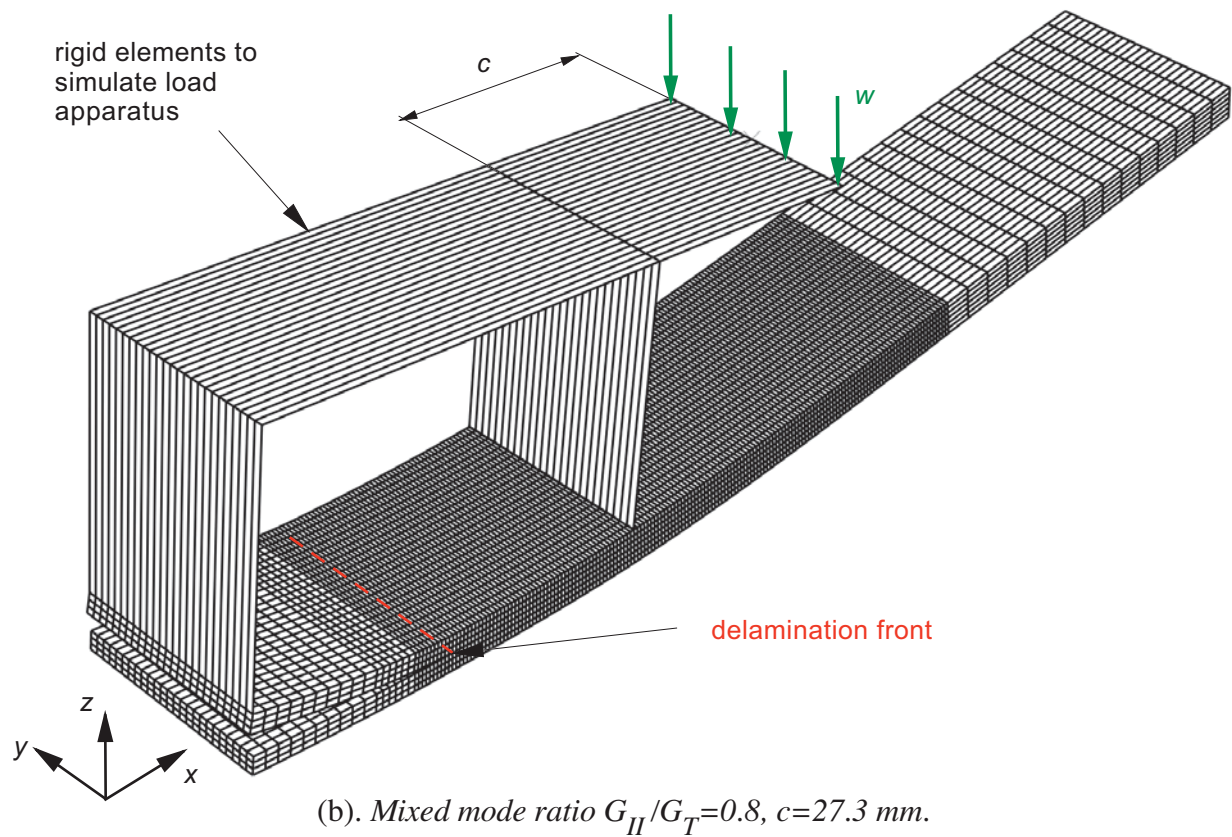
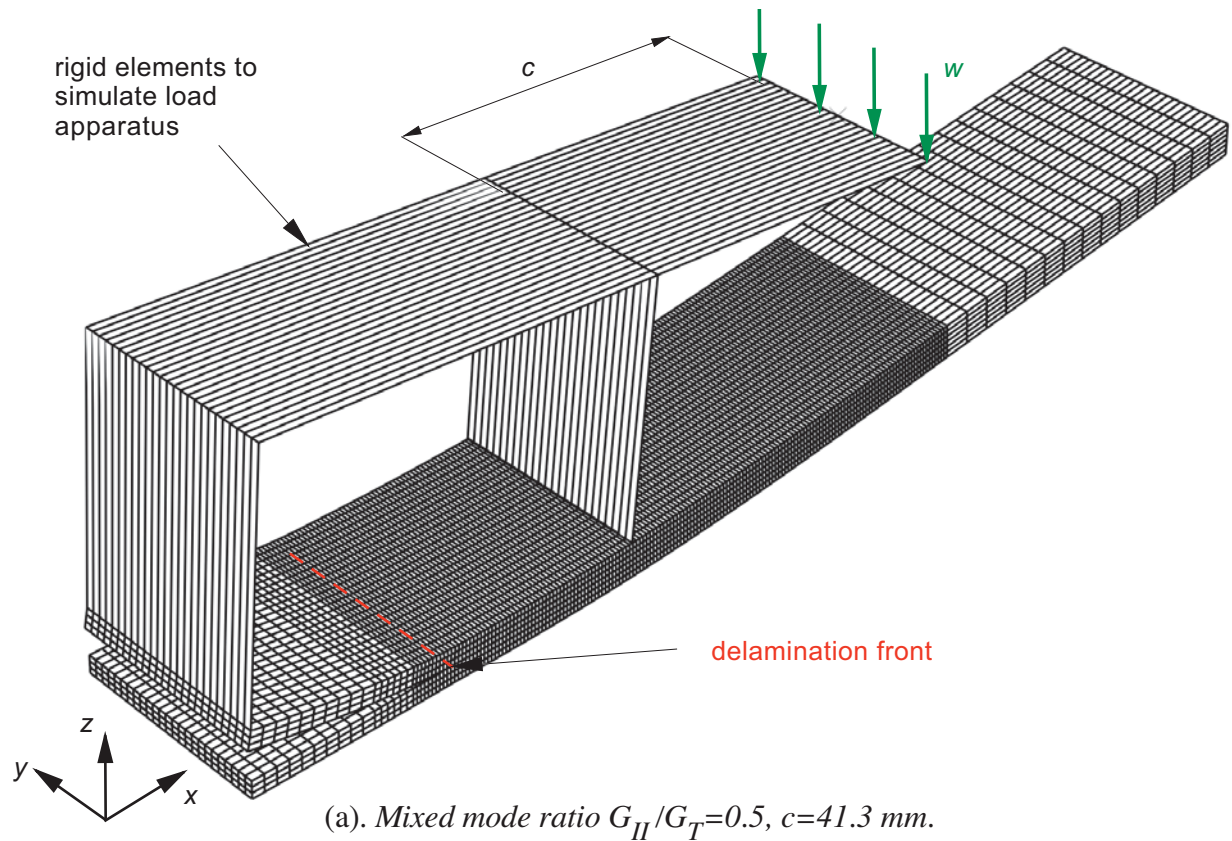


Figure 6. Deformed 3D FE-models of a MMB specimen with different mixed mode ratios.

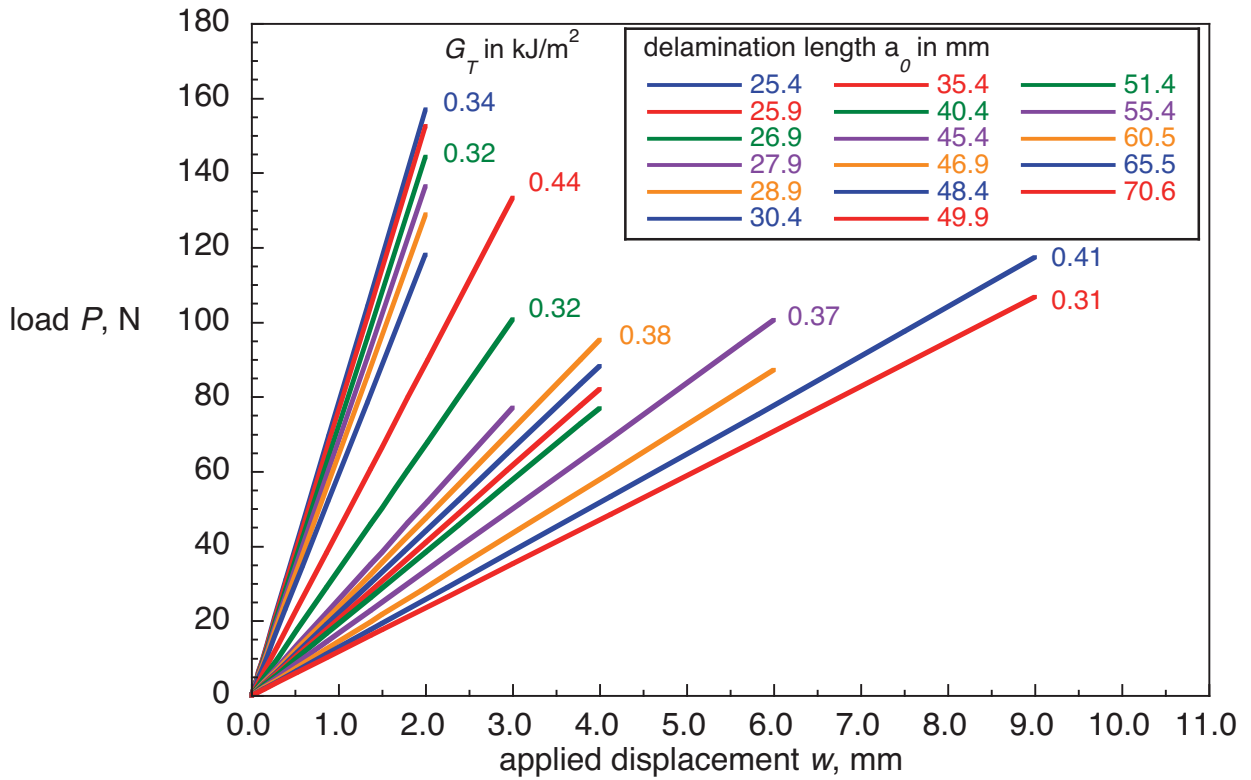


Figure 7. Load-displacement behavior for MMB specimens (20% mode II) with different delamination lengths a_0 .

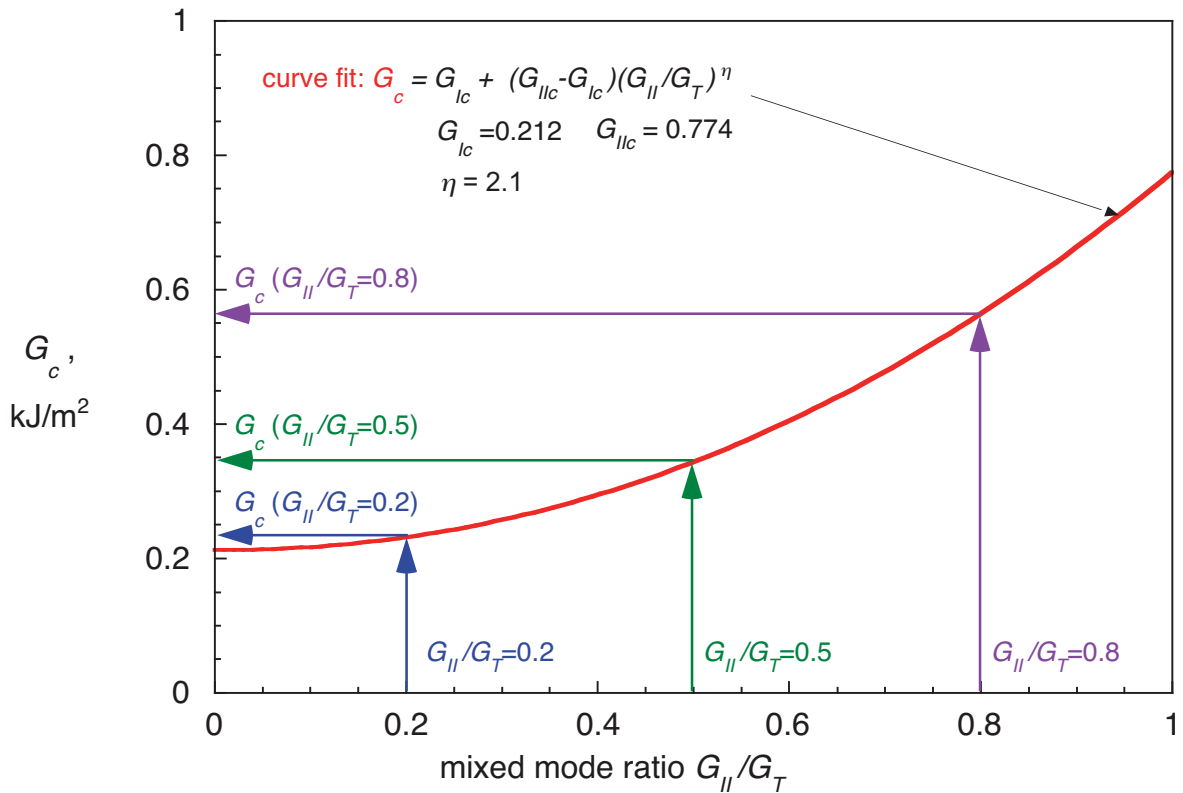


Figure 8. Use of mixed-mode fracture criterion to obtain G_c for different mode ratios G_{II}/G_T .

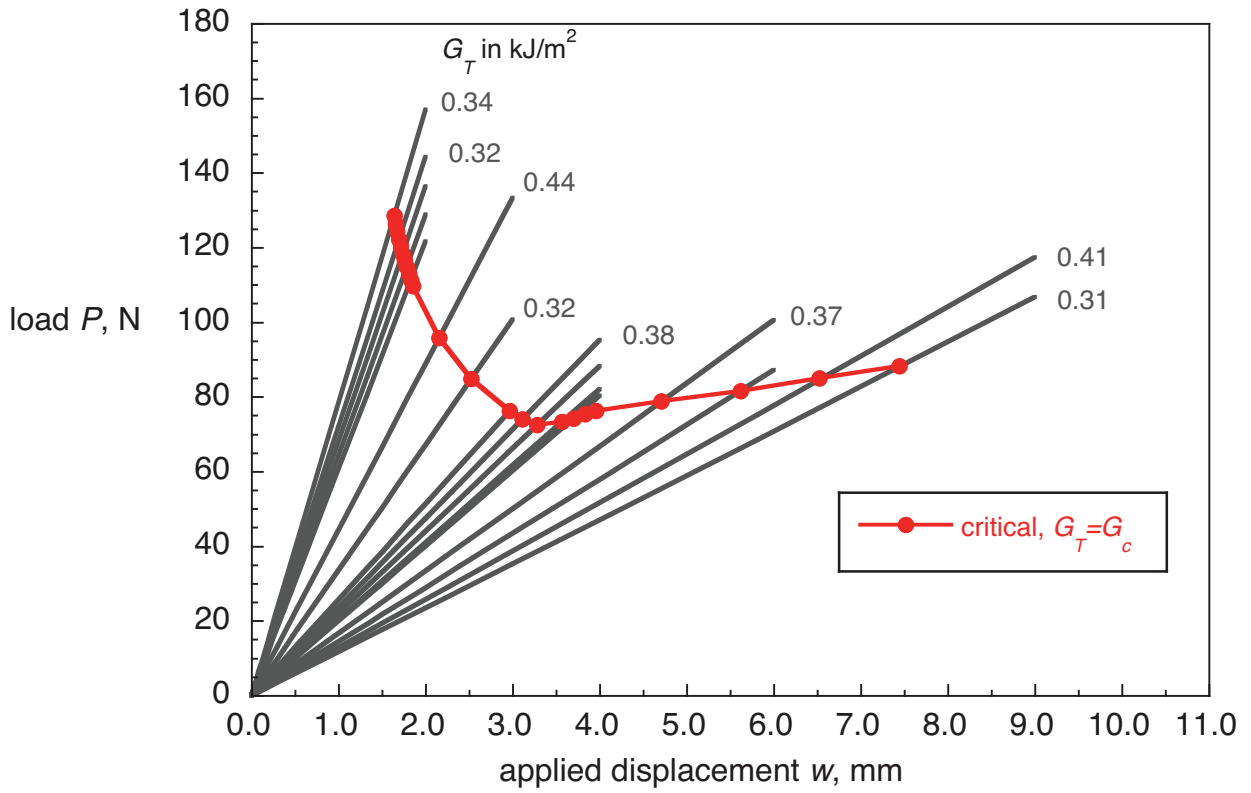


Figure 9. Calculated critical load-displacement behavior for a MMB specimen (20% mode II).

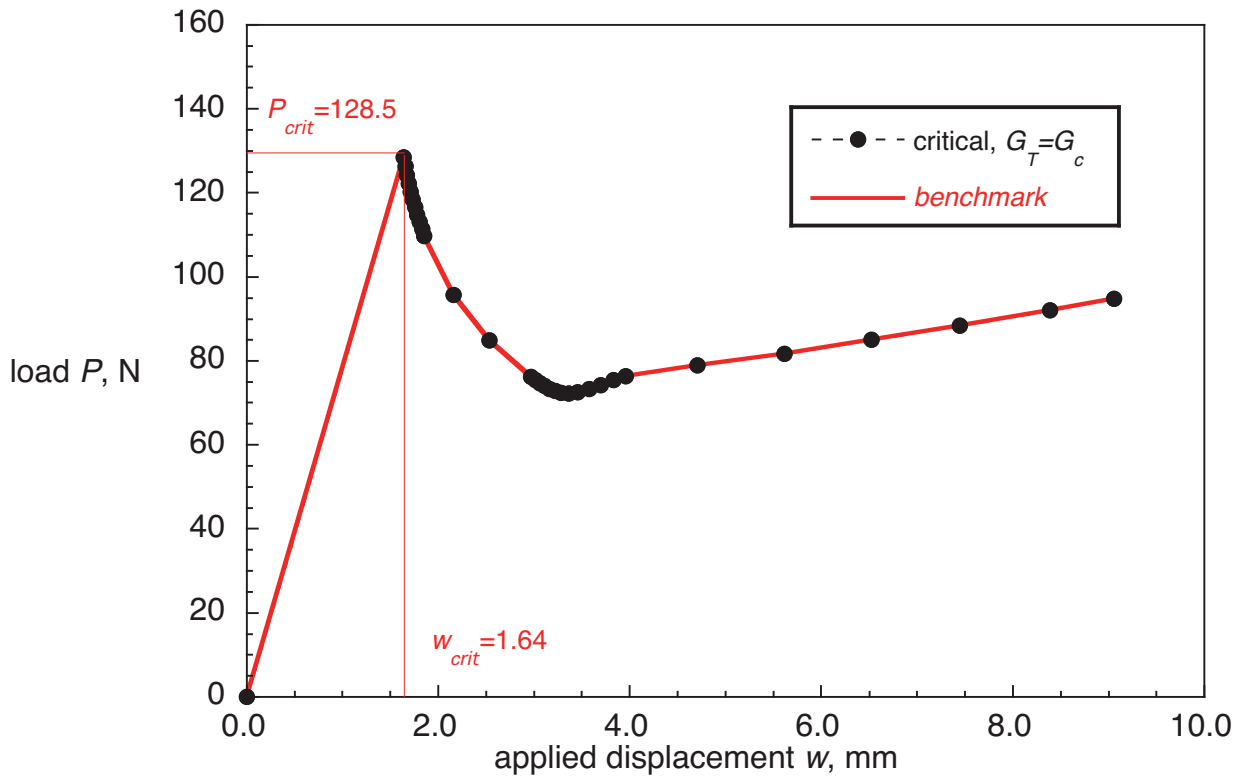


Figure 10. Calculated critical behavior and resulting benchmark case for applied displacement, w , for a MMB specimen (20% mode II).

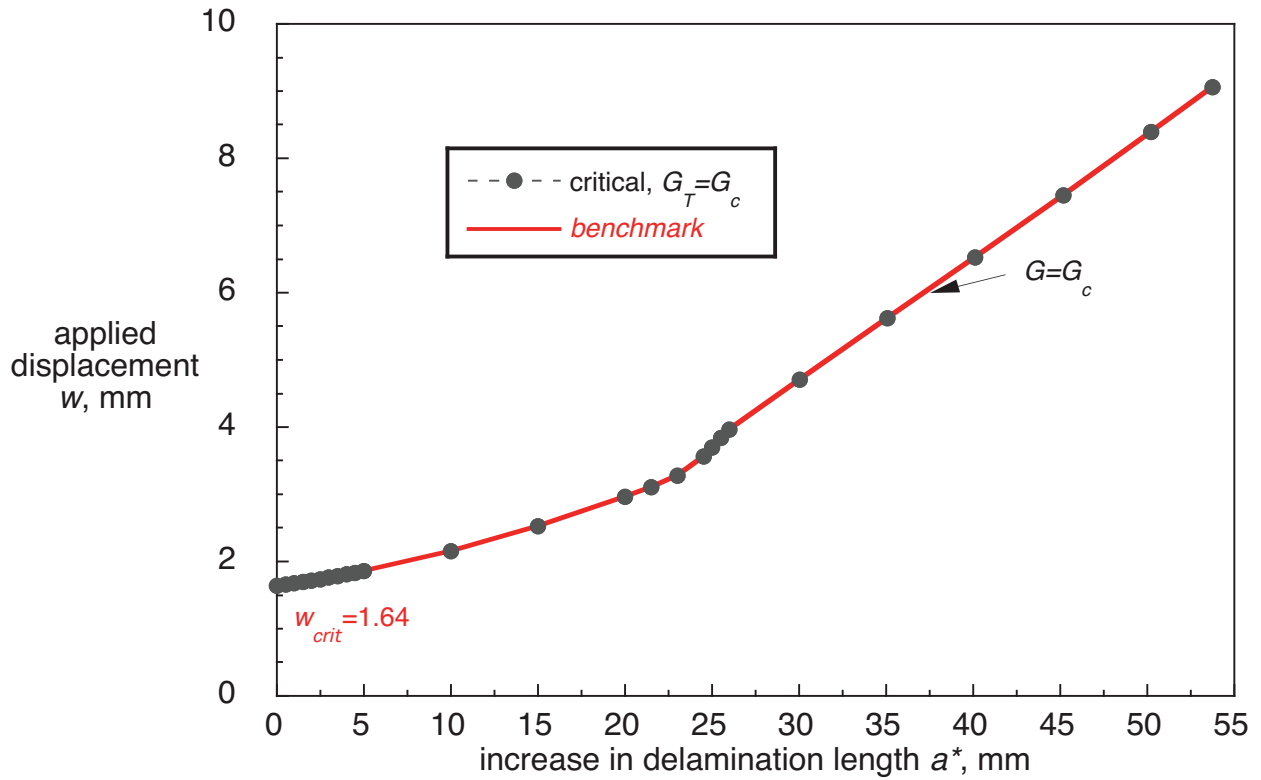


Figure 11. Benchmark case for applied displacement, w , plotted versus increase in delamination length, a^* , for a MMB specimen (20% mode II).

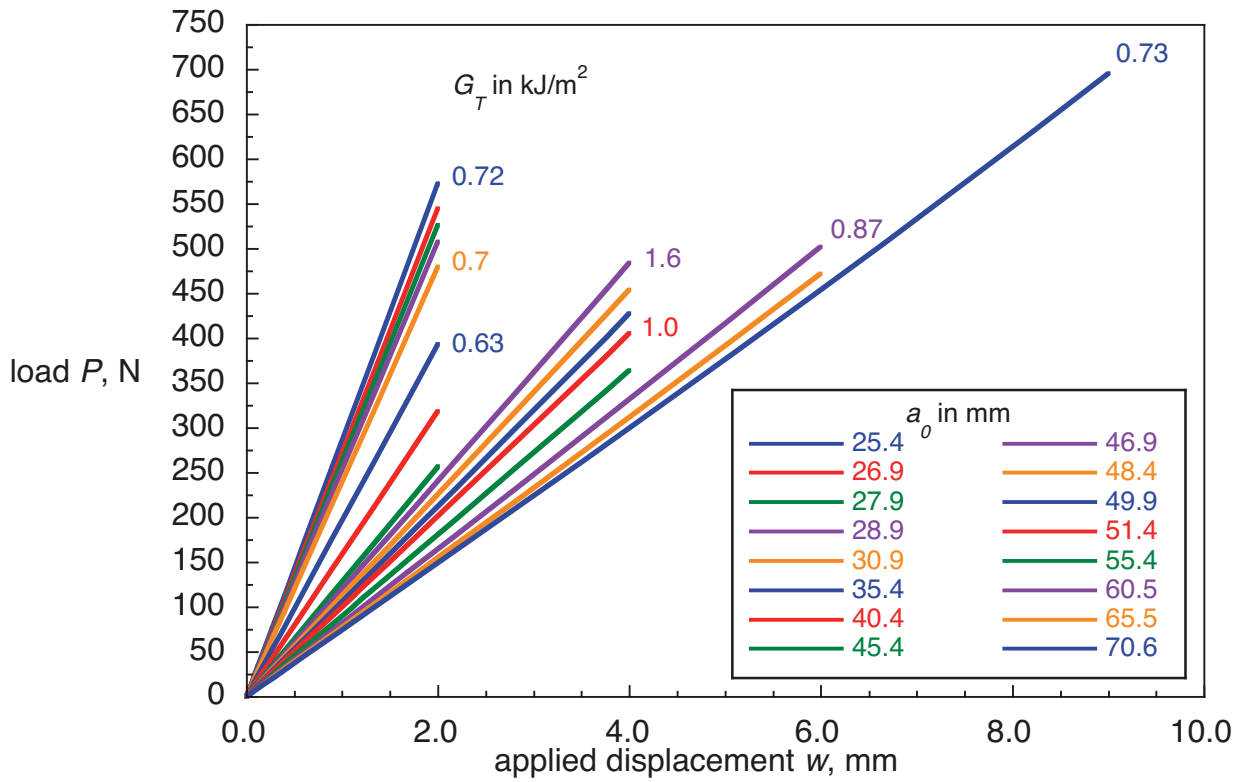


Figure 12. Load-displacement behavior for MMB specimens (50% mode II) with different delamination lengths a_0 .

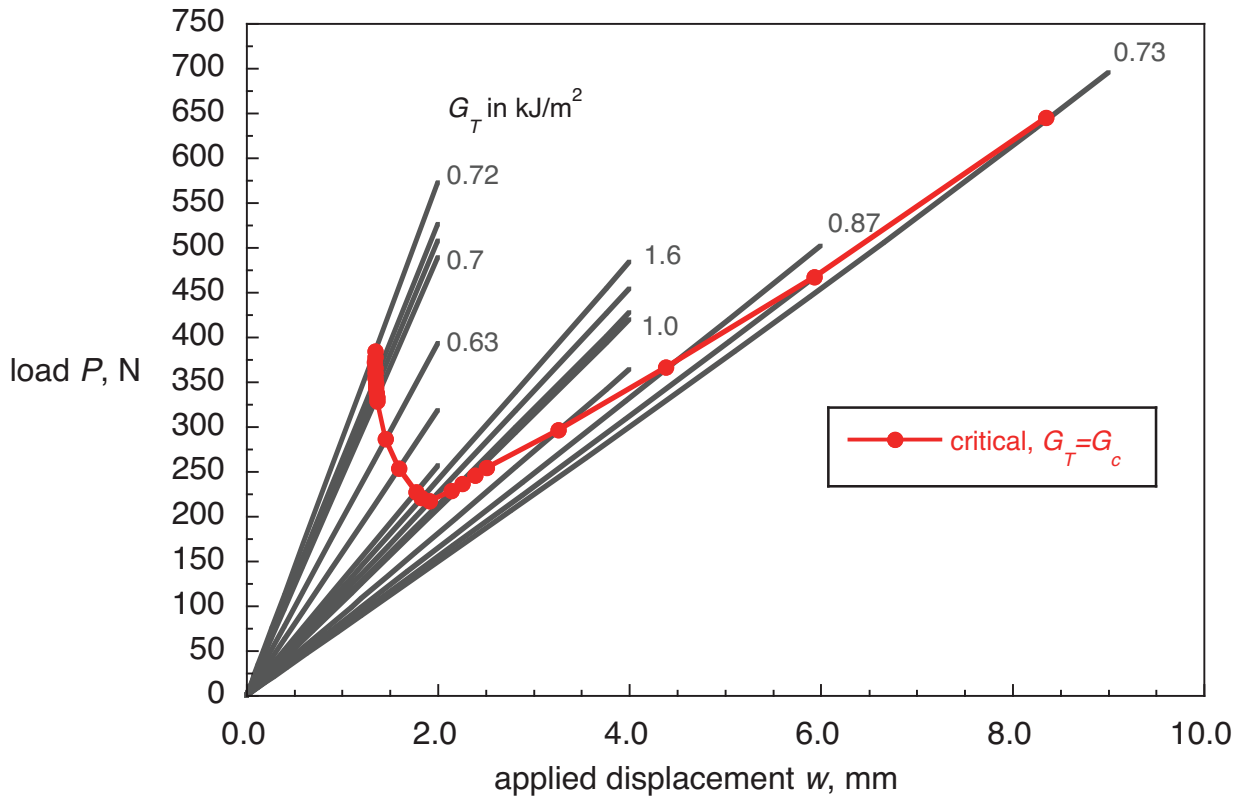


Figure 13. Calculated critical load-displacement behavior for a MMB specimen (50% mode II).

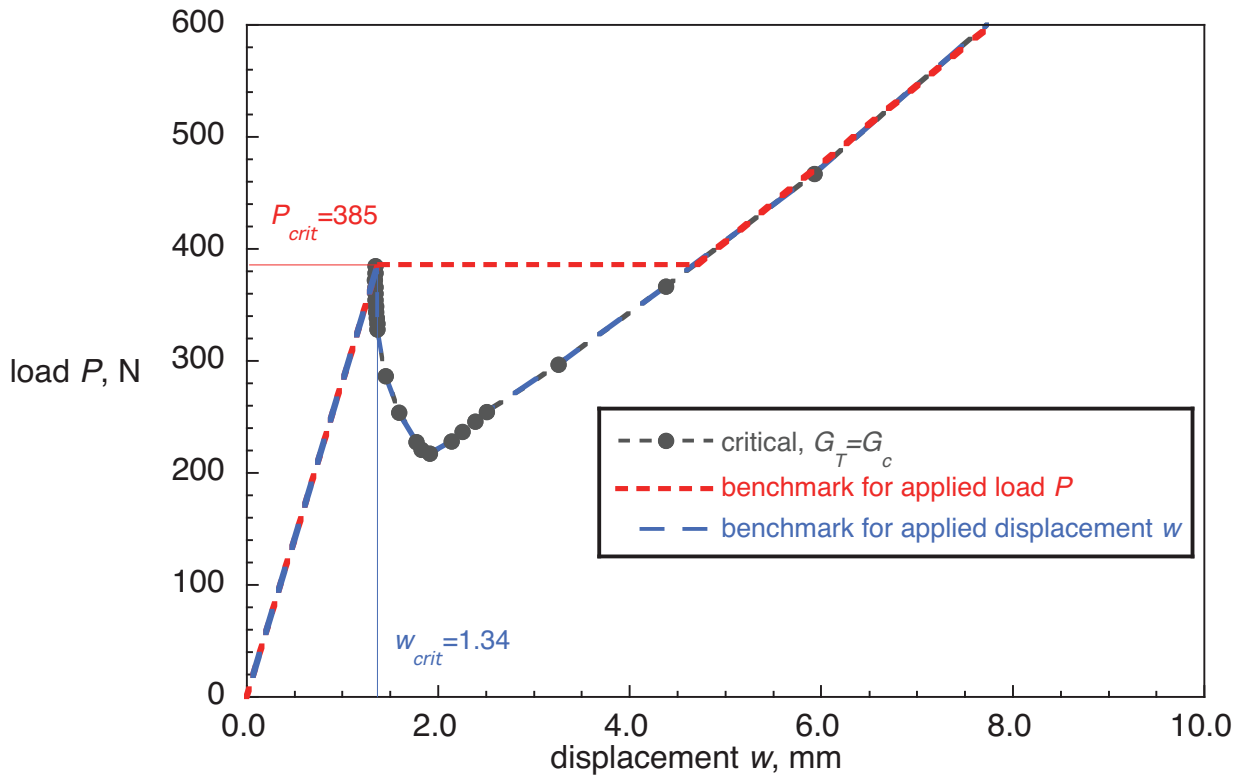


Figure 14. Calculated critical behavior and resulting benchmark cases for applied load, P , and displacement, w , for a MMB specimen (50% mode II).

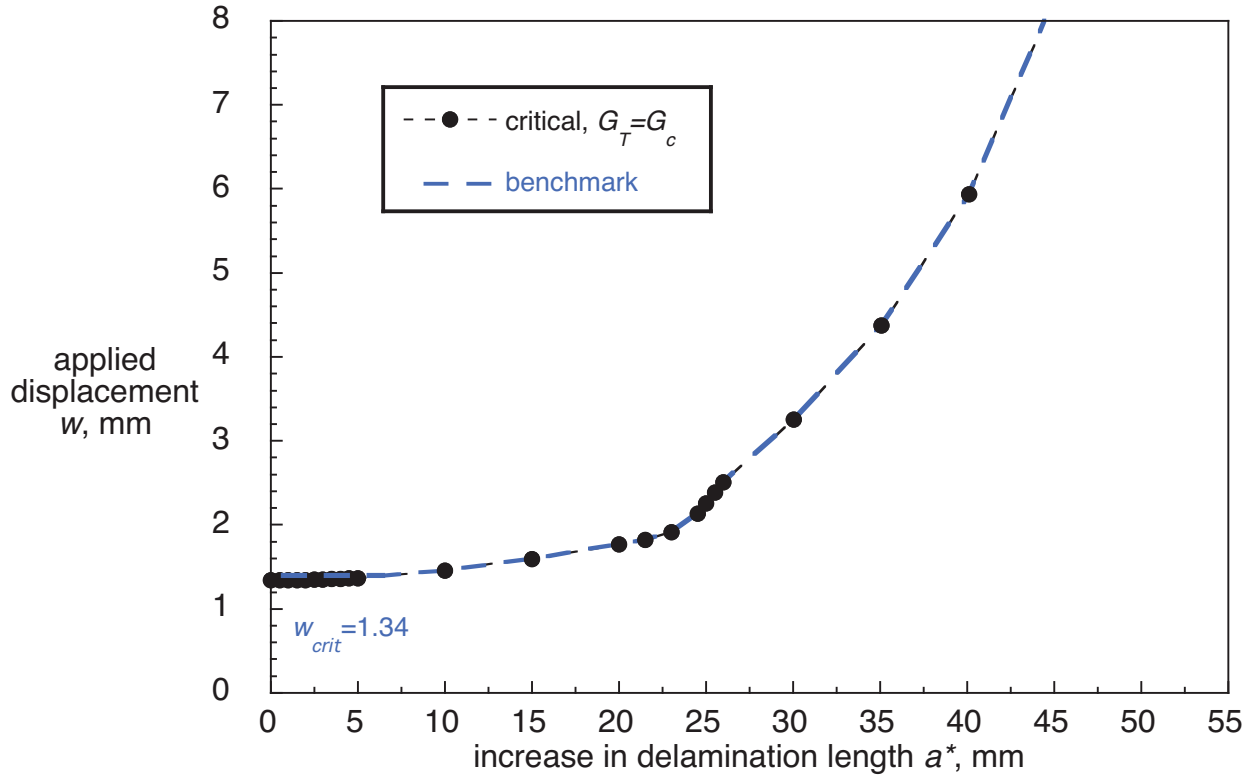


Figure 15. Benchmark case for applied displacement, w , plotted versus increase in delamination length, a^* , for a MMB specimen (50% mode II).

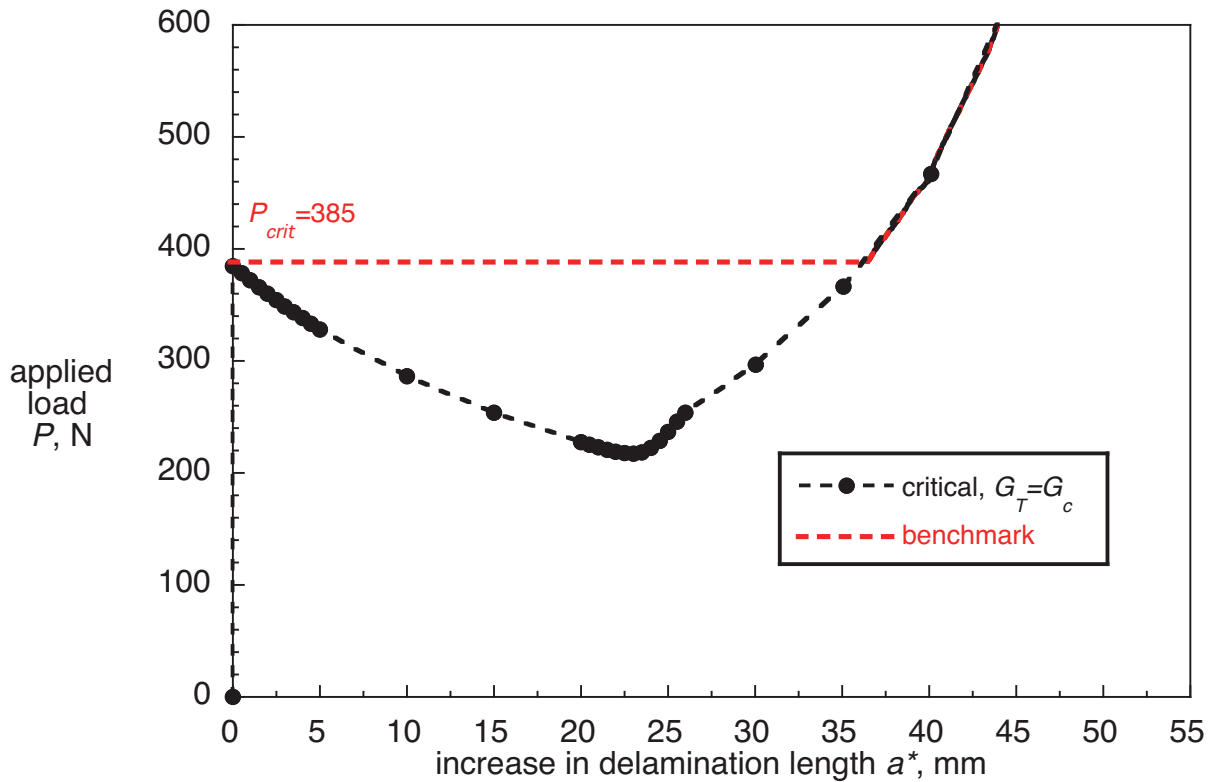


Figure 16. Benchmark case for applied load, P , plotted versus increase in delamination length, a^* , for a MMB specimen (50% mode II).

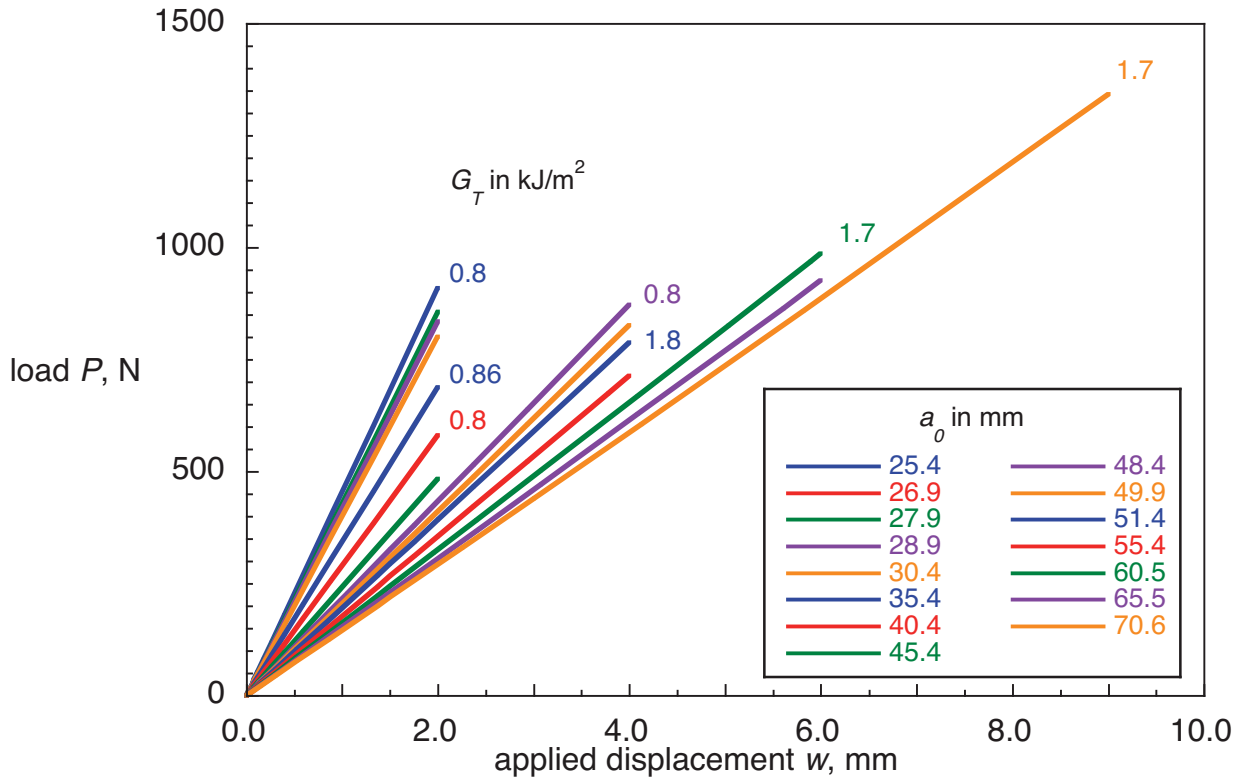


Figure 17. Load-displacement behavior for MMB specimens (80% mode II) with different delamination lengths, a_0 .

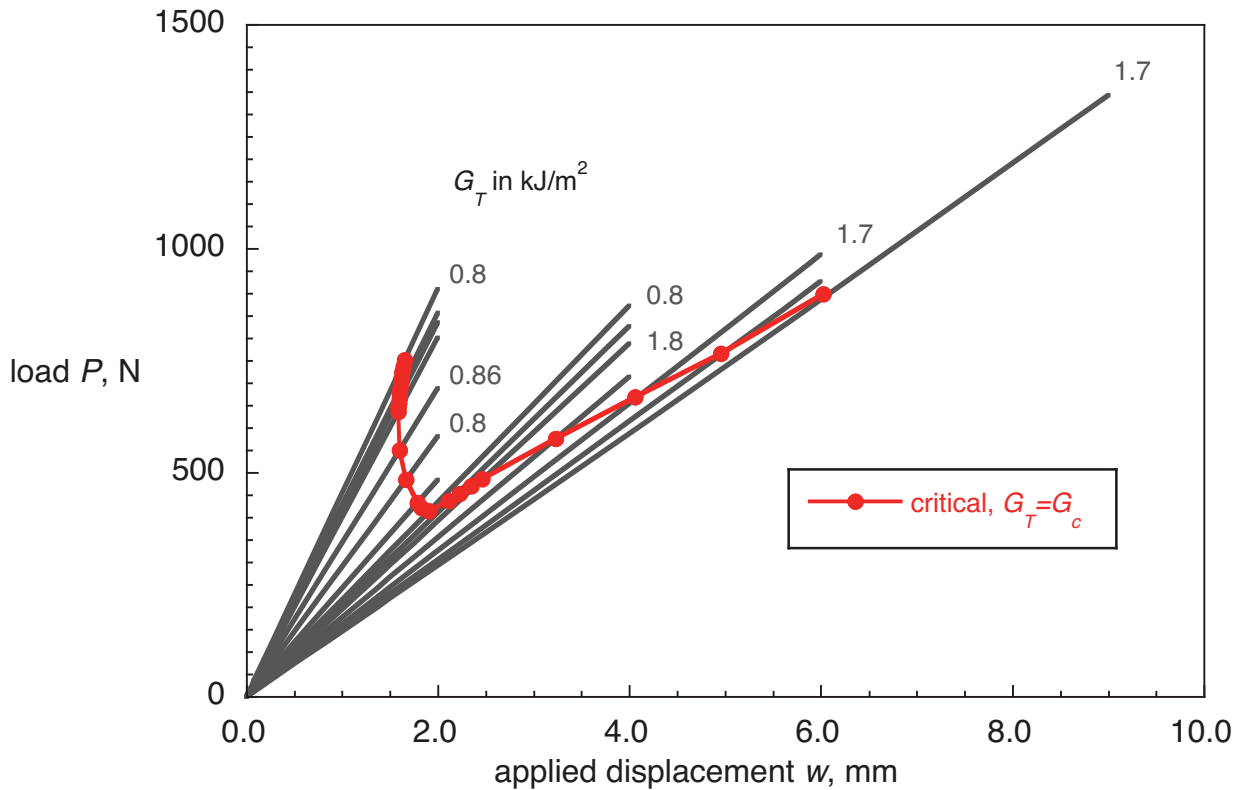


Figure 18. Calculated critical load-displacement behavior for a MMB specimen (80% mode II).

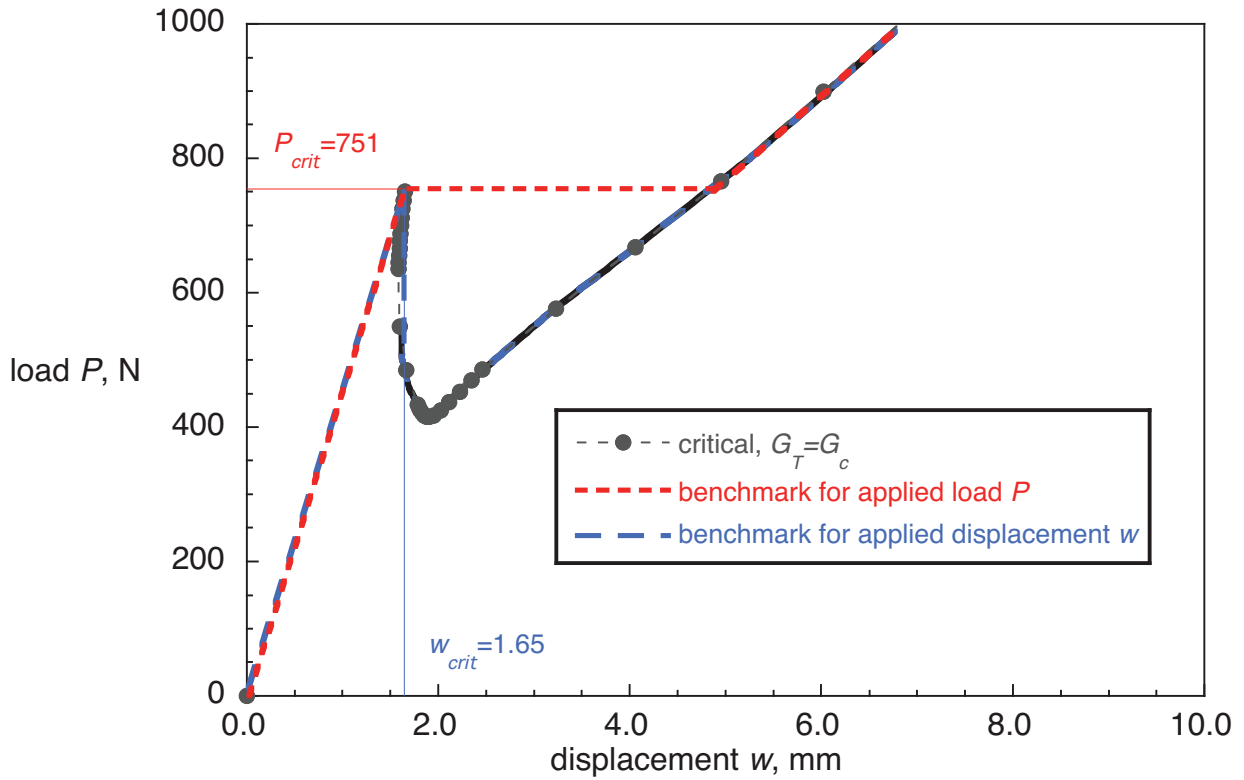


Figure 19. Calculated critical behavior and resulting benchmark cases for applied load, P , and displacement, w , for a MMB specimen (80% mode II).

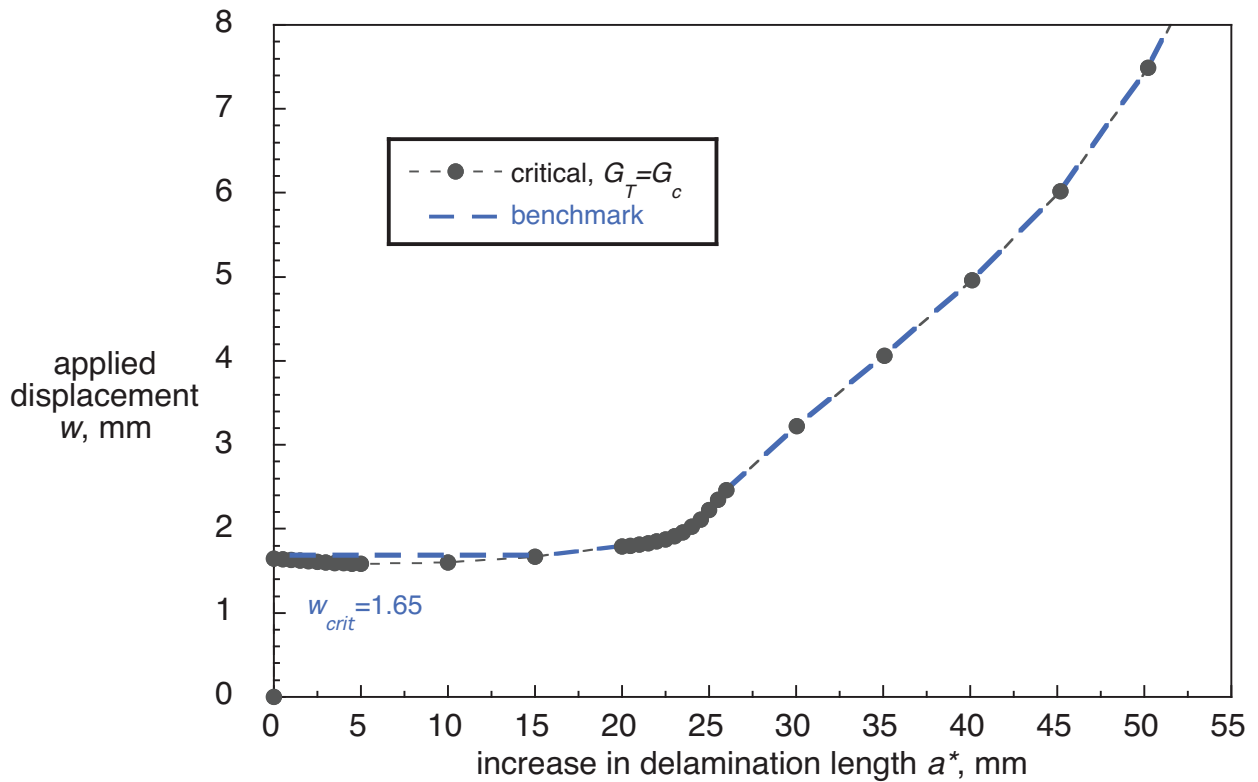


Figure 20. Benchmark case for applied displacement, w , plotted versus increase in delamination length, a^* , for a MMB specimen (80% mode II).

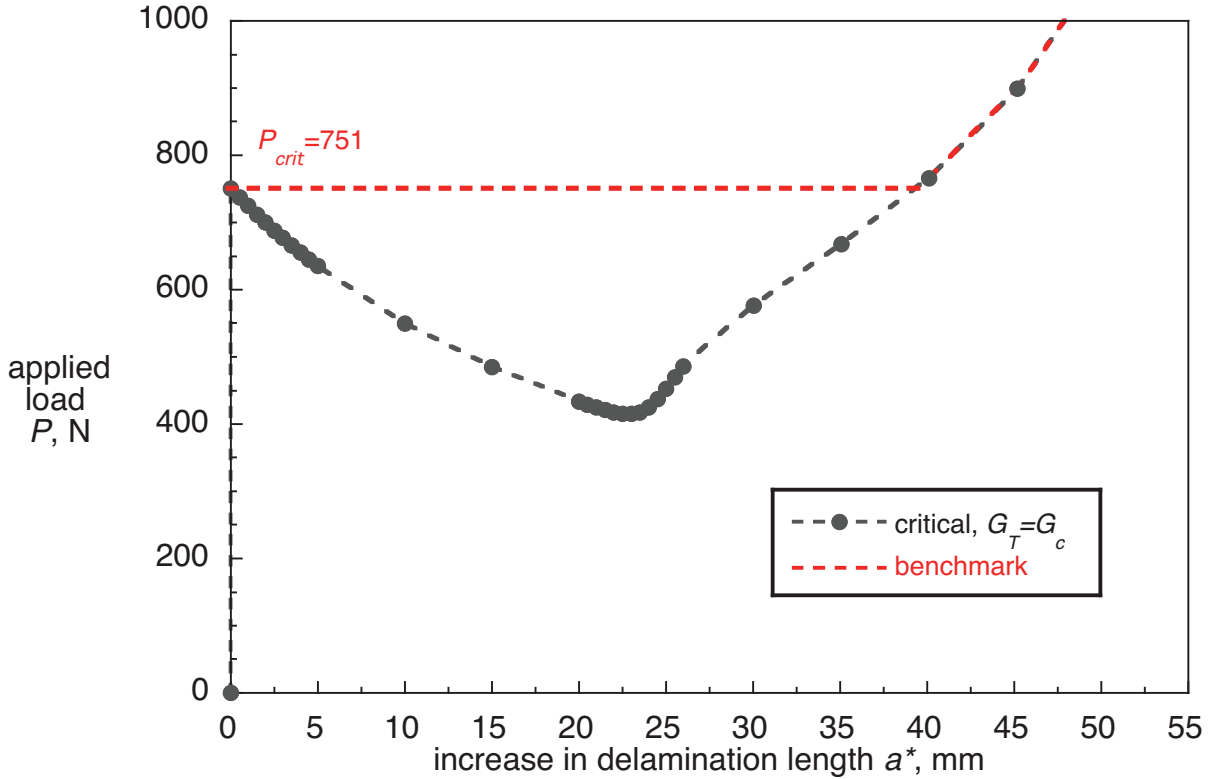


Figure 21. Benchmark case for applied load, P , plotted versus increase in delamination length, a^* , for a MMB specimen (80% mode II).

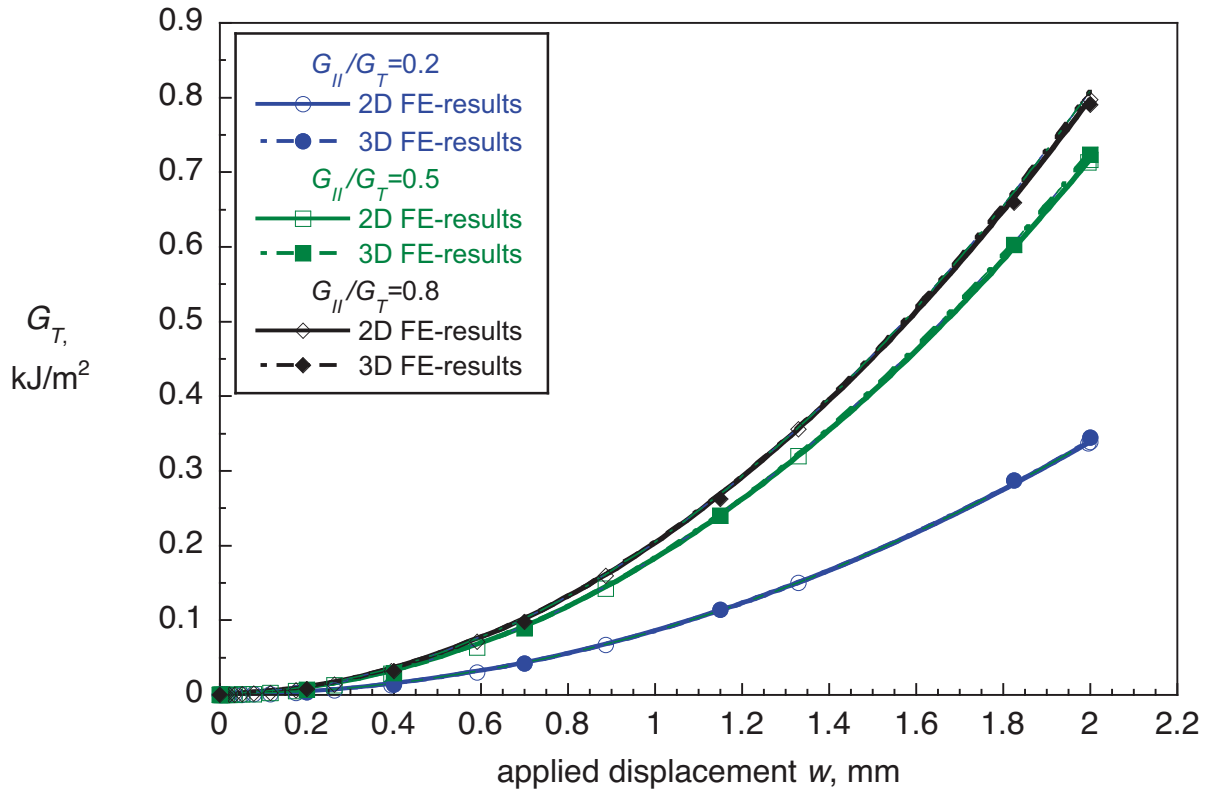


Figure 22. Computed total energy release rate.

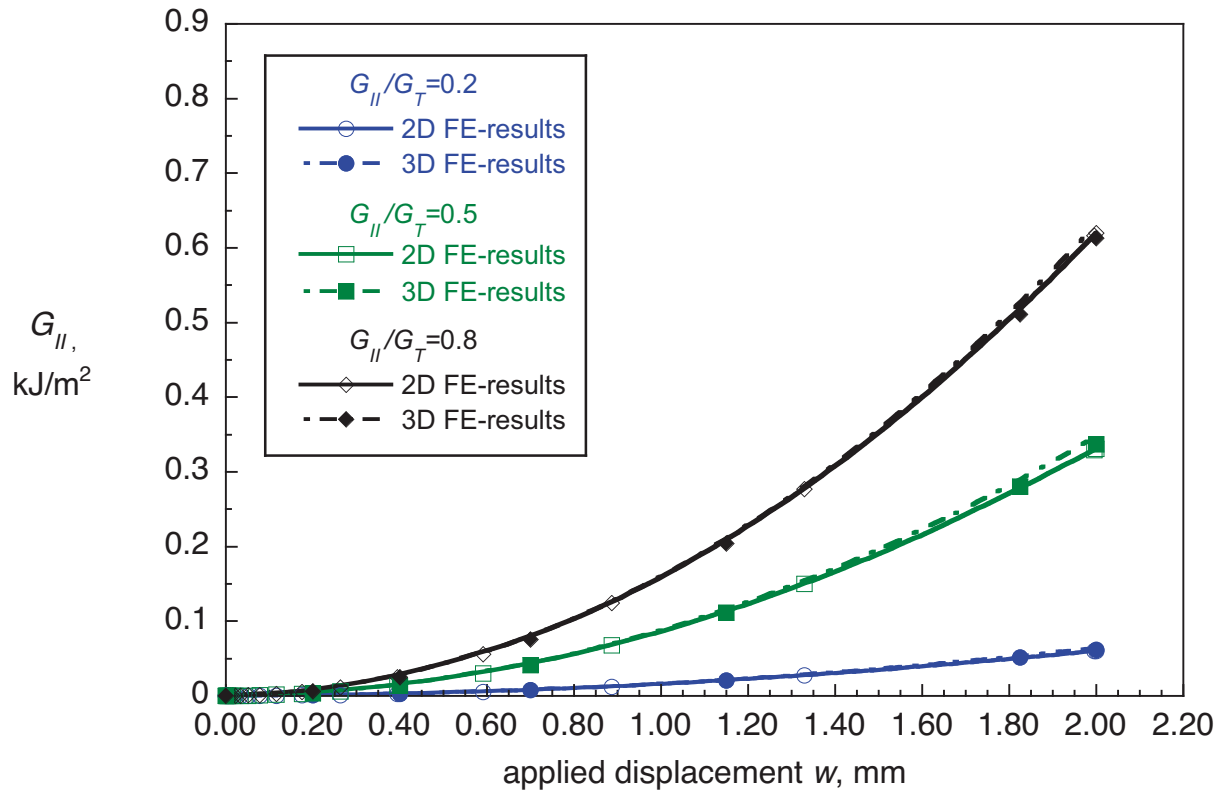


Figure 23. Computed mode II energy release rate component.

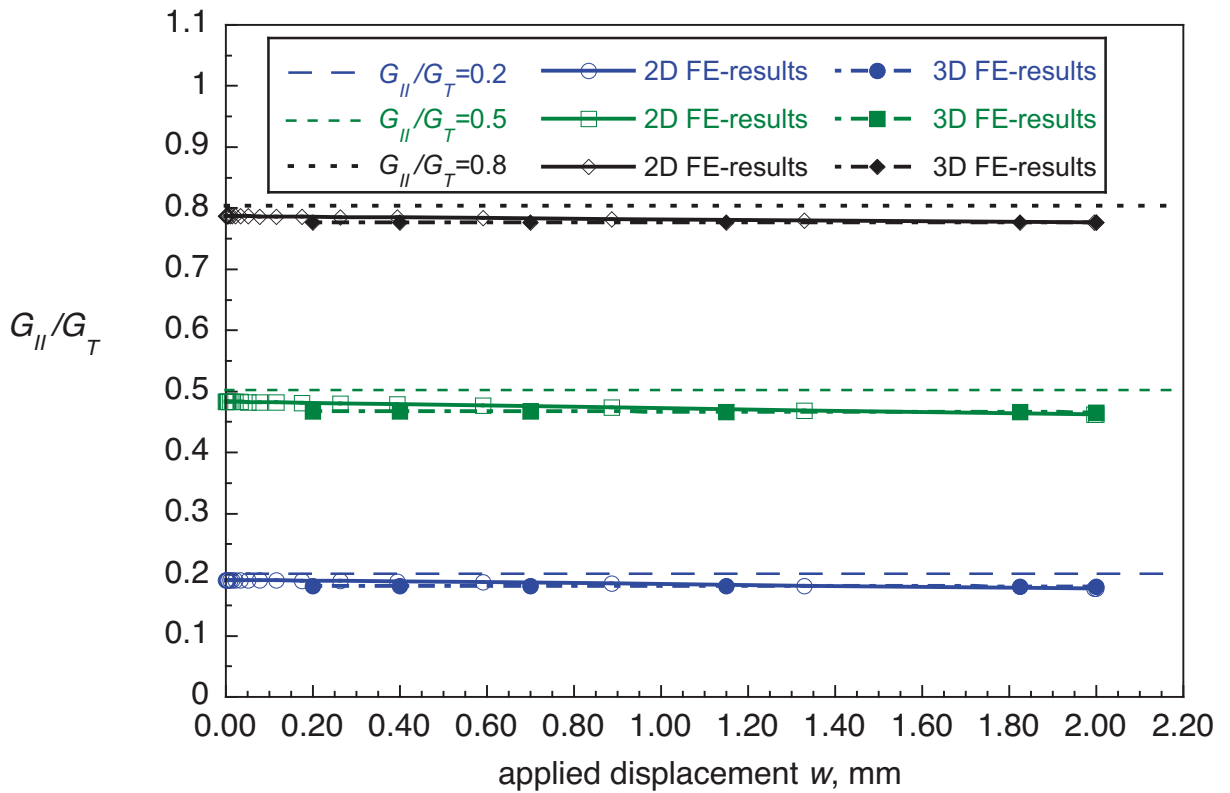


Figure 24. Computed mixed-mode ratio.

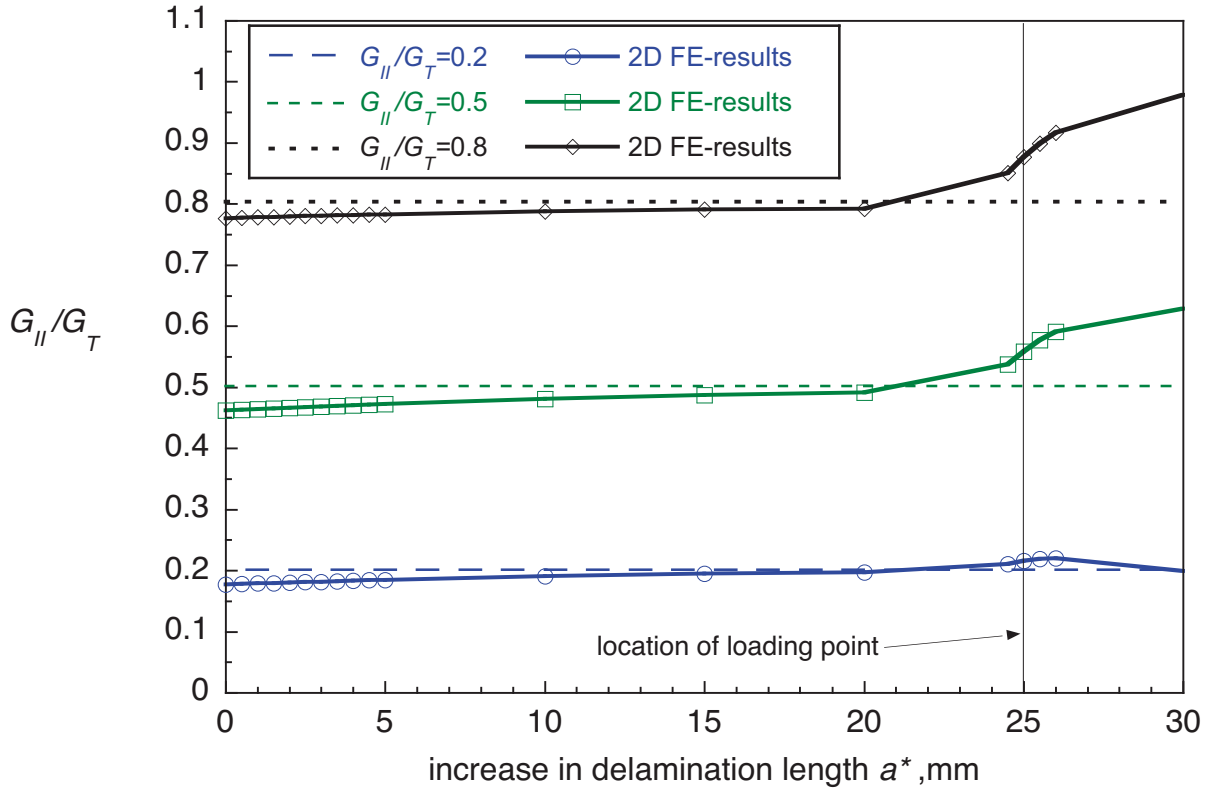


Figure 25. Dependence of computed mixed-mode ratio on delamination length.

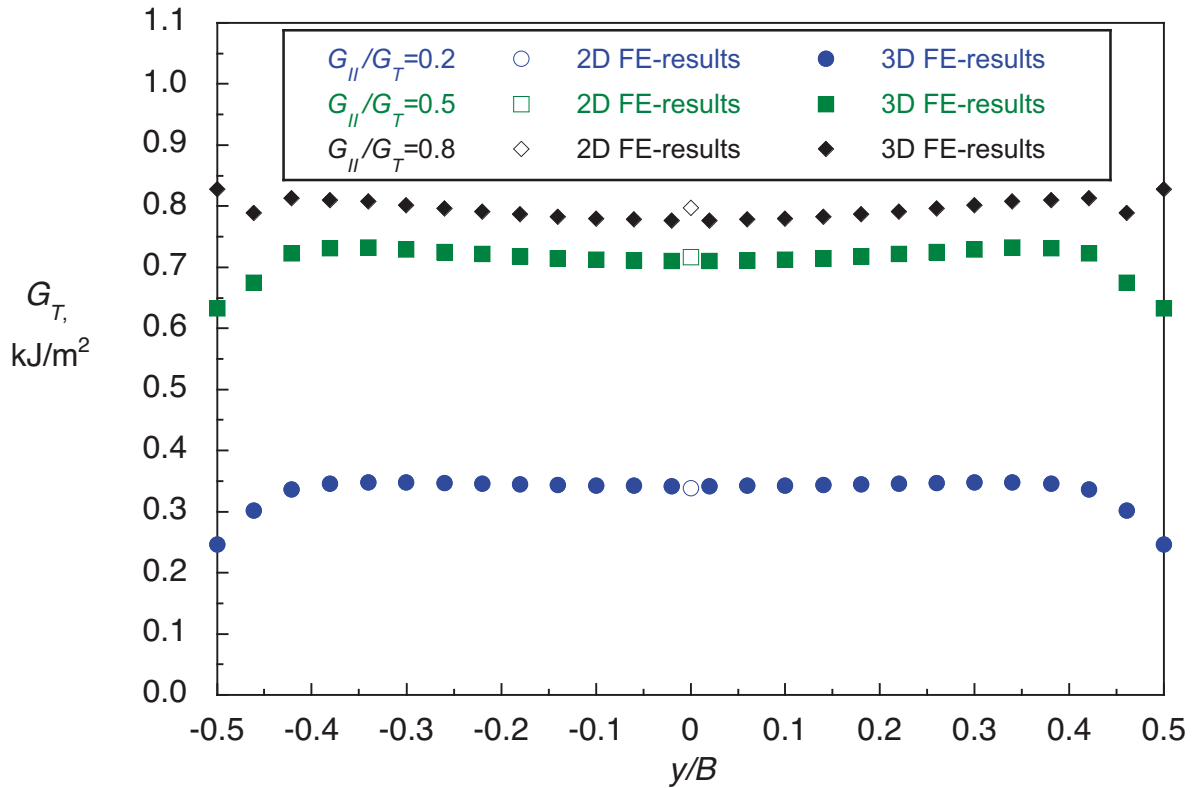


Figure 26. Computed total energy release rate distribution across the width of a MMB specimen.

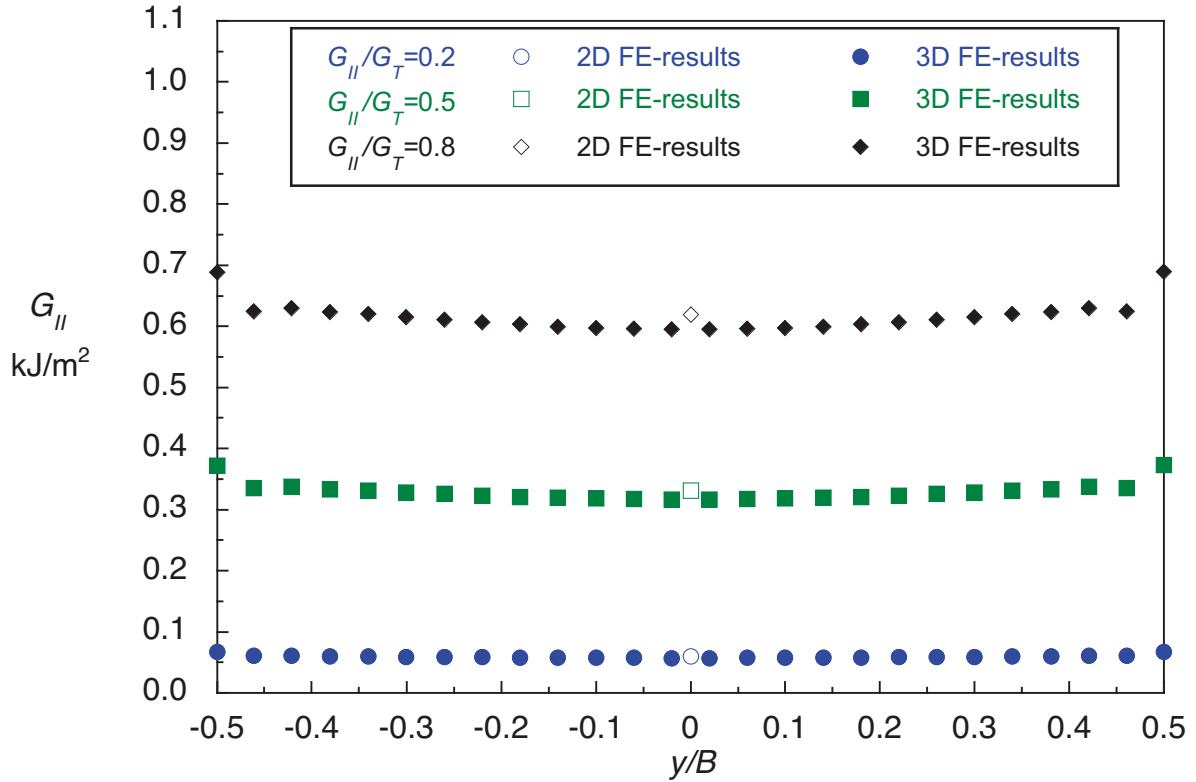


Figure 27. Computed mode II energy release rate distribution across the width of a MMB specimen.

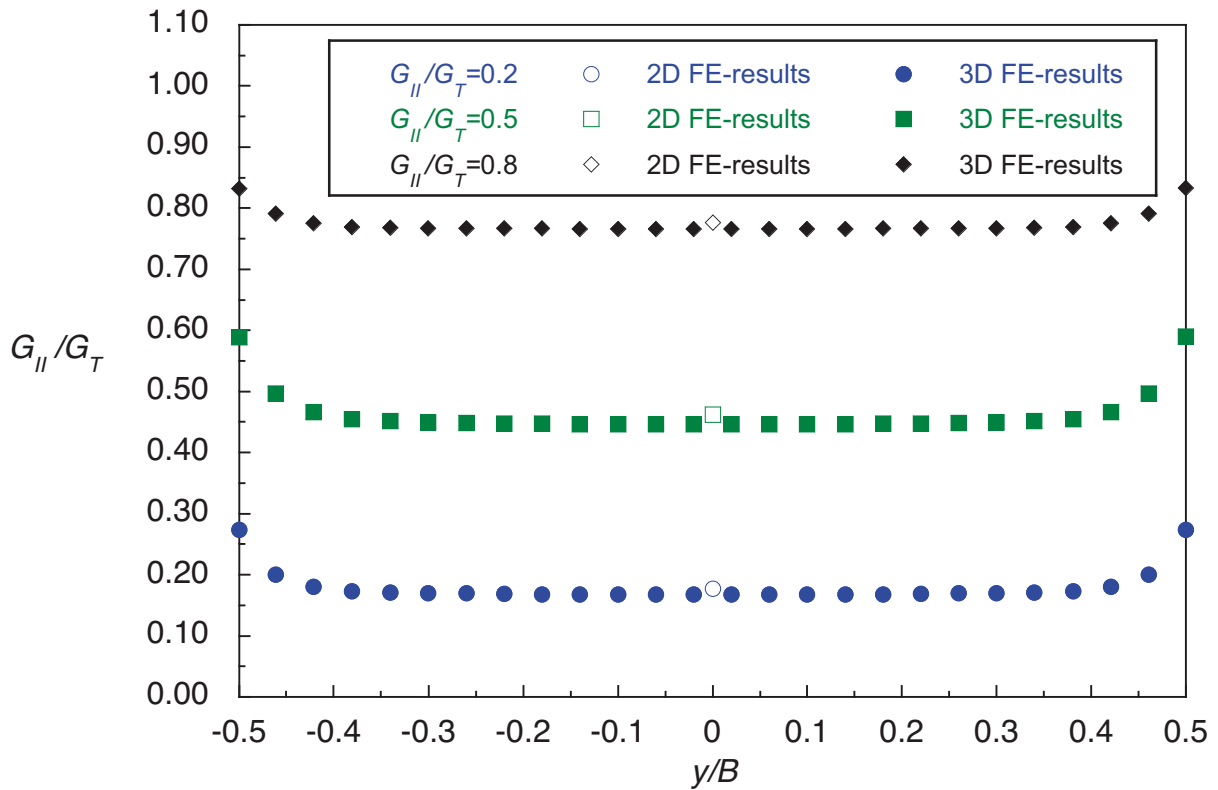


Figure 28. Computed mixed-mode ratio distribution across the width of a MMB specimen.

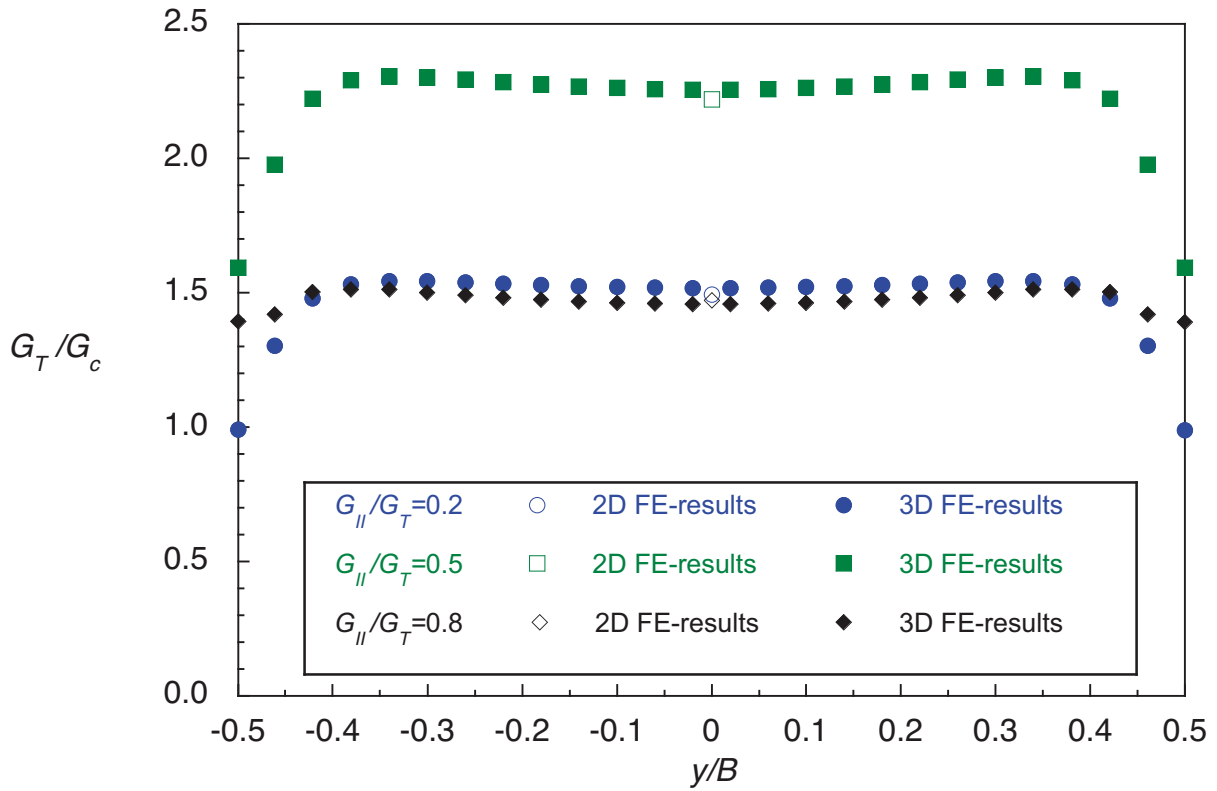


Figure 29. Failure index distribution across the width of a MMB specimen.

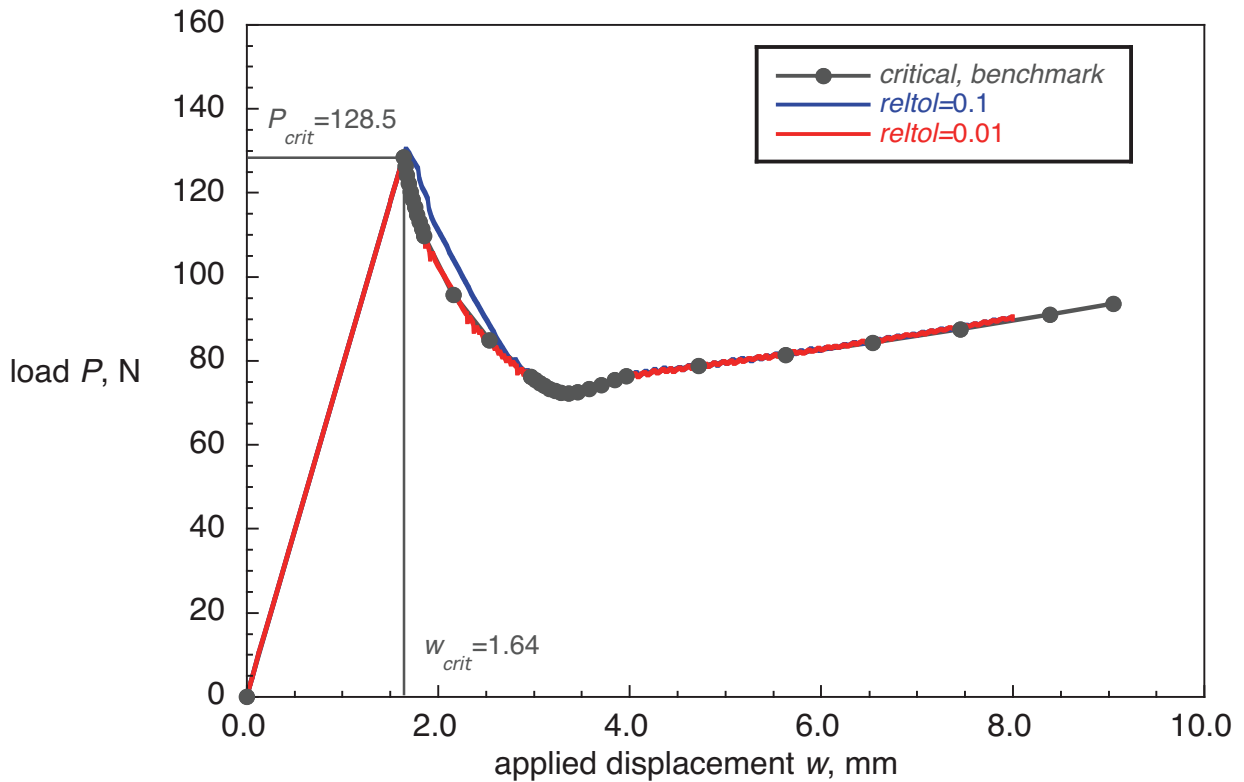


Figure 30. Computed critical load-displacement behavior for a MMB specimen (20% mode II) obtained from two-dimensional planar models (CPE4I) with different release tolerance settings.

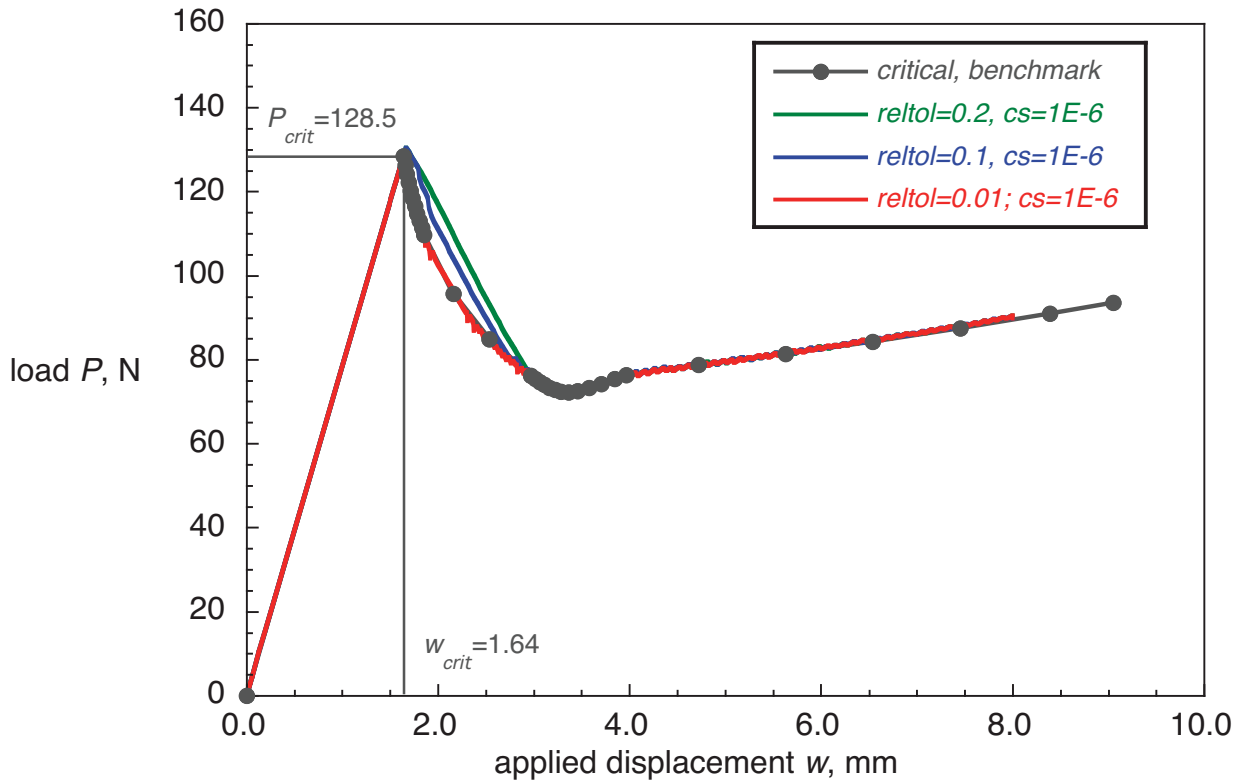


Figure 31. Computed critical load-displacement behavior for a MMB specimen (20% mode II) obtained from two-dimensional planar models (CPE4I) with added contact stabilization.

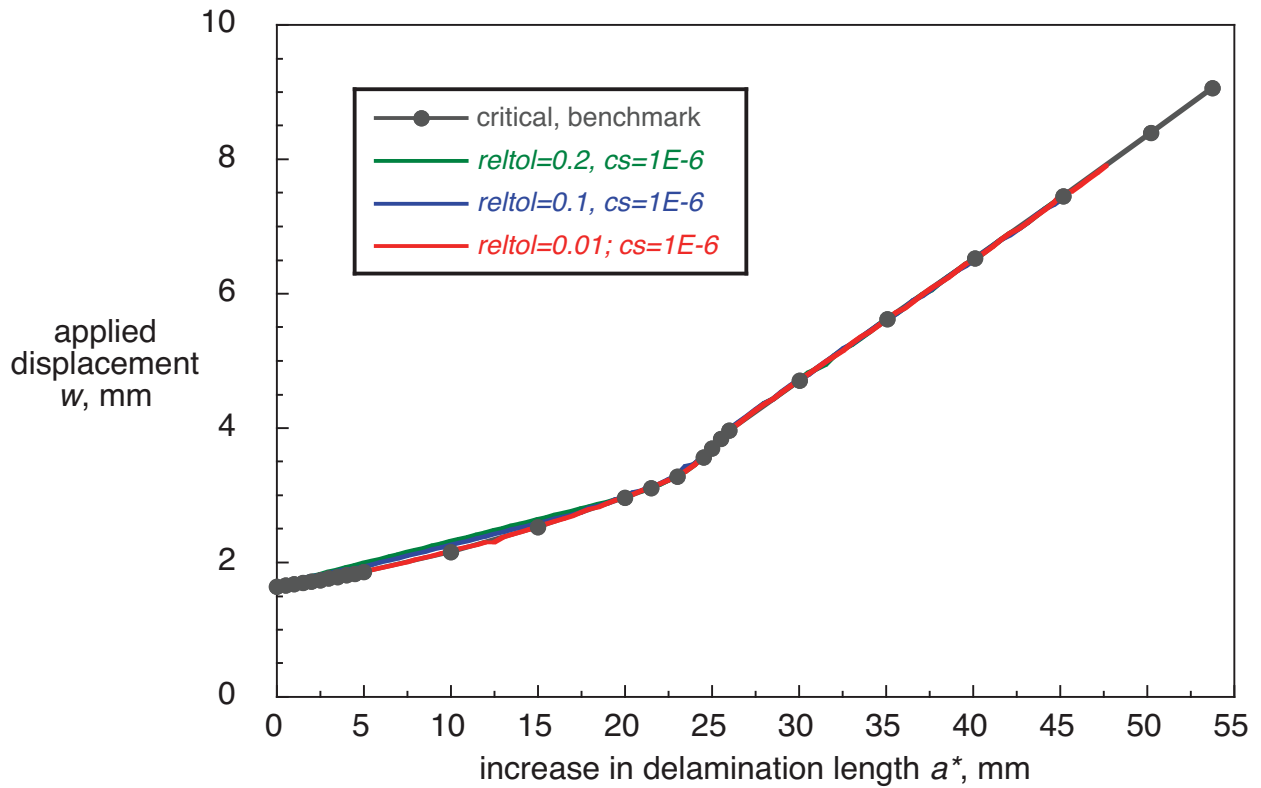


Figure 32. Computed displacement-propagation behavior for a MMB specimen (20% mode II) obtained from two-dimensional planar models (CPE4I) with added contact stabilization.

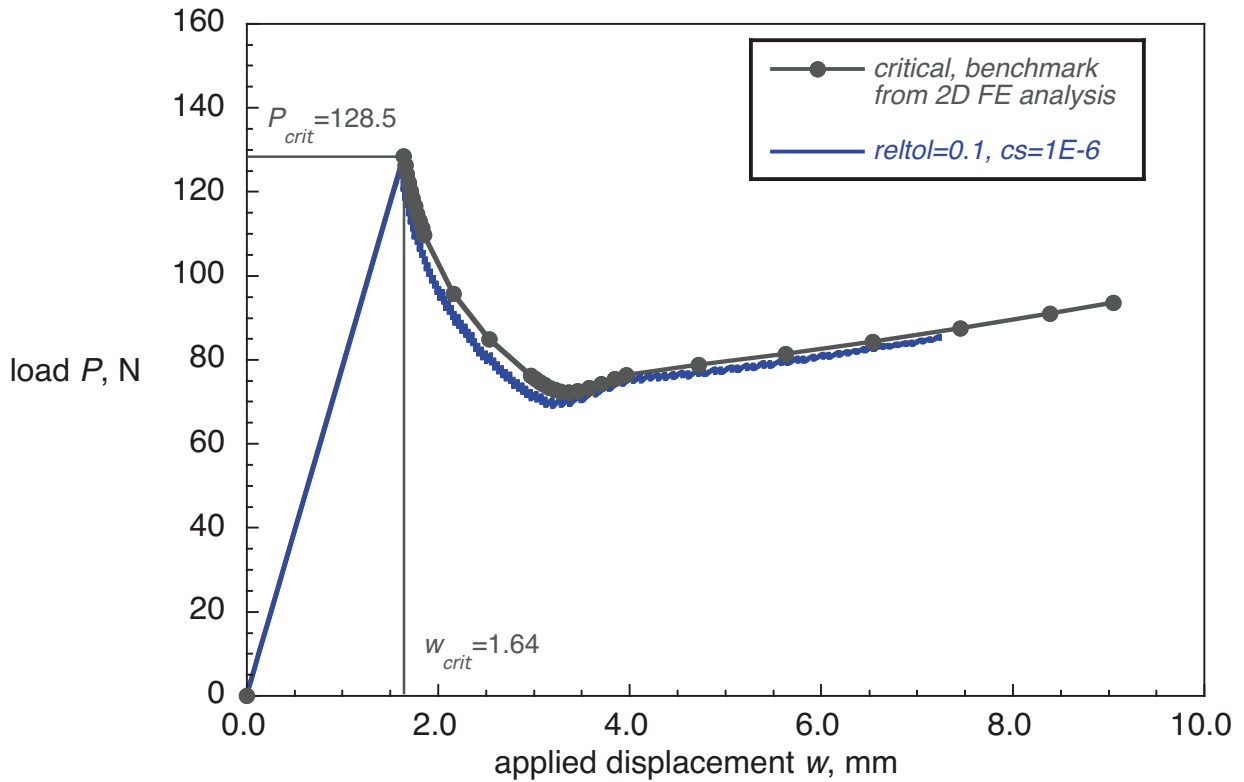


Figure 33. Computed critical load-displacement behavior for MMB specimen (20% mode II) obtained from three-dimensional solid models (C3D8I) with added contact stabilization.

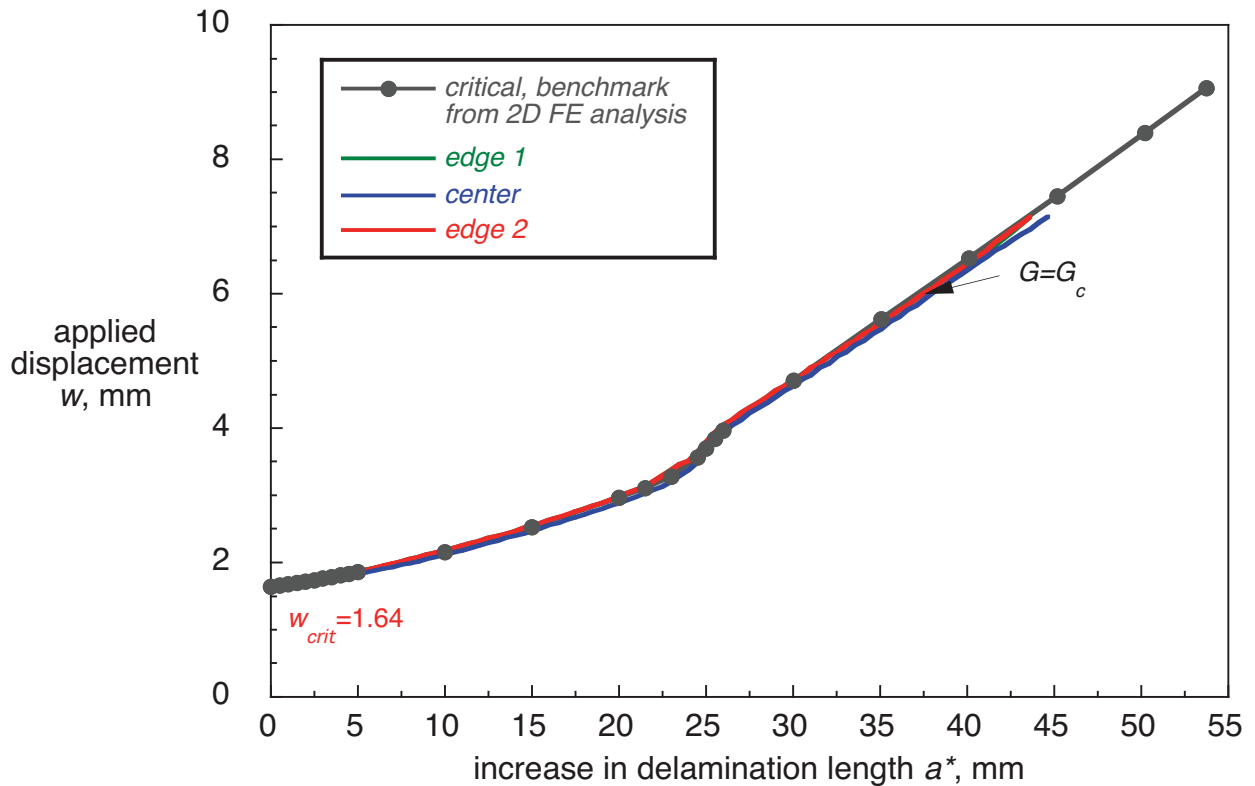


Figure 34. Computed displacement-propagation behavior for a MMB specimen (20% mode II) obtained from three-dimensional solid models (C3D8I) with added contact stabilization.

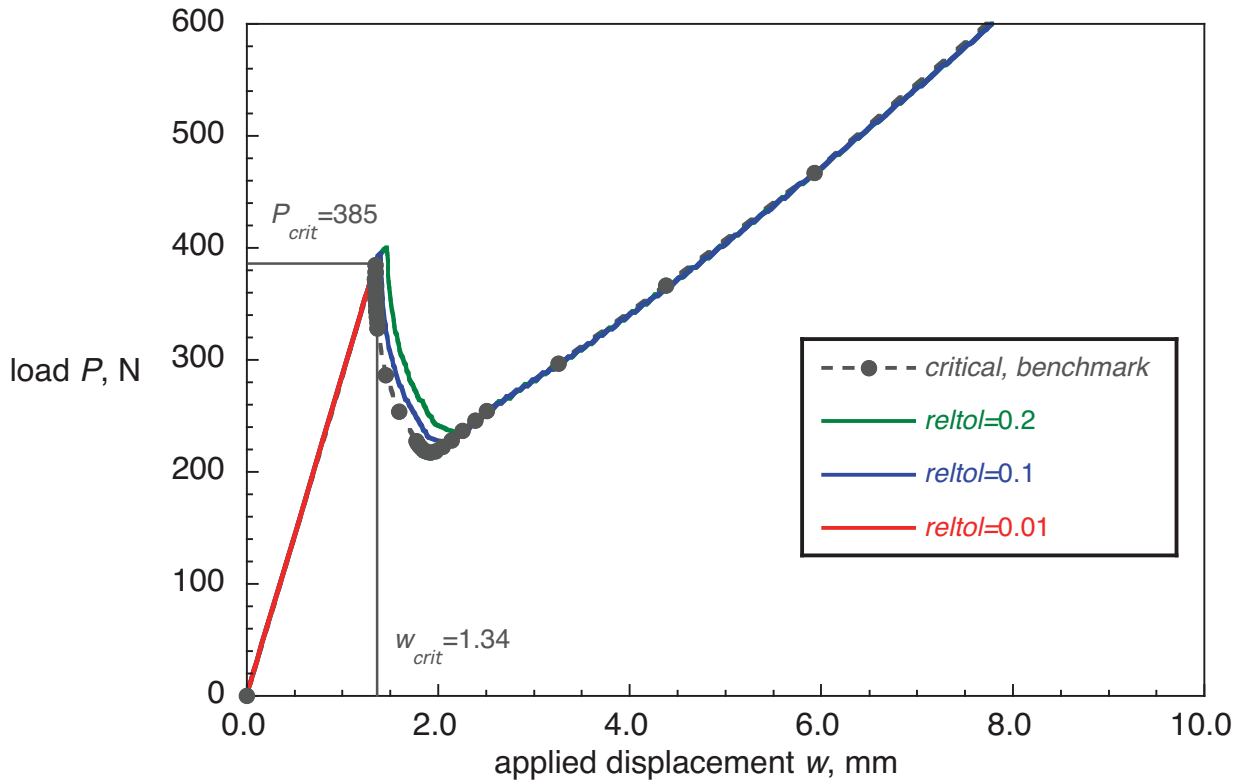


Figure 35. Computed critical load-displacement behavior for MMB specimen (50% mode II) obtained from two-dimensional planar models (CPE4I) with different release tolerance settings.

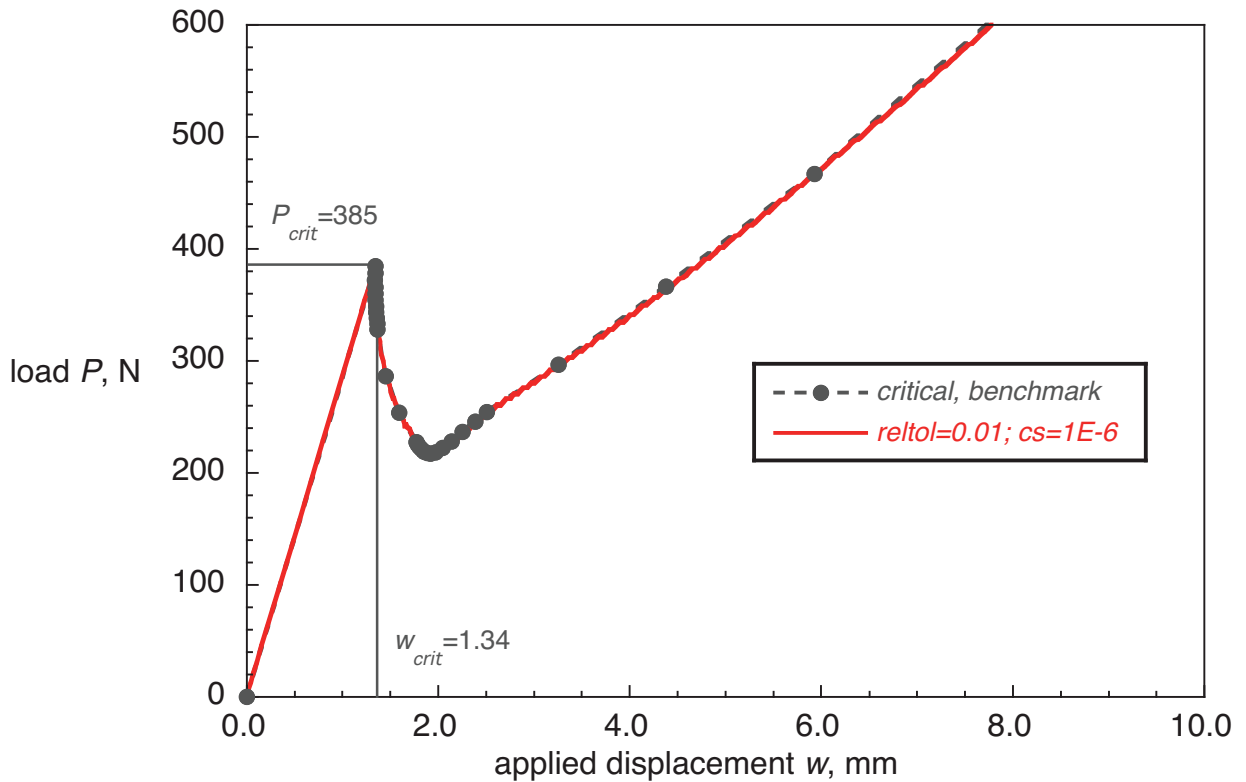


Figure 36. Computed critical load-displacement behavior for MMB specimen (50% mode II) obtained from two-dimensional planar models (CPE4I) with added contact stabilization.

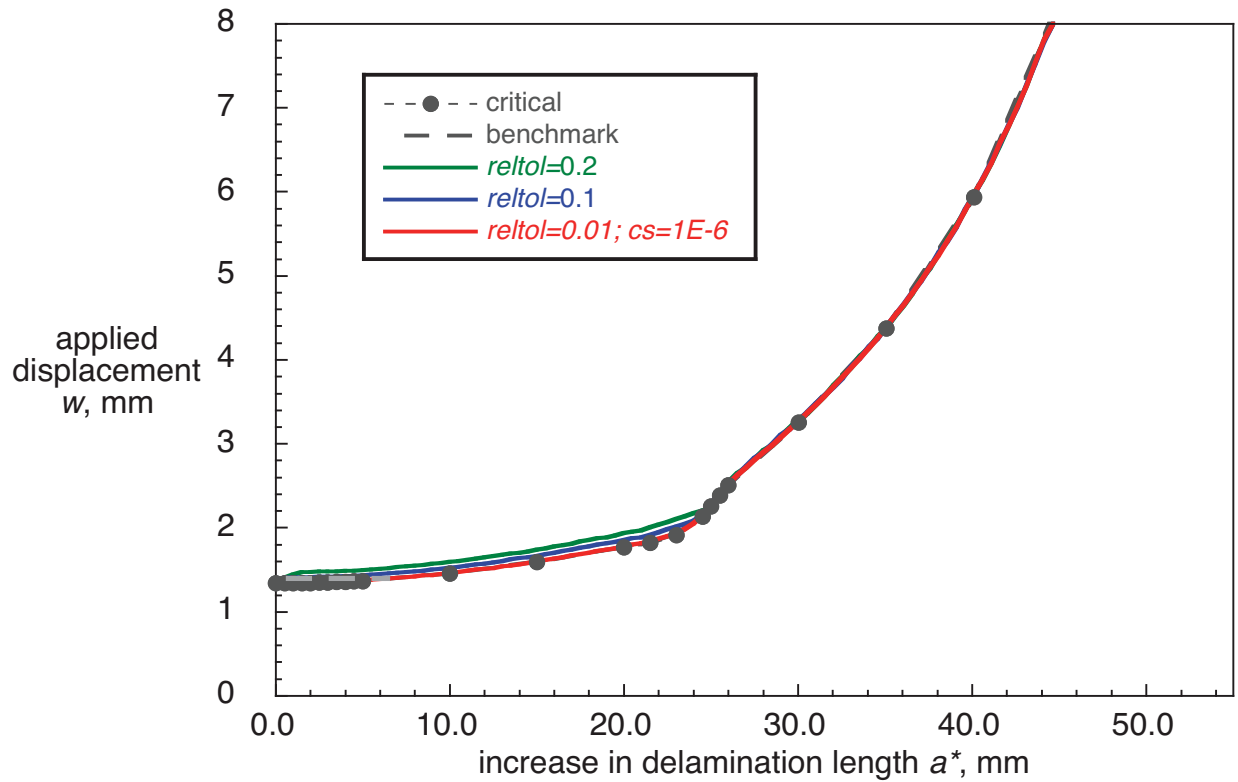


Figure 37. Computed critical displacement-propagation behavior for MMB specimen (50% mode II) obtained from two-dimensional planar models.

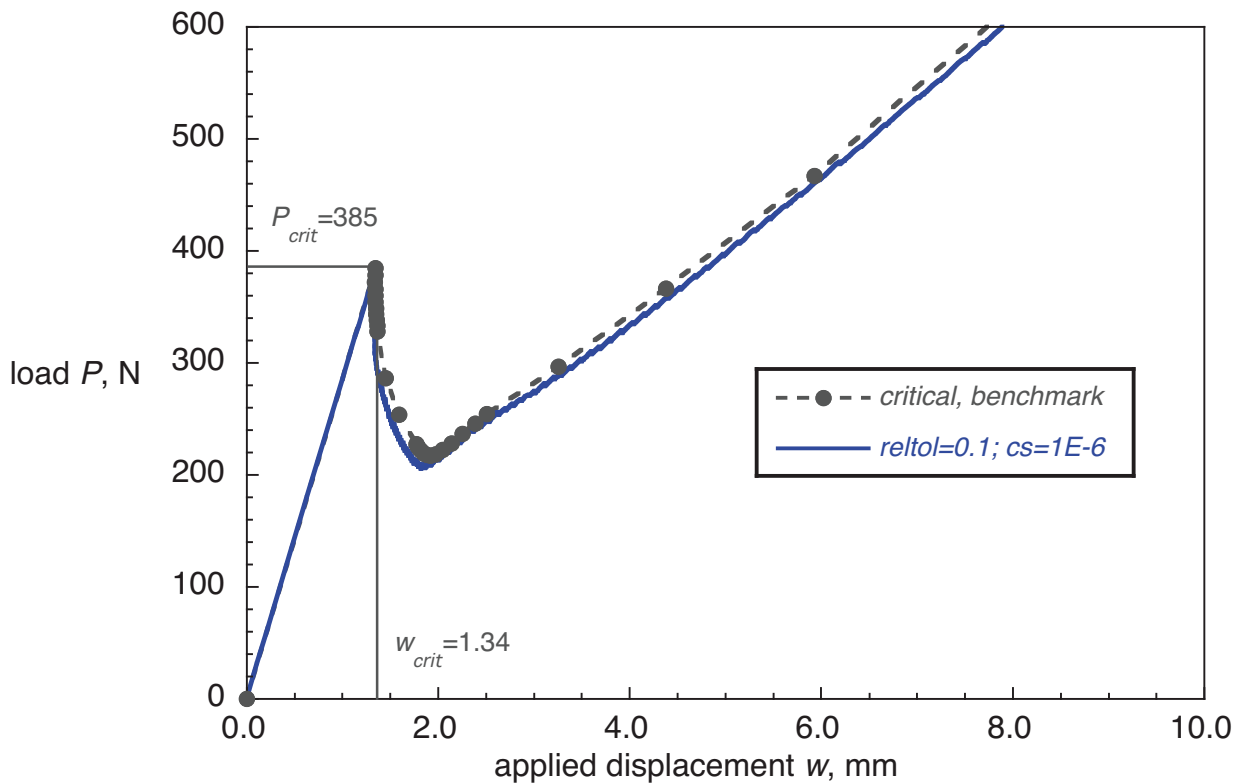


Figure 38. Computed critical load-displacement behavior for MMB specimen (50% mode II) obtained from three-dimensional solid models (C3D8I) with added contact stabilization.

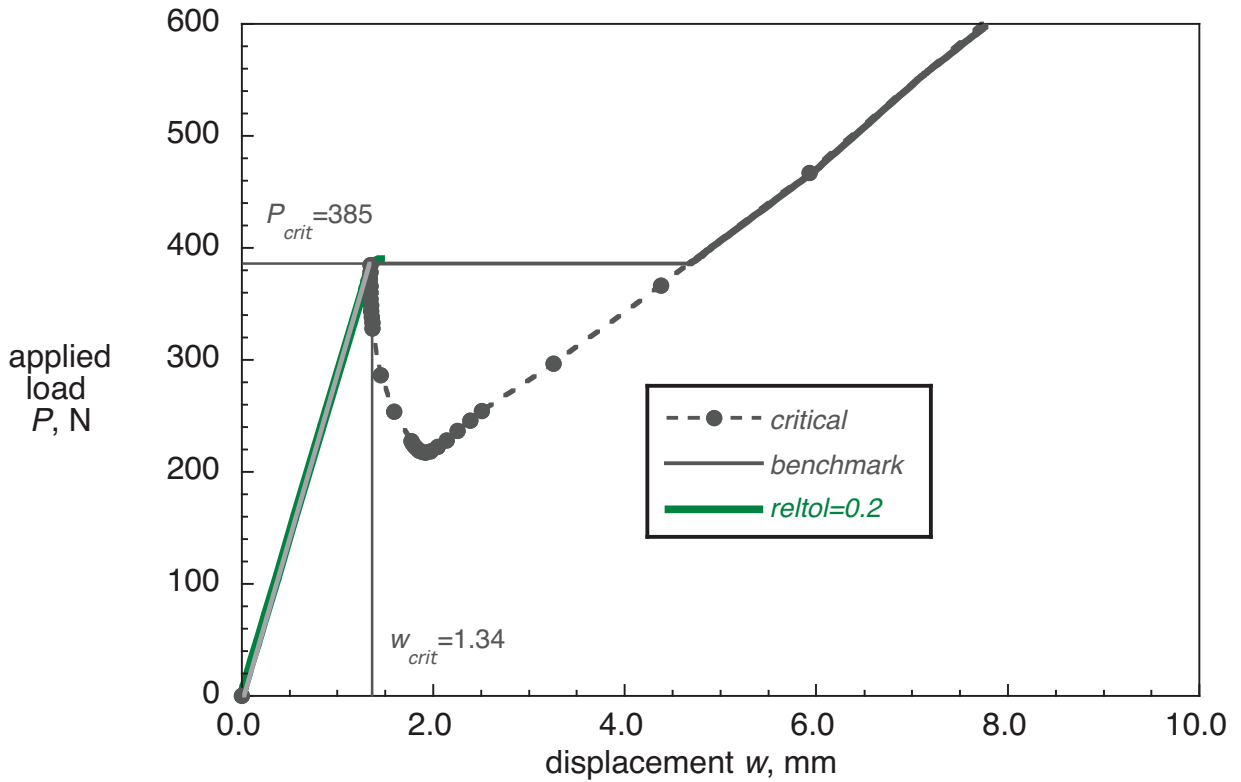


Figure 39. Computed critical load-displacement behavior for MMB specimen (50% mode II) obtained from two-dimensional planar models (CPE4I) with different release tolerance settings.

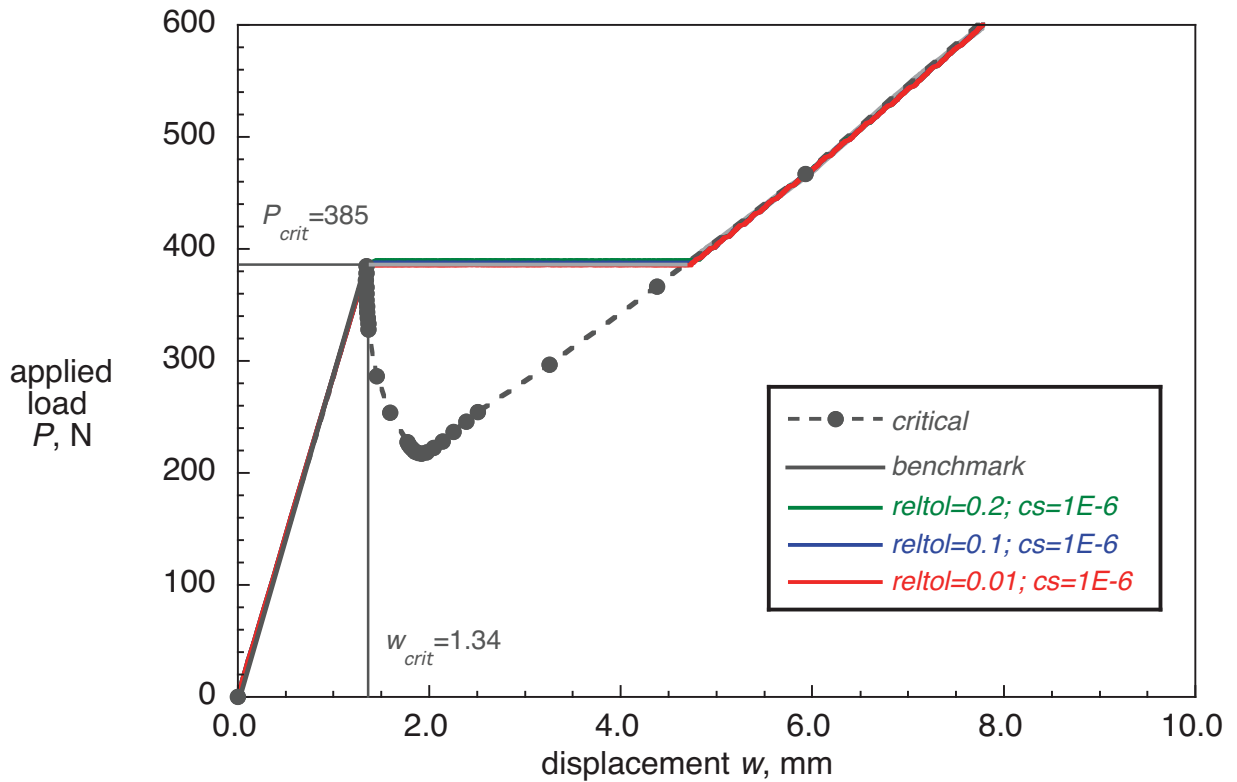


Figure 40. Computed critical load-displacement behavior for MMB specimen (50% mode II) obtained from two-dimensional planar models (CPE4I) with added contact stabilization.

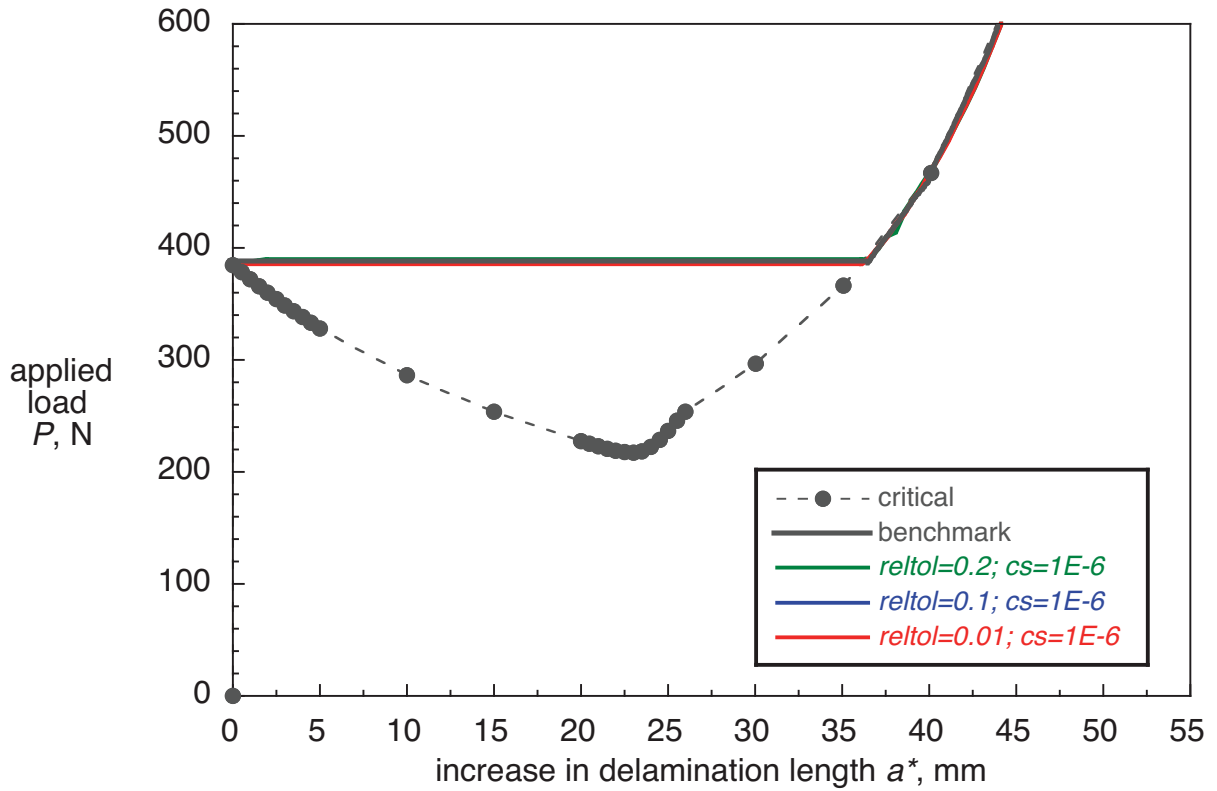


Figure 41. Computed critical load-propagation behavior for MMB specimen (50% mode II) obtained from two-dimensional planar models.

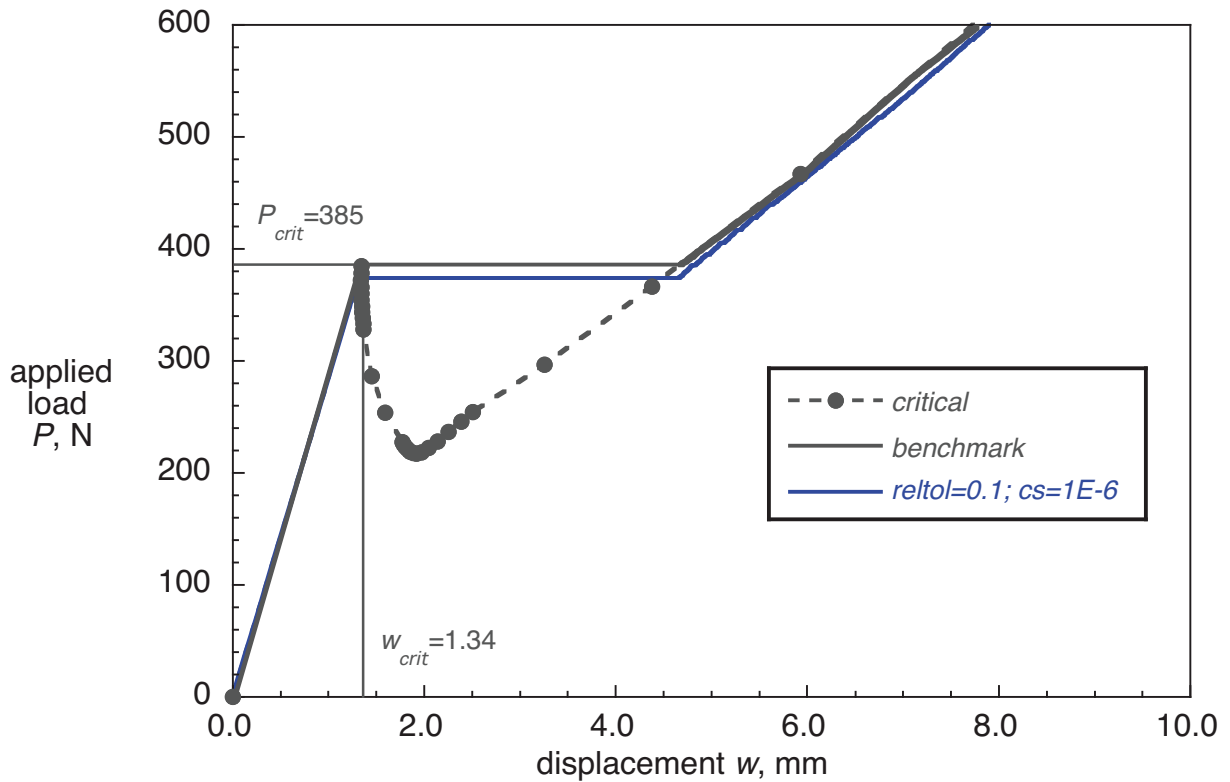


Figure 42. Computed critical load-displacement behavior for MMB specimen (50% mode II) obtained from three-dimensional solid models (C3D8I) with added contact stabilization.

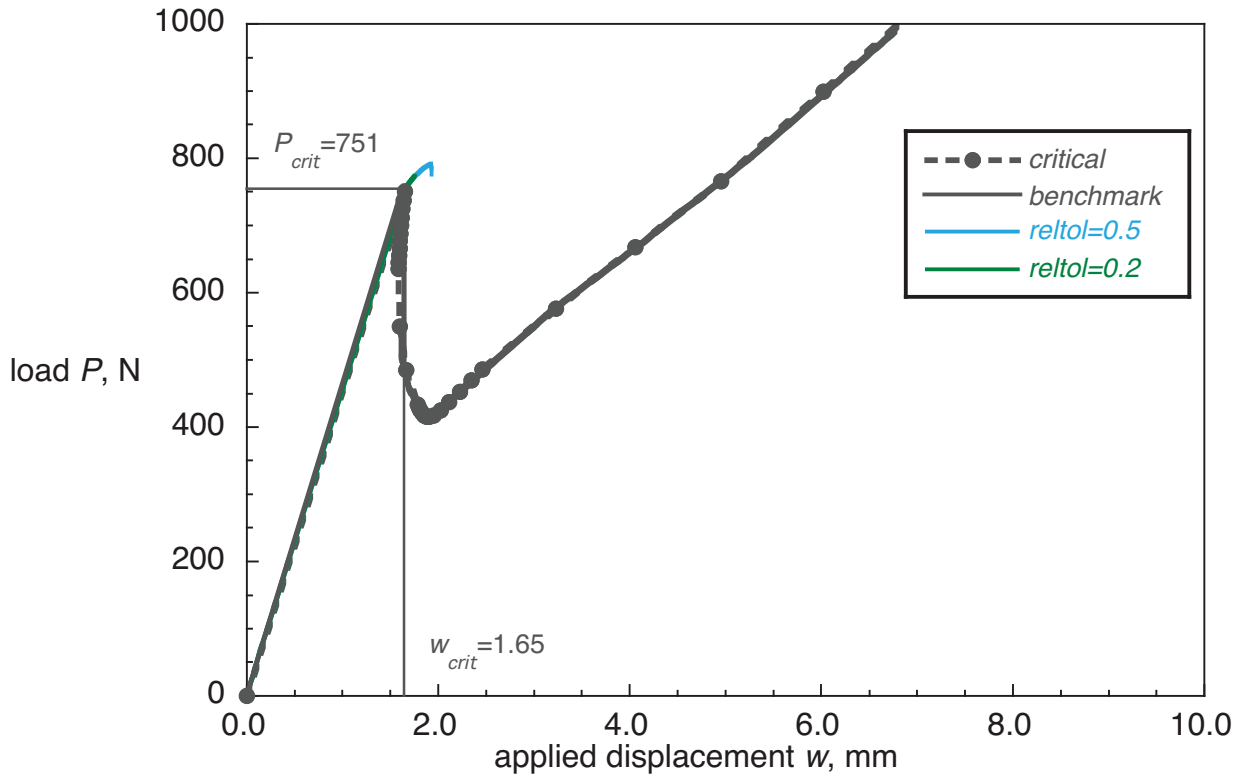


Figure 43. Computed critical load-displacement behavior for MMB specimen (80% mode II) obtained from two-dimensional planar models (CPE4I) with different release tolerance settings.

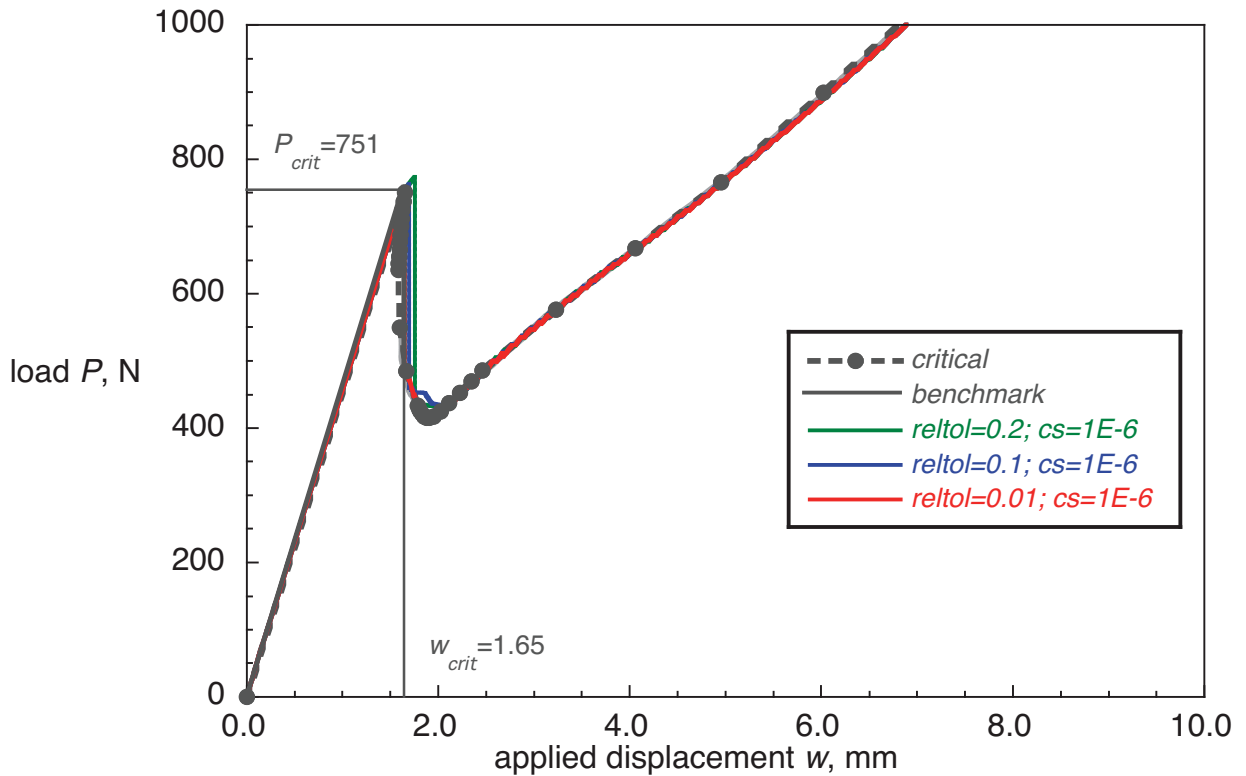


Figure 44. Computed critical load-displacement behavior for MMB specimen (80% mode II) obtained from two-dimensional planar models (CPE4I) with added contact stabilization.

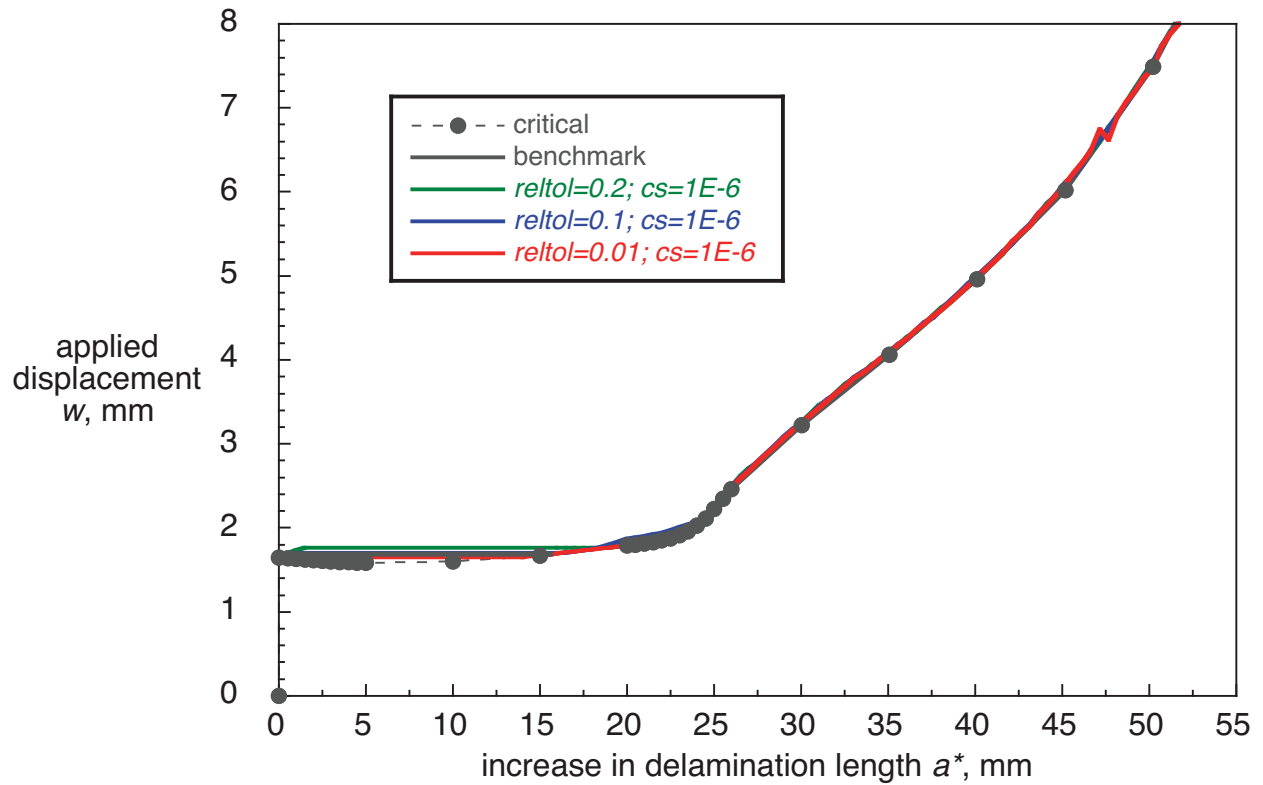


Figure 45. Computed critical displacement-propagation behavior for MMB specimen (80% mode II) obtained from two-dimensional planar models.

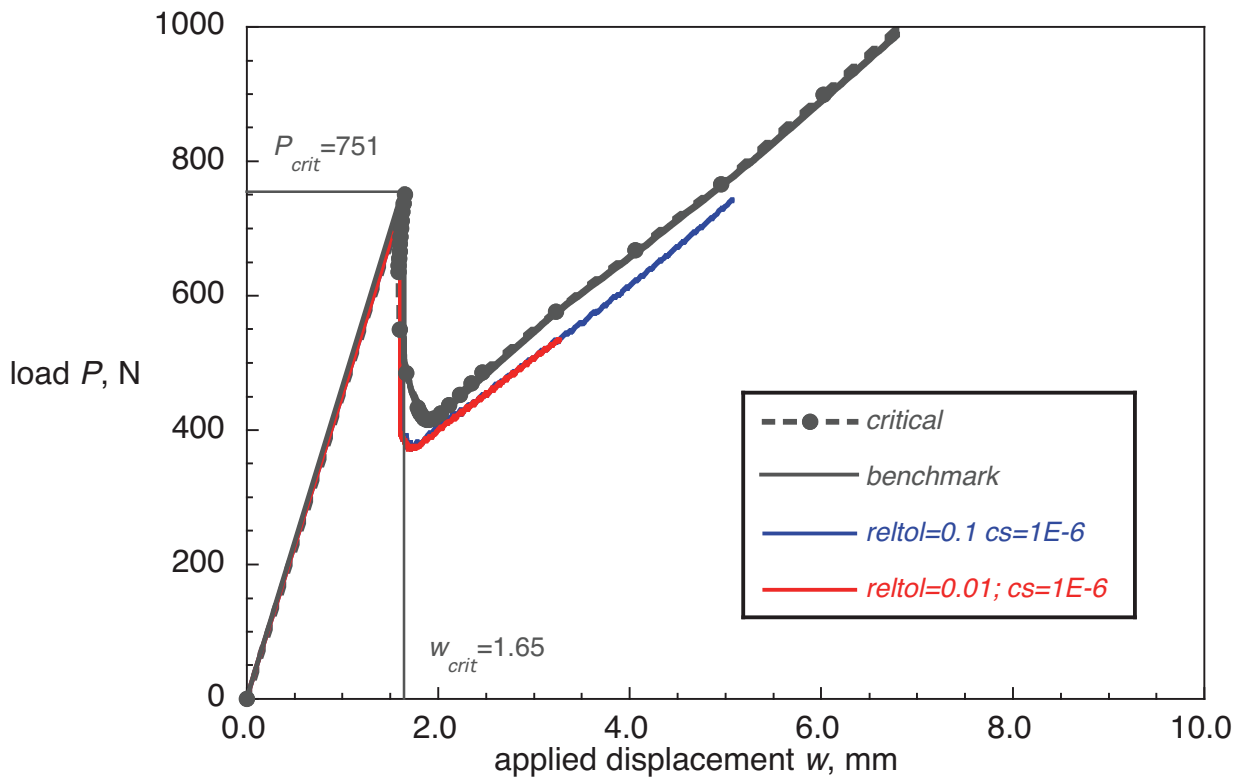


Figure 46. Computed critical load-displacement behavior for MMB specimen (80% mode II) obtained from three-dimensional solid models (C3D8I) with added contact stabilization.

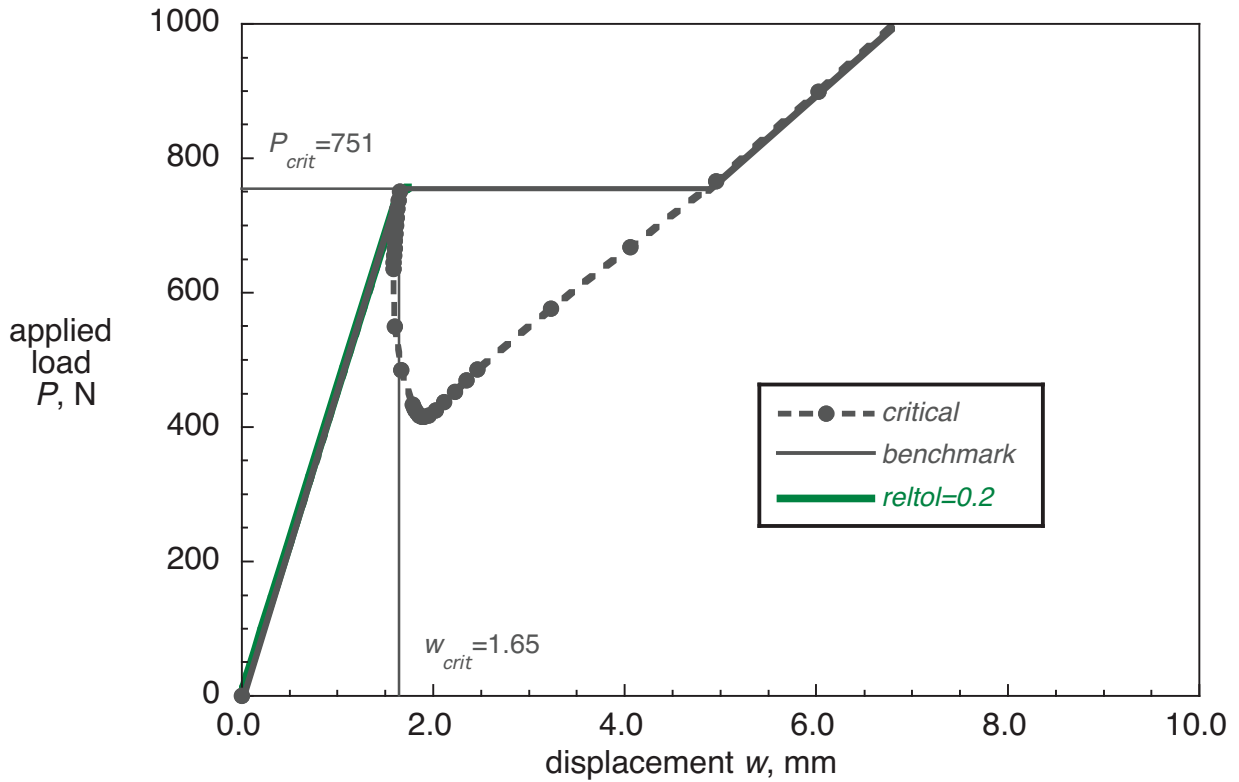


Figure 47. Computed critical load-displacement behavior for MMB specimen (80% mode II) obtained from two-dimensional planar models (CPE4I) with different release tolerance settings.

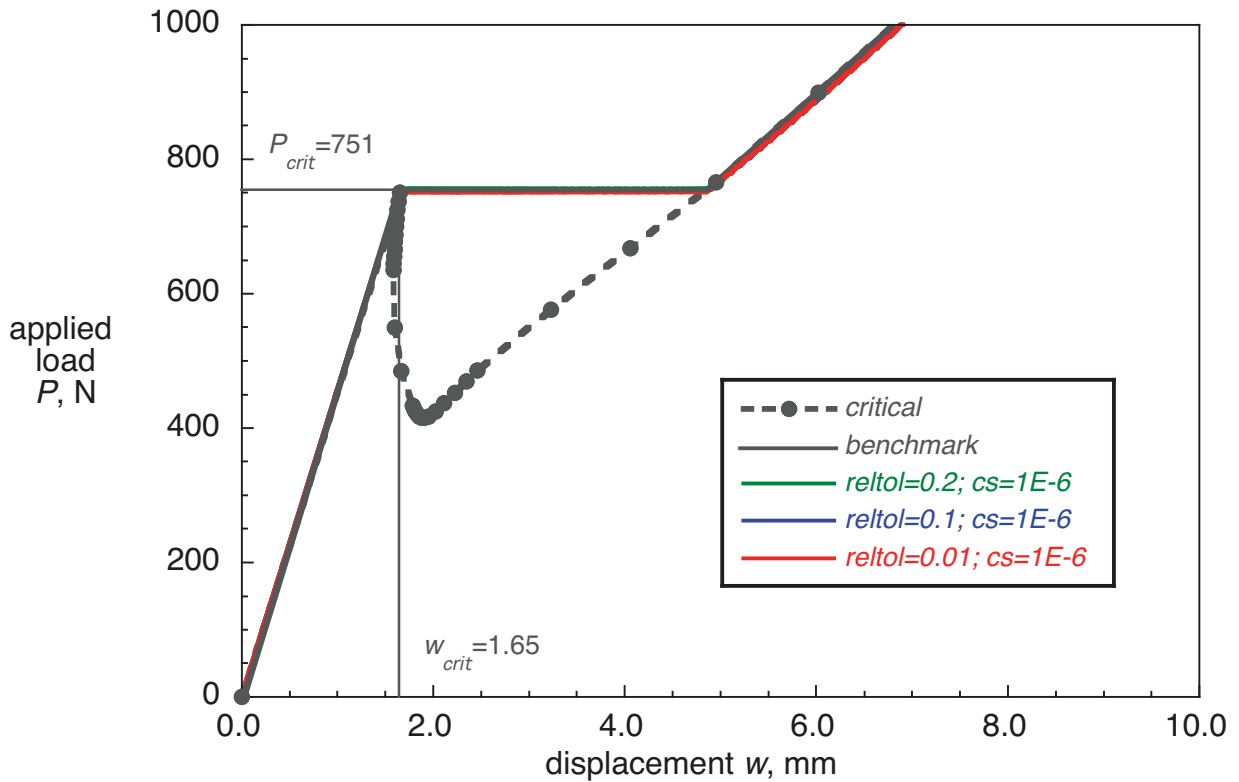


Figure 48. Computed critical load-displacement behavior for MMB specimen (80% mode II) obtained from two-dimensional planar models (CPE4I) with added contact stabilization.

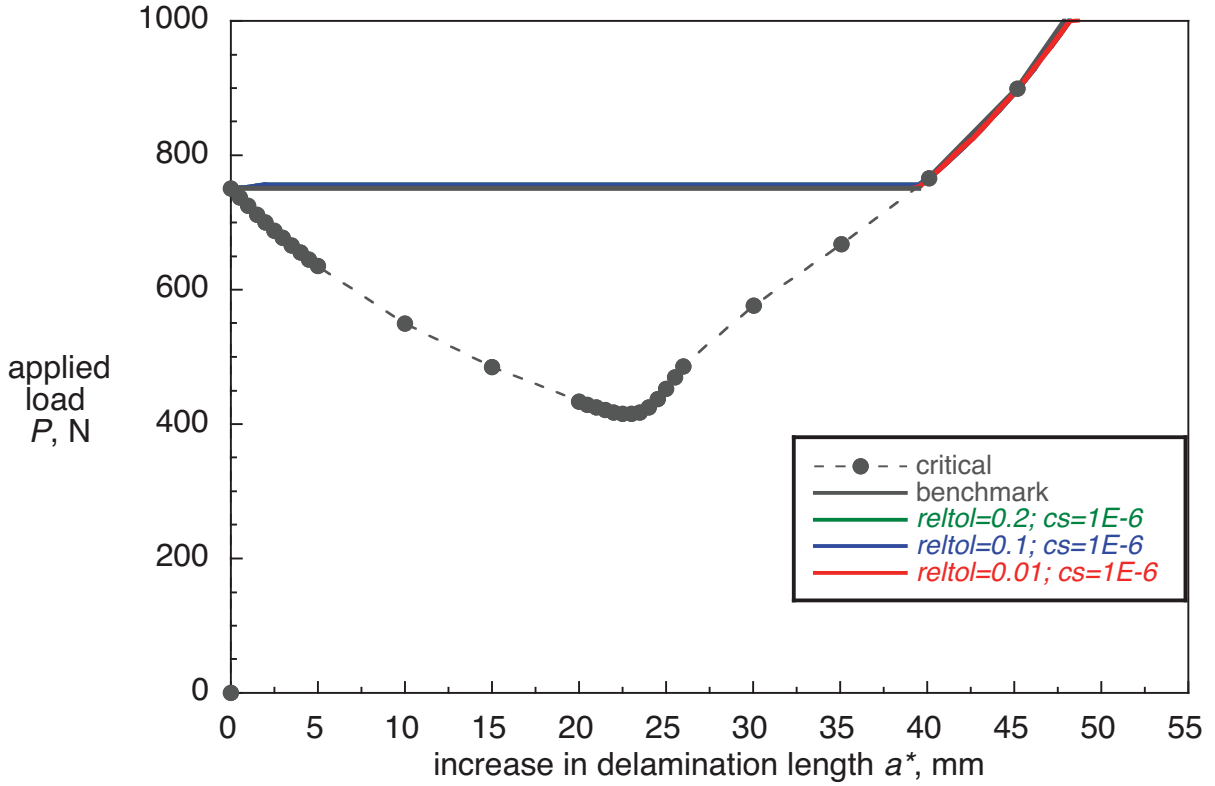


Figure 49. Computed critical load-propagation behavior for MMB specimen (80% mode II) obtained from two-dimensional planar models.

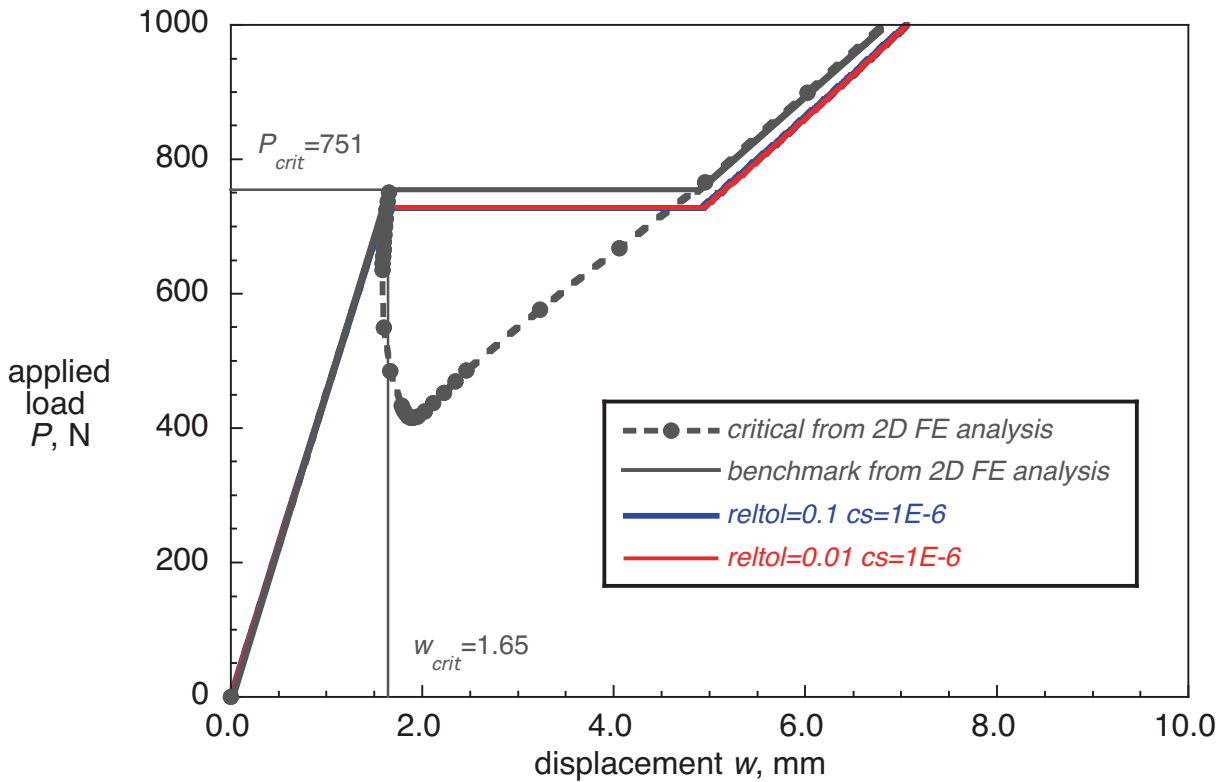


Figure 50. Computed critical load-displacement behavior for MMB specimen (80% mode II) obtained from three-dimensional solid models (C3D8I) with added contact stabilization.

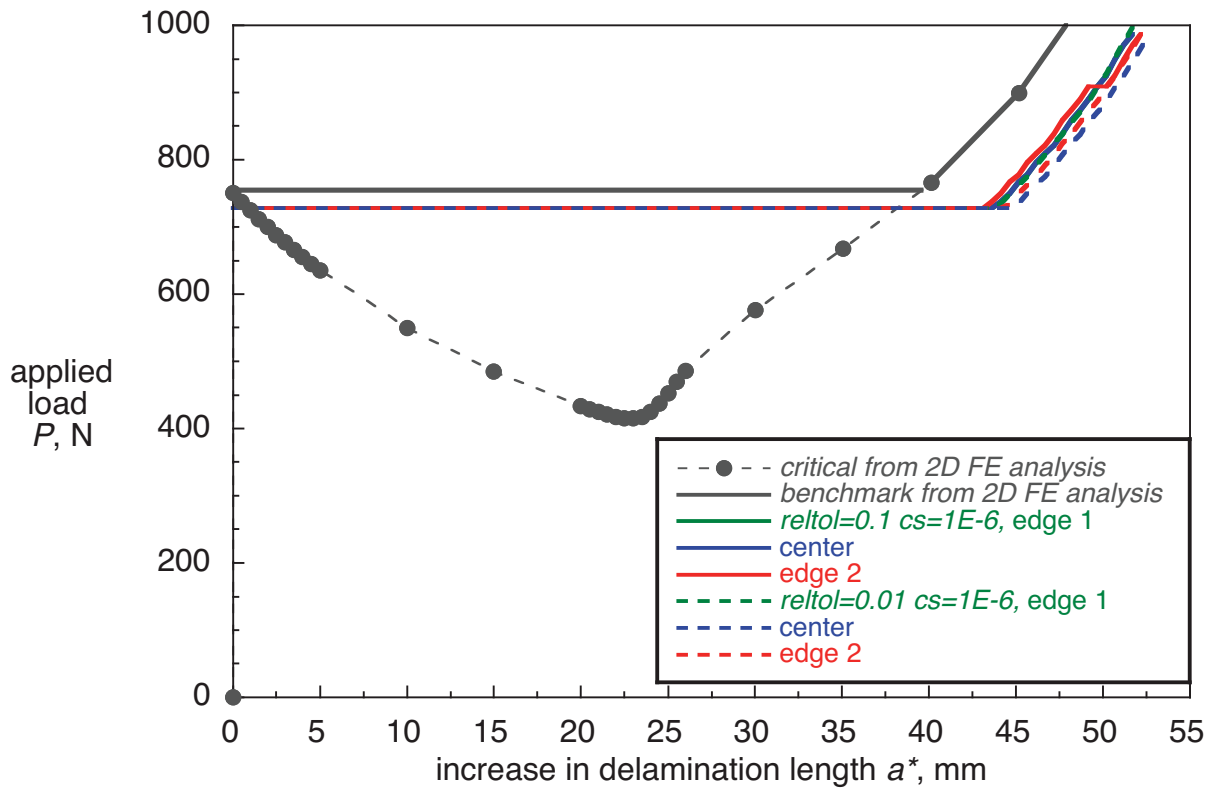
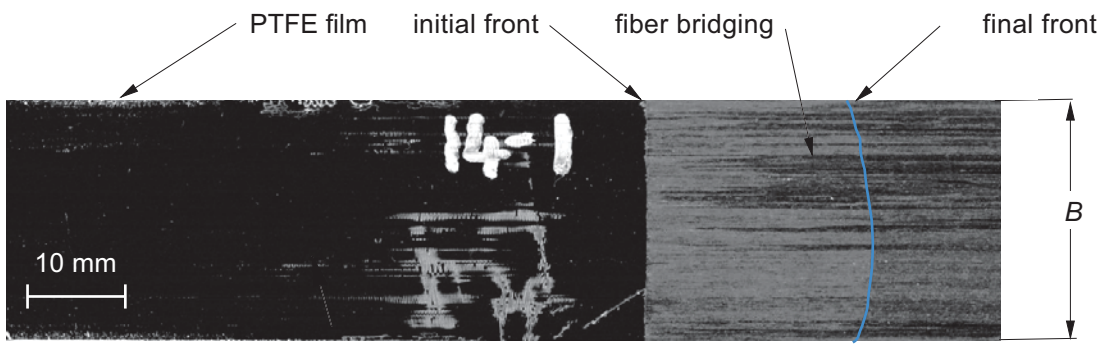
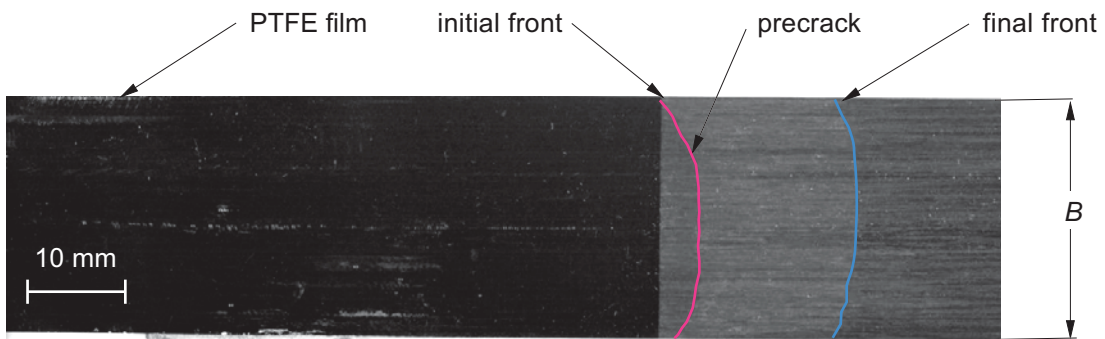


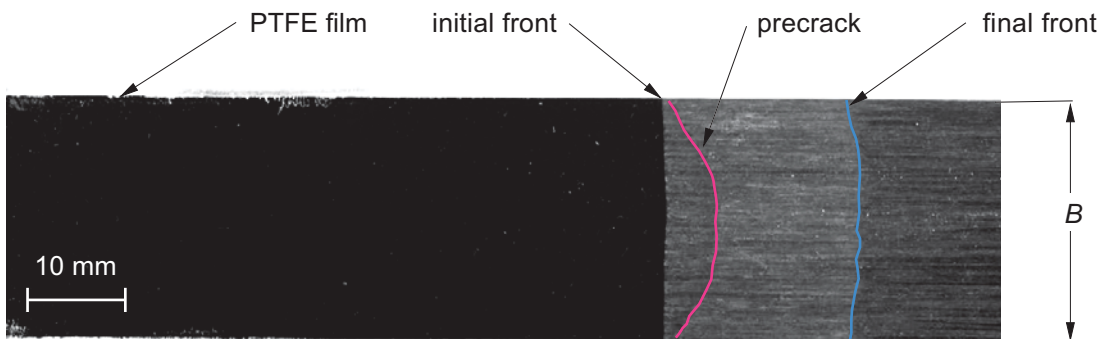
Figure 51. Computed critical load-propagation behavior for MMB specimen (80% mode II) obtained from three-dimensional solid models (C3D8I) with added contact stabilization.



a. 20% mode II.

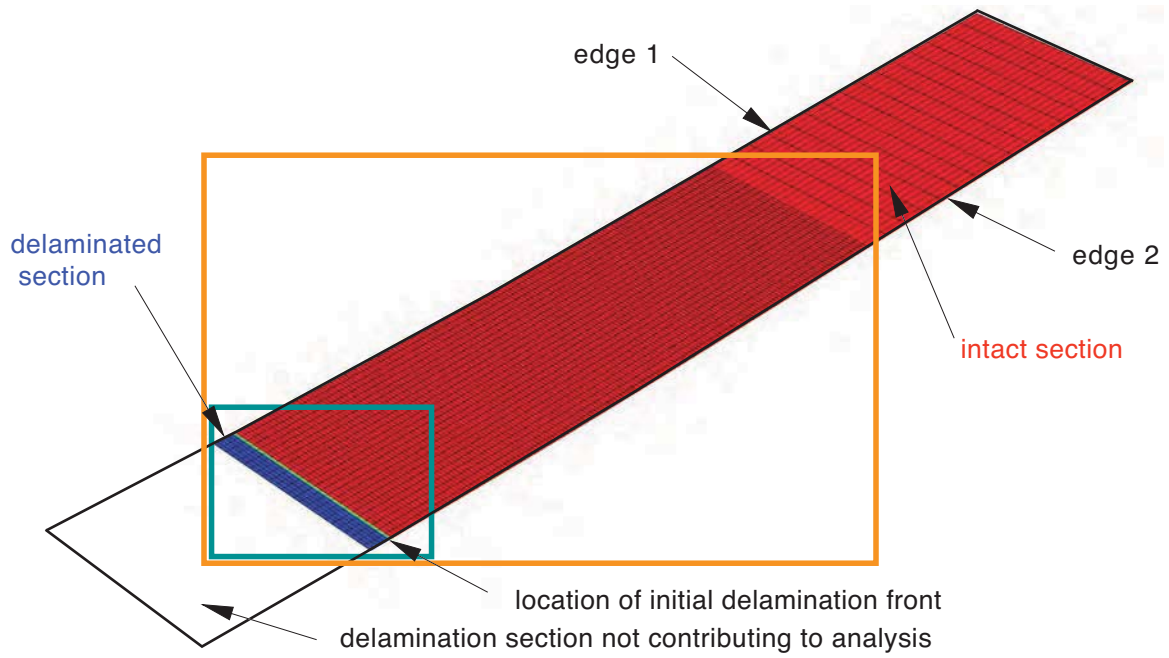


b. 50% mode II.

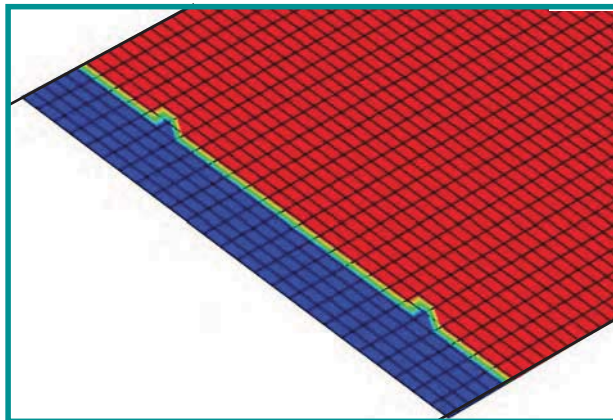


c. 80% mode II.

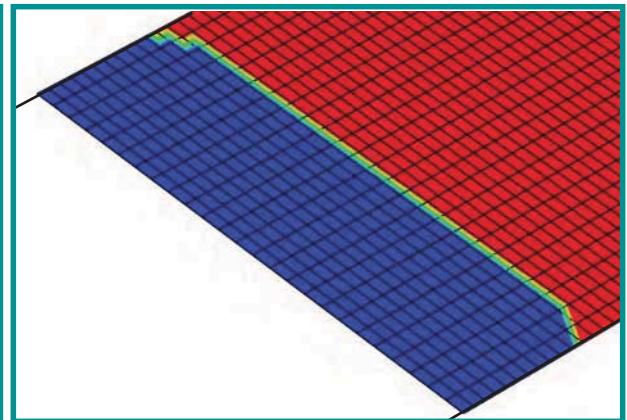
Figure 52. Fracture surfaces of typical MMB specimens [7].



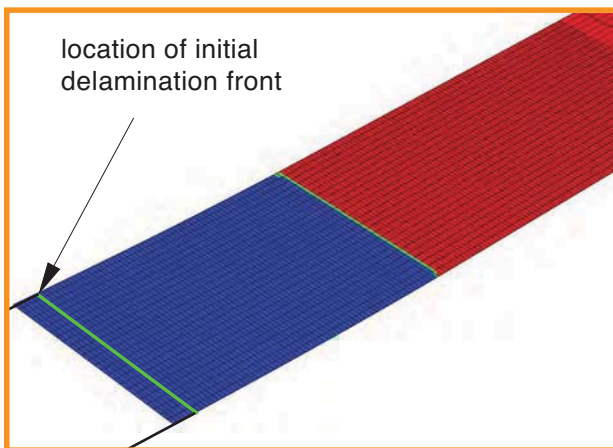
a. Initial delamination front shape (Bottom surface of FE model in Figure 5).



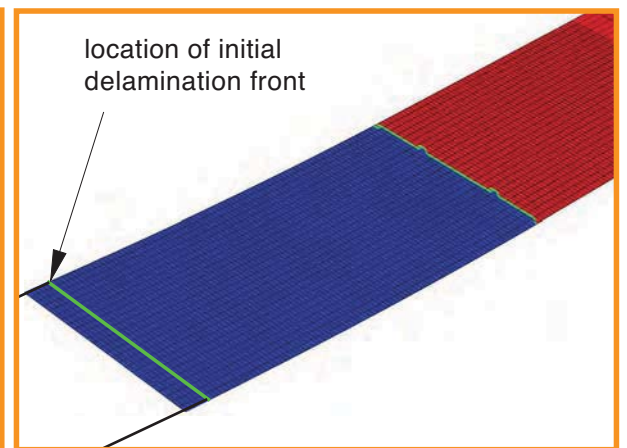
b. Detail of first delamination propagation.



c. Detail of delamination propagation.

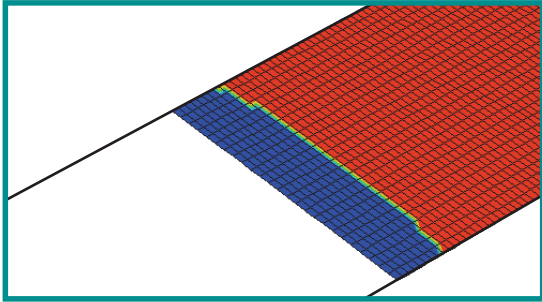


d. Detail of delamination propagation.

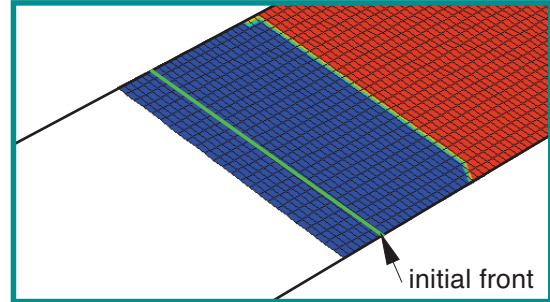


e. Detail of delamination propagation.

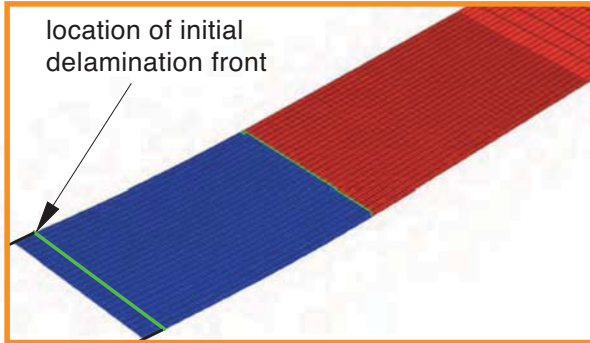
Figure 53. Computed delamination front shape for MMB specimen (20% mode II).



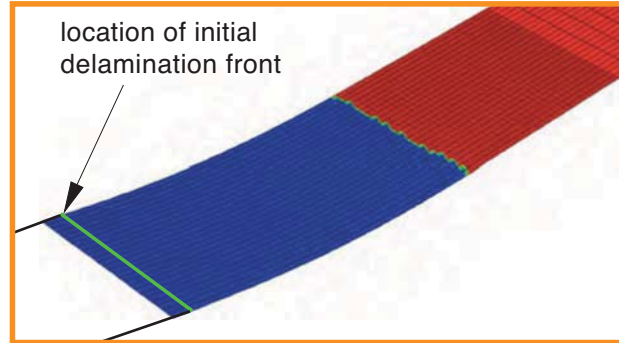
a. Detail of first delamination propagation.



b. Detail of early propagation.

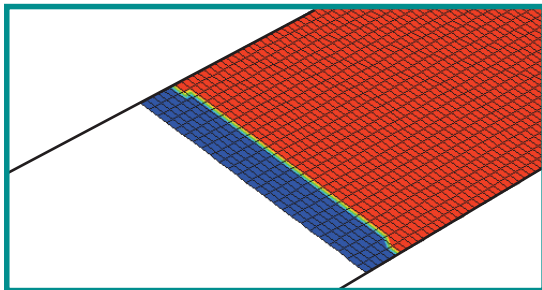


c. Detail of advanced propagation.

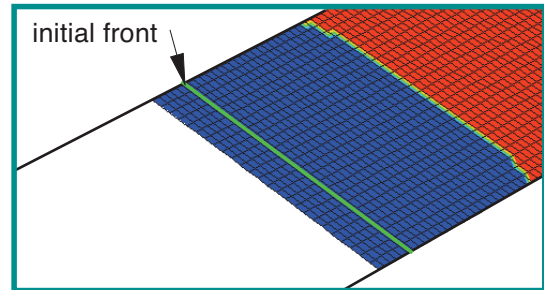


d. Detail of final front.

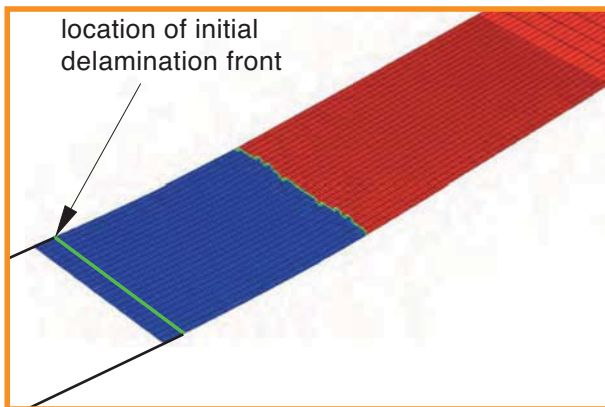
Figure 54. Computed delamination front for MMB specimen (50% G_{II} - applied displacement).



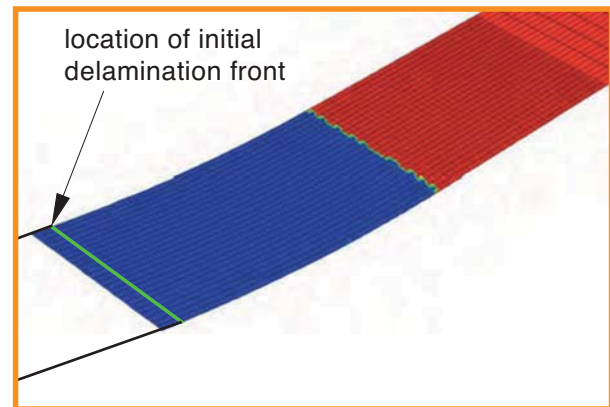
a. Detail of first delamination propagation.



b. Detail of early propagation.

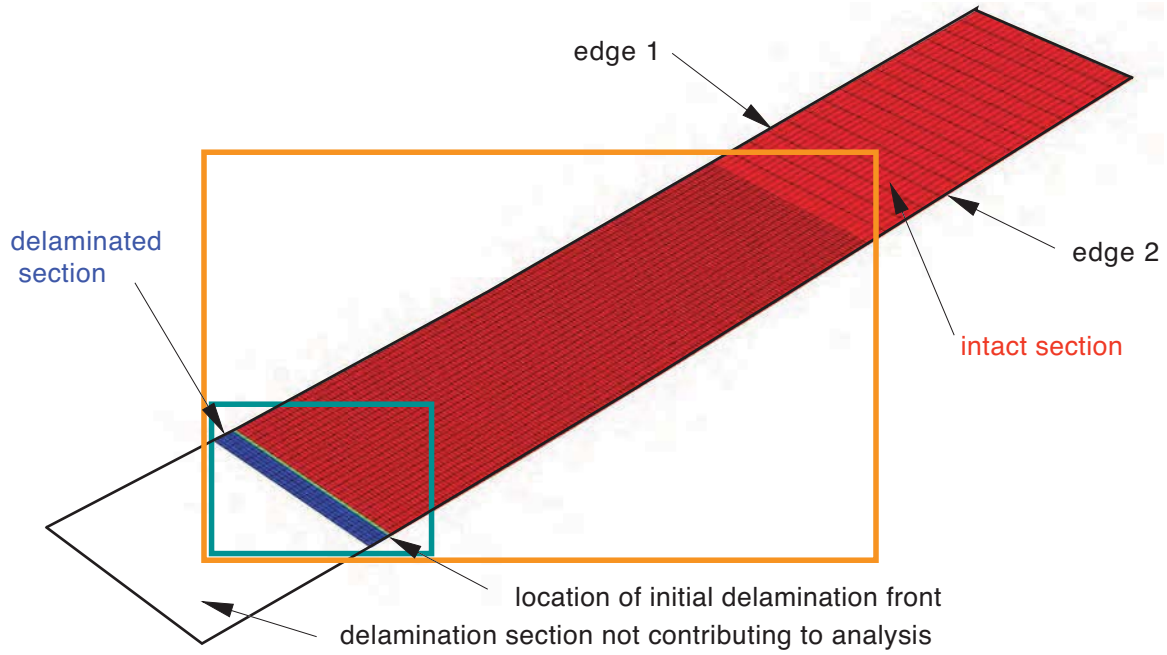


c. Detail of advanced propagation.

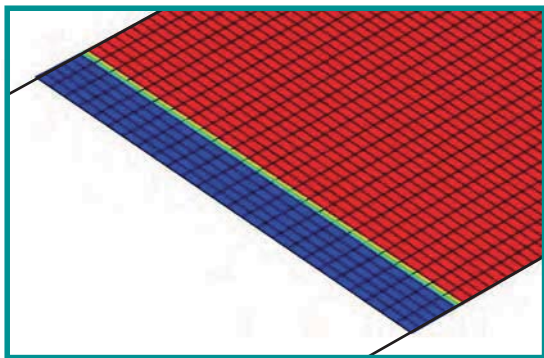


d. Detail of final front.

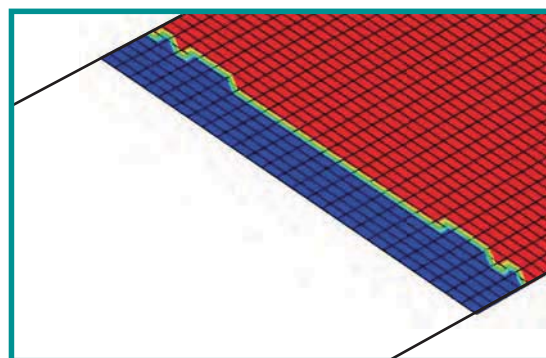
Figure 55. Computed delamination front for MMB specimen (50% G_{II} - applied load).



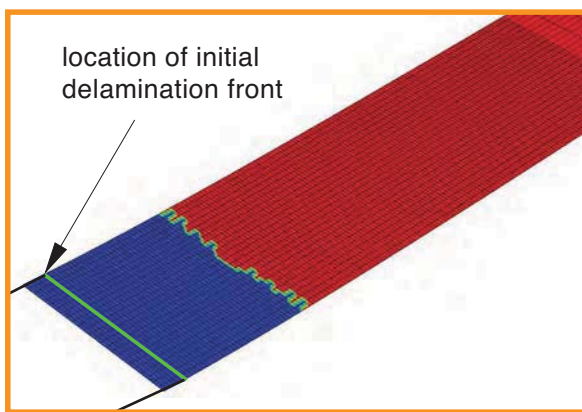
a. Initial delamination front shape (Bottom surface of FE model in Figure 5).



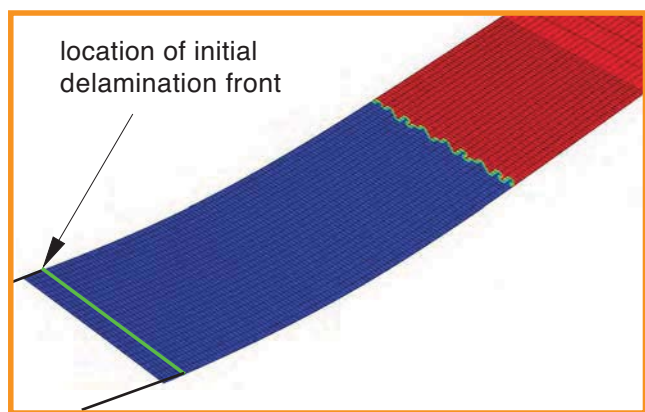
b. Detail of first initial delamination front.



c. Detail of first delamination propagation.

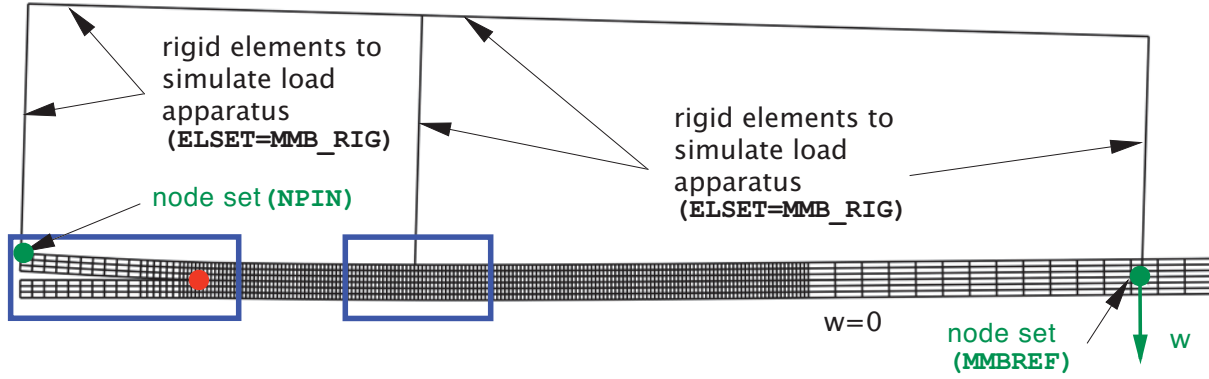


d. Detail of delamination propagation.

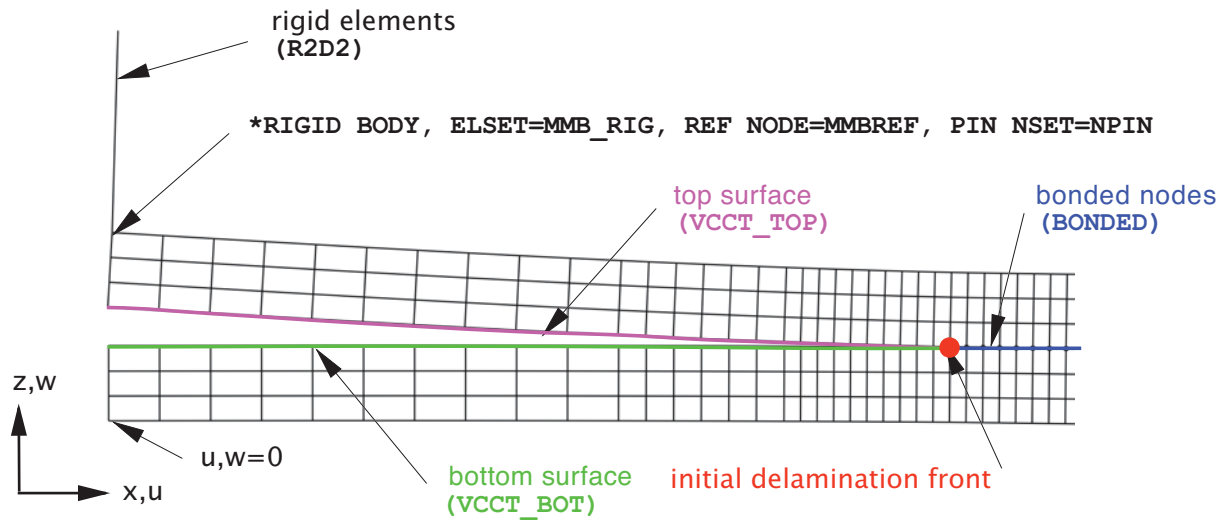


e. Detail of delamination propagation.

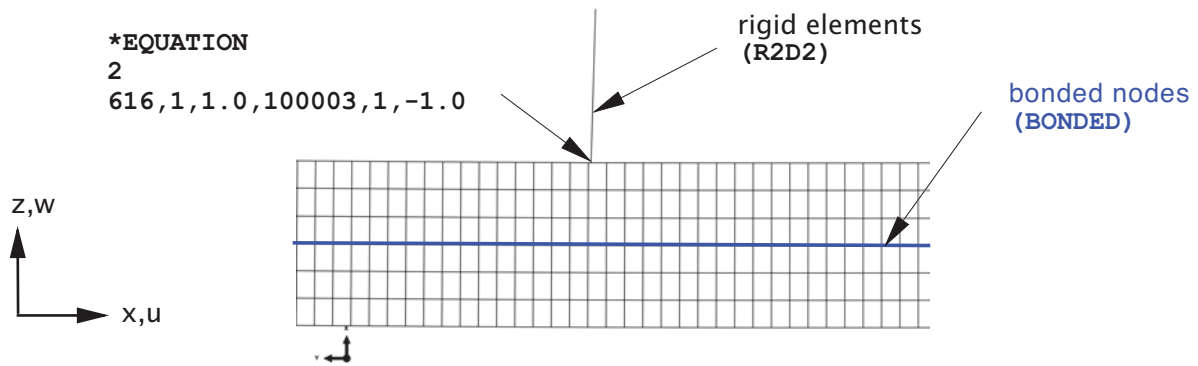
Figure 56. Computed delamination front shape for MMB specimen (80% mode II).



(a). View of full model.



(b). Detail of specimen tip and crack tip zone.



(c). Detail of load introduction zone.

Figure A1. Deformed 2D FE-model of a MMB specimen.

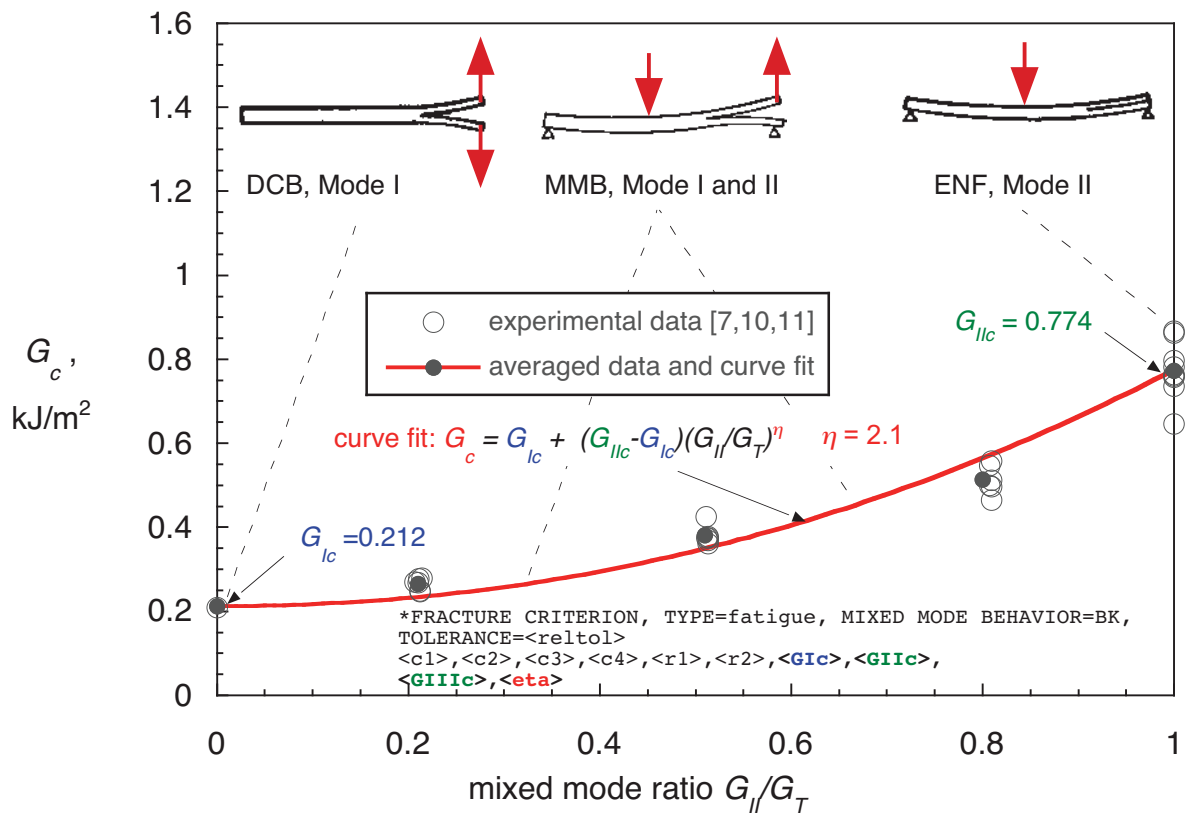


Figure A2. Mixed mode fracture criterion for IM7/8552.

REPORT DOCUMENTATION PAGE

*Form Approved
OMB No. 0704-0188*

The public reporting burden for this collection of information is estimated to average 1 hour per response, including the time for reviewing instructions, searching existing data sources, gathering and maintaining the data needed, and completing and reviewing the collection of information. Send comments regarding this burden estimate or any other aspect of this collection of information, including suggestions for reducing this burden, to Department of Defense, Washington Headquarters Services, Directorate for Information Operations and Reports (0704-0188), 1215 Jefferson Davis Highway, Suite 1204, Arlington, VA 22202-4302. Respondents should be aware that notwithstanding any other provision of law, no person shall be subject to any penalty for failing to comply with a collection of information if it does not display a currently valid OMB control number.
PLEASE DO NOT RETURN YOUR FORM TO THE ABOVE ADDRESS.

1. REPORT DATE (DD-MM-YYYY) 01-04-2012		2. REPORT TYPE Contractor Report		3. DATES COVERED (From - To)	
4. TITLE AND SUBTITLE Development and Application of Benchmark Examples for Mixed-Mode I/II Quasi-Static Delamination Propagation Predictions				5a. CONTRACT NUMBER	
				5b. GRANT NUMBER NNL09AA00A	
				5c. PROGRAM ELEMENT NUMBER	
6. AUTHOR(S) Krueger, Ronald				5d. PROJECT NUMBER	
				5e. TASK NUMBER	
				5f. WORK UNIT NUMBER 877868.02.07.07.05.01.01	
7. PERFORMING ORGANIZATION NAME(S) AND ADDRESS(ES) NASA Langley Research Center Hampton, VA 23681-2199				8. PERFORMING ORGANIZATION REPORT NUMBER NIA Report No. 2012-01	
9. SPONSORING/MONITORING AGENCY NAME(S) AND ADDRESS(ES) National Aeronautics and Space Administration Washington, DC 20546-0001				10. SPONSOR/MONITOR'S ACRONYM(S) NASA	
				11. SPONSOR/MONITOR'S REPORT NUMBER(S) NASA/CR-2012-217562	
12. DISTRIBUTION/AVAILABILITY STATEMENT Unclassified - Unlimited Subject Category 24 Availability: NASA CASI (443) 757-5802					
13. SUPPLEMENTARY NOTES Langley Technical Monitor: Jonathan B. Ransom					
14. ABSTRACT The development of benchmark examples for quasi-static delamination propagation prediction is presented and demonstrated for a commercial code. The examples are based on finite element models of the Mixed-Mode Bending (MMB) specimen. The examples are independent of the analysis software used and allow the assessment of the automated delamination propagation prediction capability in commercial finite element codes based on the virtual crack closure technique (VCCT). First, quasi-static benchmark examples were created for the specimen. Second, starting from an initially straight front, the delamination was allowed to propagate under quasi-static loading. Third, the load-displacement relationship from a propagation analysis and the benchmark results were compared, and good agreement could be achieved by selecting the appropriate input parameters. Good agreement between the results obtained from the automated propagation analysis and the benchmark results could be achieved by selecting input parameters that had previously been determined during analyses of mode I Double Cantilever Beam and mode II End Notched Flexure specimens. The benchmarking procedure proved valuable by highlighting the issues associated with choosing the input parameters of the particular implementation. Overall the results are encouraging, but further assessment for mixed-mode delamination fatigue onset and growth is required.					
15. SUBJECT TERMS benchmarking; composites; delamination; finite element analysis; fracture mechanics; virtual crack closure technique					
16. SECURITY CLASSIFICATION OF:			17. LIMITATION OF ABSTRACT	18. NUMBER OF PAGES	19a. NAME OF RESPONSIBLE PERSON
a. REPORT	b. ABSTRACT	c. THIS PAGE			STI Help Desk (email: help@sti.nasa.gov)
U	U	U	UU	62	19b. TELEPHONE NUMBER (Include area code) (443) 757-5802